Chapter 3

Results and discussion

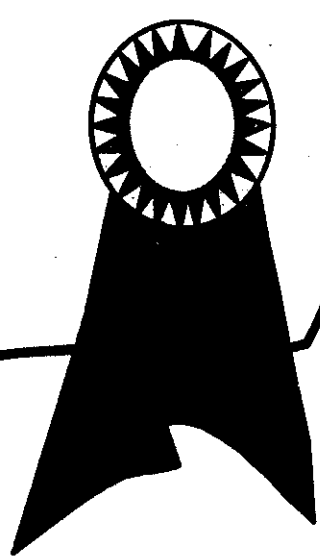

RESULTS and DISCUSSION

3.1 Zinc – Gallium Couple

3.1.1 Distribution Behaviour Investigations

The distribution behaviour of the cyclotron irradiated target materials (i.e Zn(II)) and the corresponding radiotracer product of Ga(III) in HCl and/or HNO_3 acid solutions on 12-molybdocerate gel matrix was investigated at different experimental conditions by using the static batch equilibration and the dynamic chromatographic column breakthrough methods. The experimental criteria were chosen to simulate more or less the conditions of radiochemical separation of cyclotron produced radioisotopes in the literature publications.

3.1.1.1 Static Studies

The interactions of the individual radioactive tracers of zinc(II) and gallium(III) as well as inactive copper(II) and iron(III) as interfering metal ions in HNO_3 and HCl acid solutions with the 12-molybdocerate (IV) cation exchange matrix were investigated at 25±1 °C by the batch equilibration technique. Investigations were carried out under similar experimental conditions in order to make possible comparison and assessment of the obtained distribution coefficient (K_d) values for evaluation of effective chromatographic separation and purification procedures of the target-product couples and regeneration of the column matrix. The course and mechanism of interactions of the metal ions with the 12-molybdocerate(IV) matrix, as a measure of the corresponding distribution coefficient (K_d) values, depend mainly on the physical and chemical properties of the sorbent surface, nature and concentration of the equilibrating solution and chemical state of the metal ions in solution at a constant reaction temperature. In radiochemical processing of the

cyclotron produced radioisotopes the concentrations of the target material (i.e zinc (II)) are usually in micro or macro amounts. On the other hand, the product radioisotopes of gallium (III) are in trace amounts. Therefore, the effect of metal ions concentration as well as nature and concentration of the acid solutions (HNO_3 and HCl) on the distribution behaviour of the respective radiotracer ions on 12-molybdocerate(IV) matrix in the H^+-ion form were studied. Nitric and hydrochloric acid solutions were selected to be the best candidates as equilibrating media. This selection is implemented, to some extent, to meet the medical requirements of the respective radiotracer products. The obtained distribution behaviour data of the individual metal ions is illustrated by plotting the distribution coefficient (K_d) values against the acid concentration at different metal ions concentrations in log-log plot and by drawing the breakthrough curves.

The K_d values for Zn(II) and Ga(III) in nitric and hydrochloric acid media over the investigated concentration range (0.005-0.5M acid) at 25±1°C are shown in Figures (6 and 7) and (8 and 9), respectively. In general, when a cation in solution is being exchanged for an ion of different charge values the relative affinity of the higher charge ion increases in direct proportion to the dilution of the acid solution, in absence of hydrolysis and polynuclear formation reactions. Thus, the exchange of the lower charge ion (i.e H^+) on the surface of the 12-molybdocerate(IV) exchanger with metal ions of higher charge in solution via cation exchange reaction mechanism is favoured by decreasing the acid concentrations.

3.1.1.1.1 Effect of H^+- ion Concentration

Figure 6 shows that the distribution coefficient (K_d) values of 10^{-6}M zinc(II) in nitric acid solutions decrease with increasing the acid

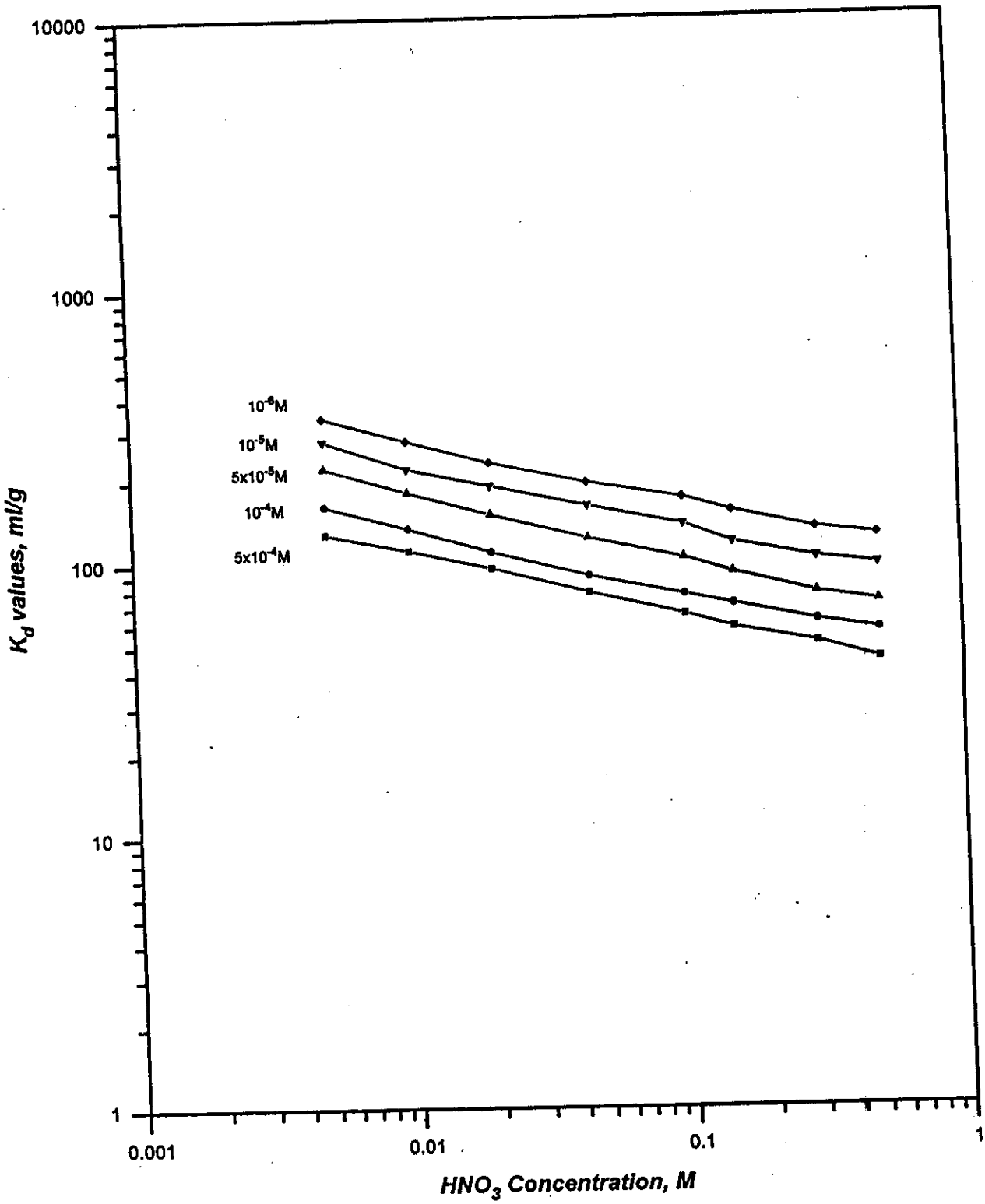

Fig.6. Distribution coefficient (K_d) values of Zn(II) in HNO_3 acid splutions on 12-molybdocerate (IV) at different Zn(II) concentrations(25+1 °C)

concentration overall the investigated range of acidity (0.005-0.5M acid). At high acid concentrations zinc (II) ions may associate with the NO_3^- anions to give neutral and / or anionic species: $[Zn(NO_3)_2]^0$, $[Zn(NO_3)_4]^{2-}$ and $[Zn(NO_3)_5]^{3-}$ which contribute to the observed decrease in the respective distribution coefficient (K_d) values with increasing the acid concentration[25,156]. In addition, the decrease in the adsorbability of Zn(II) with increasing the acid concentration can be attributed to competition between the cations of zinc (II) and H^+ in solution to exchange with H^+ ions on surface of the 12- molybdocerate (IV) matrix. Therefore, it may be deduced that cation exchange mechanism is the ruling reaction process and zinc (II) cations be exchanged for protons on the surface of the molybdate matrix. On the other hand, at low acid concentrations zinc(II) ions has a much greater tendency to form cationic species of $[Zn(OH)]^+$, Zn^{2+} and $[Zn(NO_3)]^+$ which are strongly held on the surface of 12-molybdocerate (IV) matrix by hydrolytic sorption and / or cation exchange mechanisms[24,154,155]. The hydrolytic sorption can be considered as simple condensation reaction between the hydrolysis products of Zn(II) and the sorbent material carrying excess OH- groups. Therefore; the enhanced retention of zinc(II) ions with decreasing the acid concentration may be explained by cation exchange of unhydrolyzed and hydrolytic sorption of zinc(II) cations with H^+ ions on the sorbent surface as well as precipitation of hydrolyzed zinc(II) molecules onto the sorbent surface. Direct cation exchange, hydrolytic precipitation and sorption mechanisms can be illustrated with the follwing equations;

Cation exchange in absence of hydrolysis:

$$H_nMoCe(OH)_m + M^{x+} \rightleftharpoons H_{(n-x)}MoCe(OH)_mM + xH^+$$

Hydrolytic precipitation of molecular species:

$$H_nMoCe(OH)_m + M(OH)_y \longrightarrow H_nMoCe(OH)_{m-y}O_yM + yH_2O$$

Hydrolytic sorption of cationic hydrolyzed species:

$$H_nMoCe(OH)_m + M(OH)_y^{(x-y)+} \rightleftharpoons H_{n-(x-y)}MoCe(OH)_{m-y}O_yM + (x-y)H^+ + yH_2O$$

Where; M^{x+} = The metal cation under consideration and

$H_nMoCe(OH)_m$ = The 12-molybdocerate(IV) matrix[24,160]

Figure 7 shows the distribution behaviour of 10^{-6}M gallium(III) in nitric acid solutions on the 12-molybdocerate(IV) gel. At low acid concentrations, the distribution coefficient (K_d) values of Ga(III) increase gradually to a maximum value of 685ml/g with increasing the acid concentration up to 0.05M HNO_3. This behaviour is attributed to the formation of weakly and non-sorbable hydrolyzed species of Ga(III), $[Ga(OH)_3]^0$, $[Ga(OH)_4]^-$, and $[Ga_2(OH)_8]^{2-}$ depending on the acid concentration[26,154,156]. The obtained sorption maximum at 0.05 M acid; may be due to hydrolytic sorption of hydrolyzed gallium(III) cations; e.g; $[Ga(OH)_2]^+$ and $[Ga(OH)]^{2+}$, from solution as well as direct cation exchange of unhydrolyzed gallium(III) cations with counter H^+ ions on the 12-molybdocerate gel surface. In solutions> 0.1 M nitric acid; the sorption maximum of Ga(III) is followed by a decrease in the corresponding K_d values of Ga(III); due to predomination of molecular Ga(III) nitrate and non adsorbable anionic species: $[Ga(NO_3)_4]^{1-}$ and $[Ga(NO_3)_5]^{2-}$, of Ga(III) in solution on the expense of the readily and stongly exchanging Ga(III) cation [24,25].

3.1.1.1.2 Effect of the acid Anion

Figure 8 displays the corresponding distribution coefficient (K_d) values of zinc (II) in hydrochloric acid solutions. High (K_d) values are obtained at low acid concentrations and decrease more or less linearly with increasing the acid concentration in the range of 0.005-0.5M acid. At low acid concentrations zinc (II) ions have a great tendency to form the cationic species of $[Zn(OH)]^+$, Zn^{2+} and $[Zn(Cl)]^+$ which are strongly

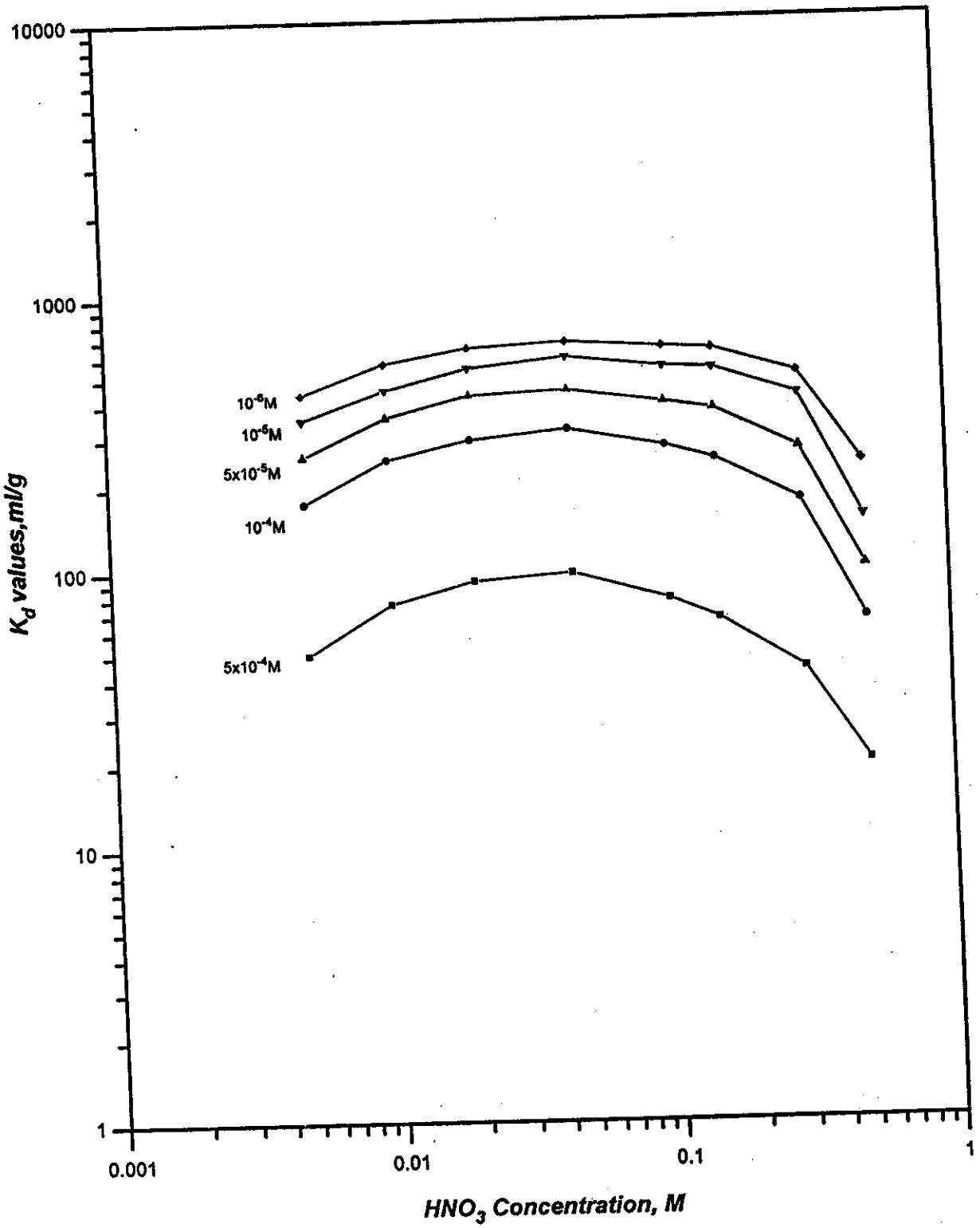

Fig.7. Distribution coefficient (K_d) values of Ga(III) in HNO_3 acid solutions on 12-molybdocerate(IV) at different Ga(III)concentrations (25+1 °C).

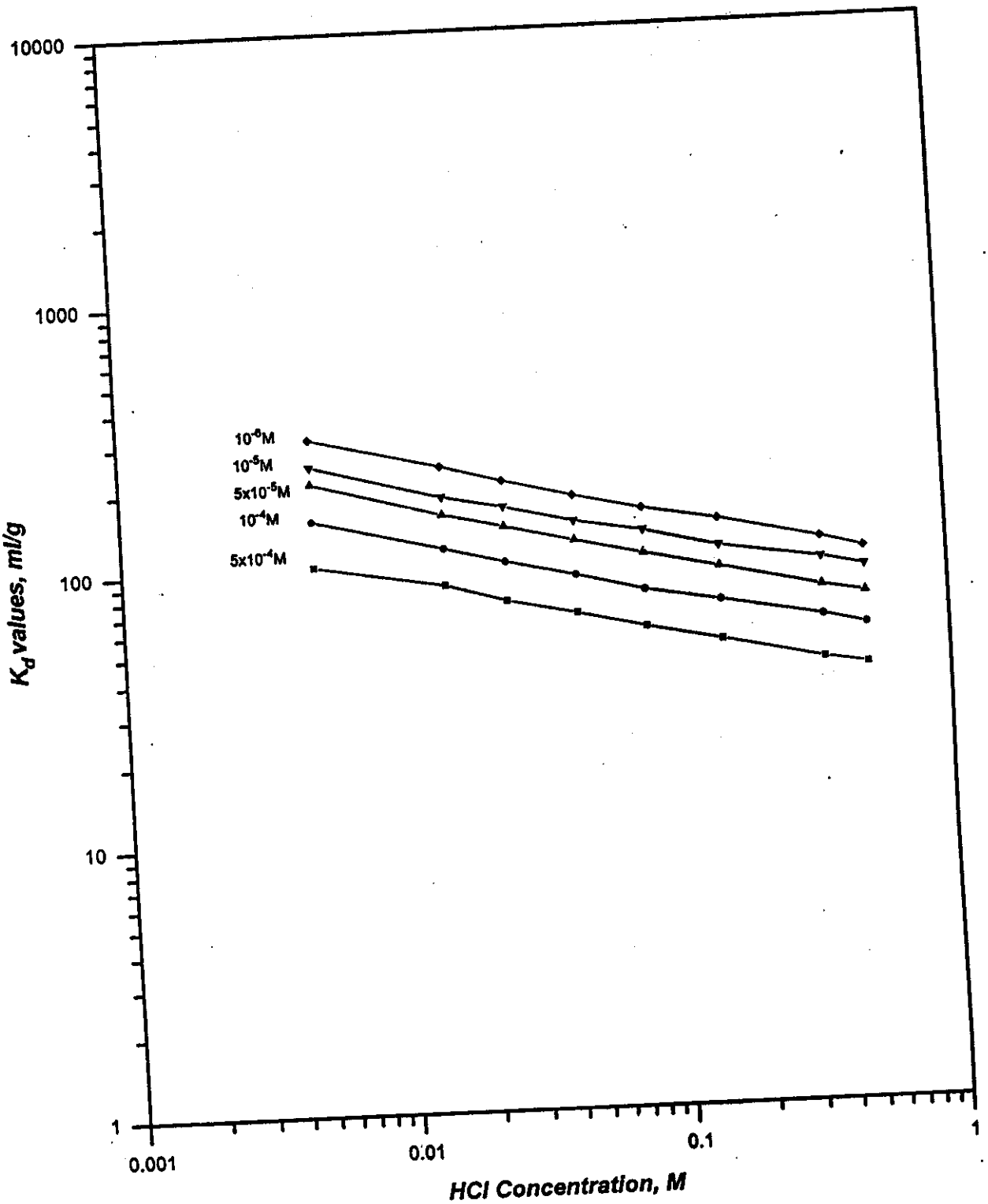

Fig.8. Distribution coefficient (K_d) values of Zn(II) in HCl acid solutions on 12-molybdocerate (IV) at different Zn(II) concentrations(25+1 °C)

retained onto the surface of 12-molybdocerate(IV) matrix by cation exchange as well as by hydrolytic sorption mechanisms. At high acid concentrations zinc (II) react with Cl^- anions to give molecular and anionic species; $[Zn(Cl)_2]^0$, $[Zn(Cl)_4]^{2-}$ and $[Zn(Cl)_6]^{4-}$, which contribute to the observed decrease in the distribution coefficient (K_d) values[25,156]. Figures 6 and 8 indicate that the sorption behaviour of zinc(II) depends to a great extent on the concentration of the competing H^+ ions in solution and to some extent on the conjugate acid anion where; the distribution coefficient (K_d) values in nitric acid media are more or less higher than those in hydrochloric acid solutions; at comparable conditions. This may be attributed to the high complexing affinity of the zinc (II) ions with Cl^- anions than NO_3^- anions in solution.

On the other hand; figures 7 and 9 show that the corresponding K_d values of gallium (III) in HNO_3 and HCl acid solution are seriously affected with the acid anion of the equilibrating media. The K_d values of gallium(III) in HNO_3 > HCl acid solutions at comparable experimental conditions. This is contributed to the formation of more stable gallium(III) chlorides than gallium nitrate complexes in hydrochloric and nitric acid solutions, respectively[25,165].

3.1.1.1.3 Effect of Concentration of the Radiotracers

Figures (6 and 7) and (8 and 9) display the effect of zinc (II) and gallium (III) concentrations ranging from 10^{-6} to $5x10^{-4}$ M in nitric and hydrochloric acid solutions on their distribution behaviour on 12-molybdocerate. It is obvious that the K_d values of the respective metal ions decrease with increasing the concentration of the radiotracer in the equilibrating solution. In all cases; the corresponding K_d values of gallium (III) are higher than that of zinc (II) at comparable conditions.

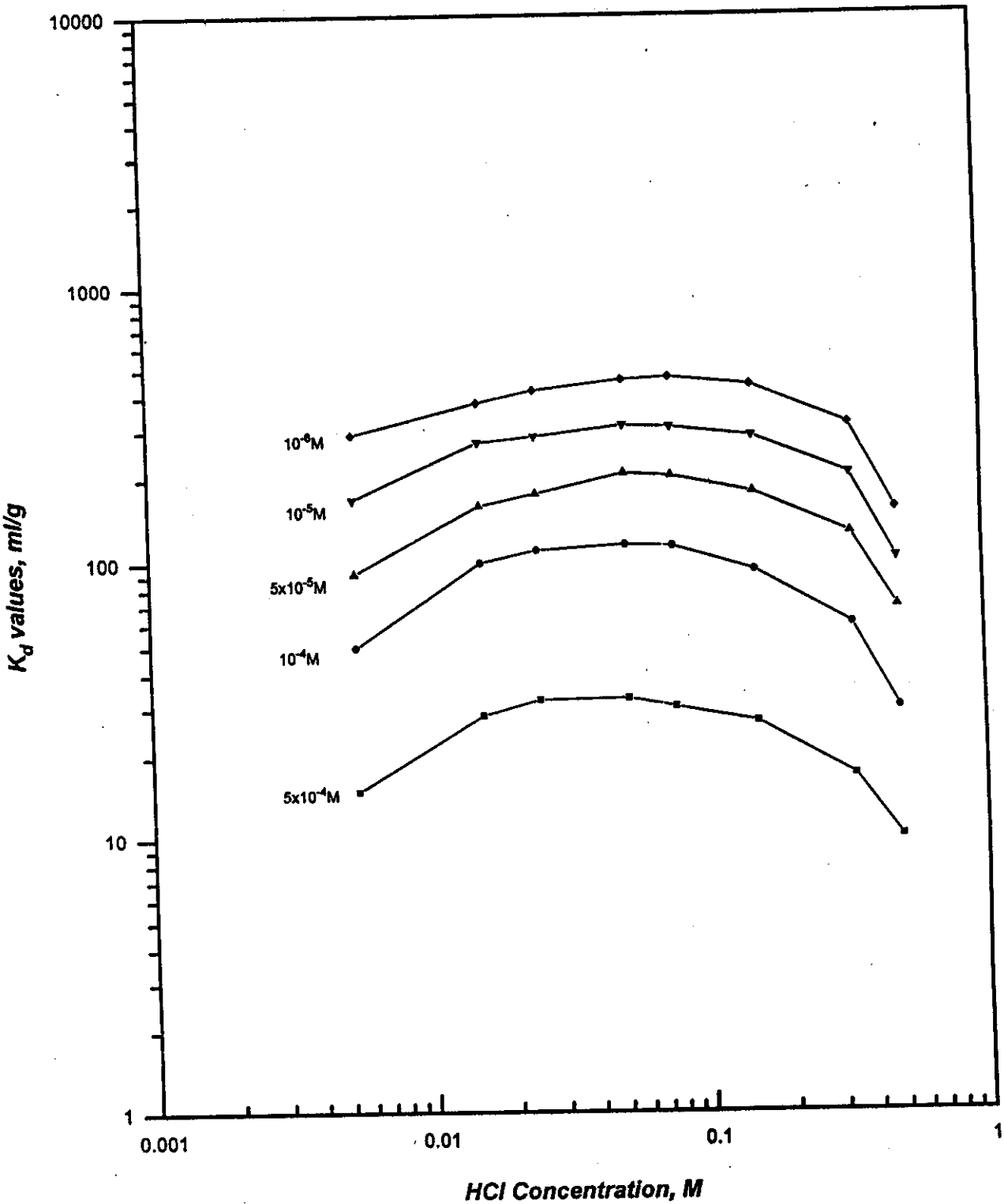

Fig.9. Distribution coefficient (K_d) values of Ga(III) in HCl acid solution on 12-molybdocerate (IV) at different Ga(III) concentrations(25+1 °C).

It indicates that gallium is strongly retained on the 12-molybdocerate (IV) matrix than its zinc (II) target at similar conditions. It could be deduced that separation of trace amounts of gallium (III) radiotracer, as the cyclotron product, from macro or micro amounts of the zinc(II) target (~5 x 10^{-4} M Zn(II)) dissolved in HCl or HNO_3 acid solutions is feasible by using 12-molybdocerate(IV) matrix.

3.1.1.1.4 Interfering Radiocontaminants

The presence of foreign elements such as copper(II) and iron(III) in the target solute as interfering impurities was considered. Radiocontaminants may be originated for example from the copper base metal to which the zinc (II) target was electroplated during the acid etching of the target after irradiation and / or from iron that may be present as an impurity in the targets. These radioactive impurities can compete during the separation and/or purification process with the respective radioactive isotopes on the 12-molybdocerate(IV) matrix. The distribution behaviour of copper(II) and iron(III) in nitric and hydrochloric acid solutions on the sorbent material was carried out by the batch equilibration method. The concentrations of the corresponding copper(II) metal ions was determined radiometrically and iron(III) by spectrophotometric method[159]. Figures (10 and 11) and (12 and 13) display the distribution coefficient (K_d) values of 10^{-6}M copper (II) and iron(III) in nitric and hydrochloric acid solutions on the 12-molybdocerate (IV) matrix dried at 50 ^{o}C in the range of 0.005 - 0.5 M acid and different metal ions concentrations on a log – log plot. It is shown that the K_d values of copper and iron have maximum values of about 80 and 100 ml/g and 40 and 60 ml/g in 0.005 M nitric and hydrochloric acid solutions; respectively. The corresponding (K_d) values decrease linearly with increasing the acid concentration to 40 and

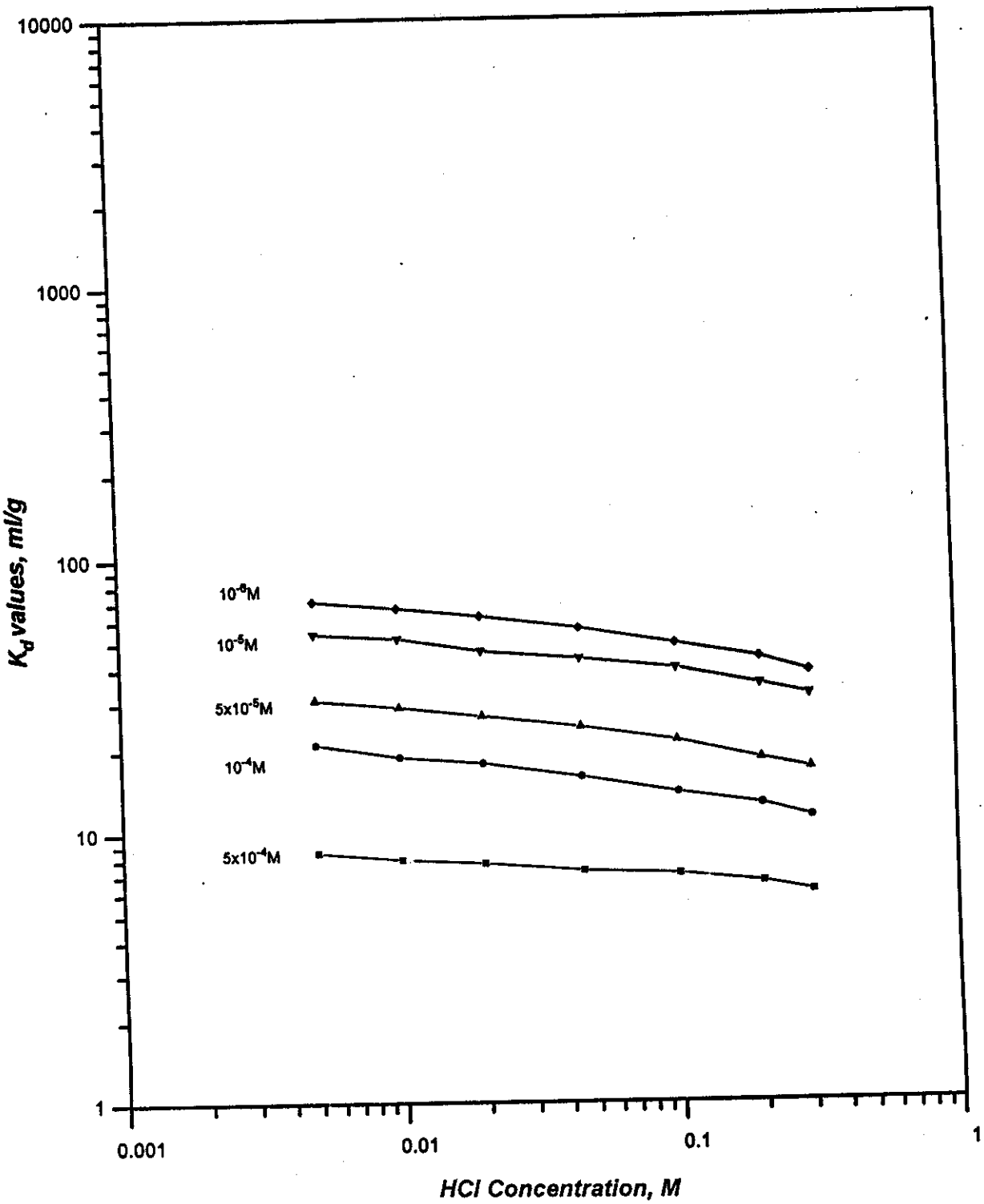

Fig.10. Distribution coefficient (K_d) values of Cu(II) in HNO_3 acid solutions on 12-molybdocerateat (IV) at different Cu(II) concentrations(25+1 °C).

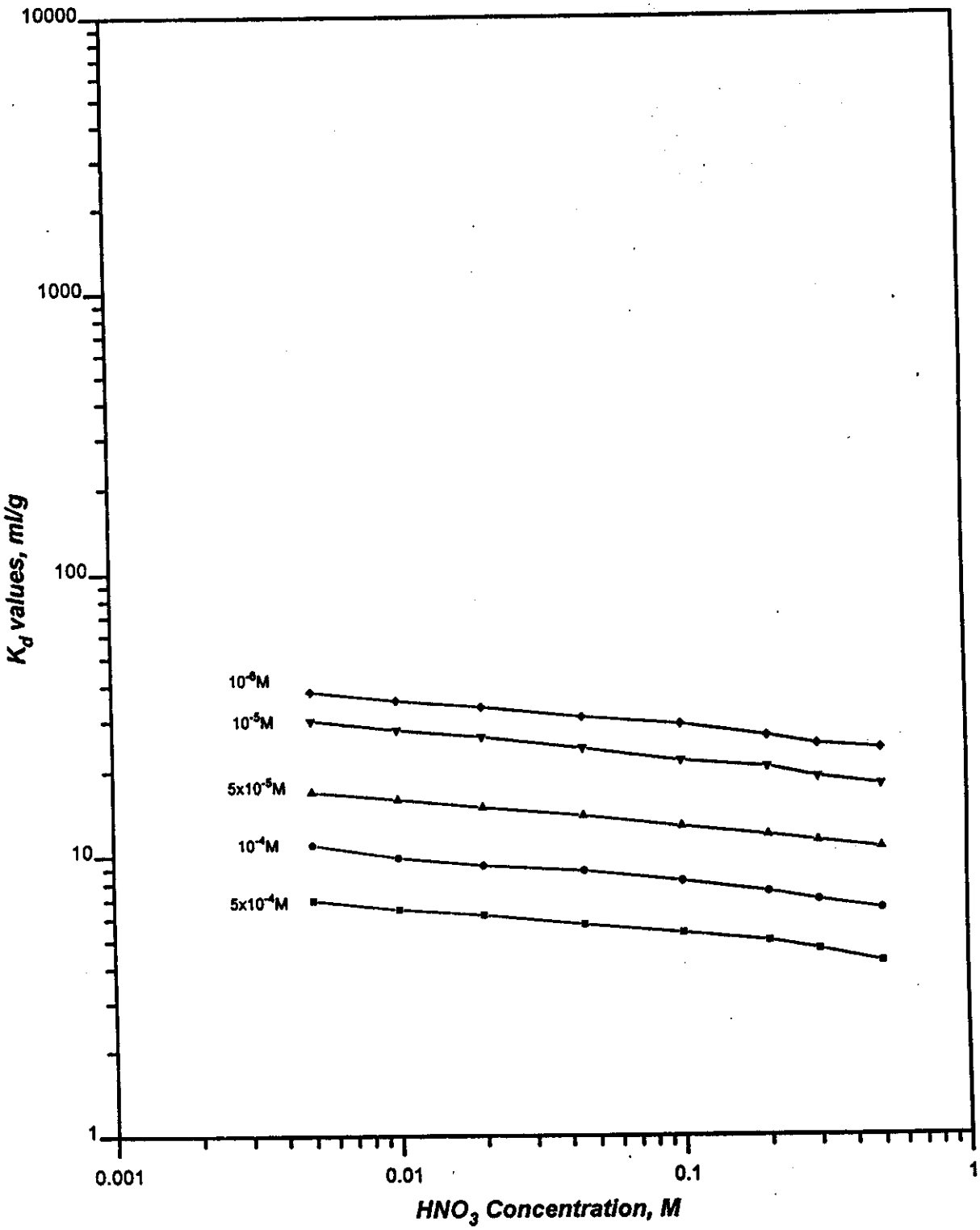

Fig.11. Distribution coefficients(K_d) values of Cu(II) in HCl acid solutions on 12-molybdocerate (IV) at different Cu(II) concentration(25+1 °C).

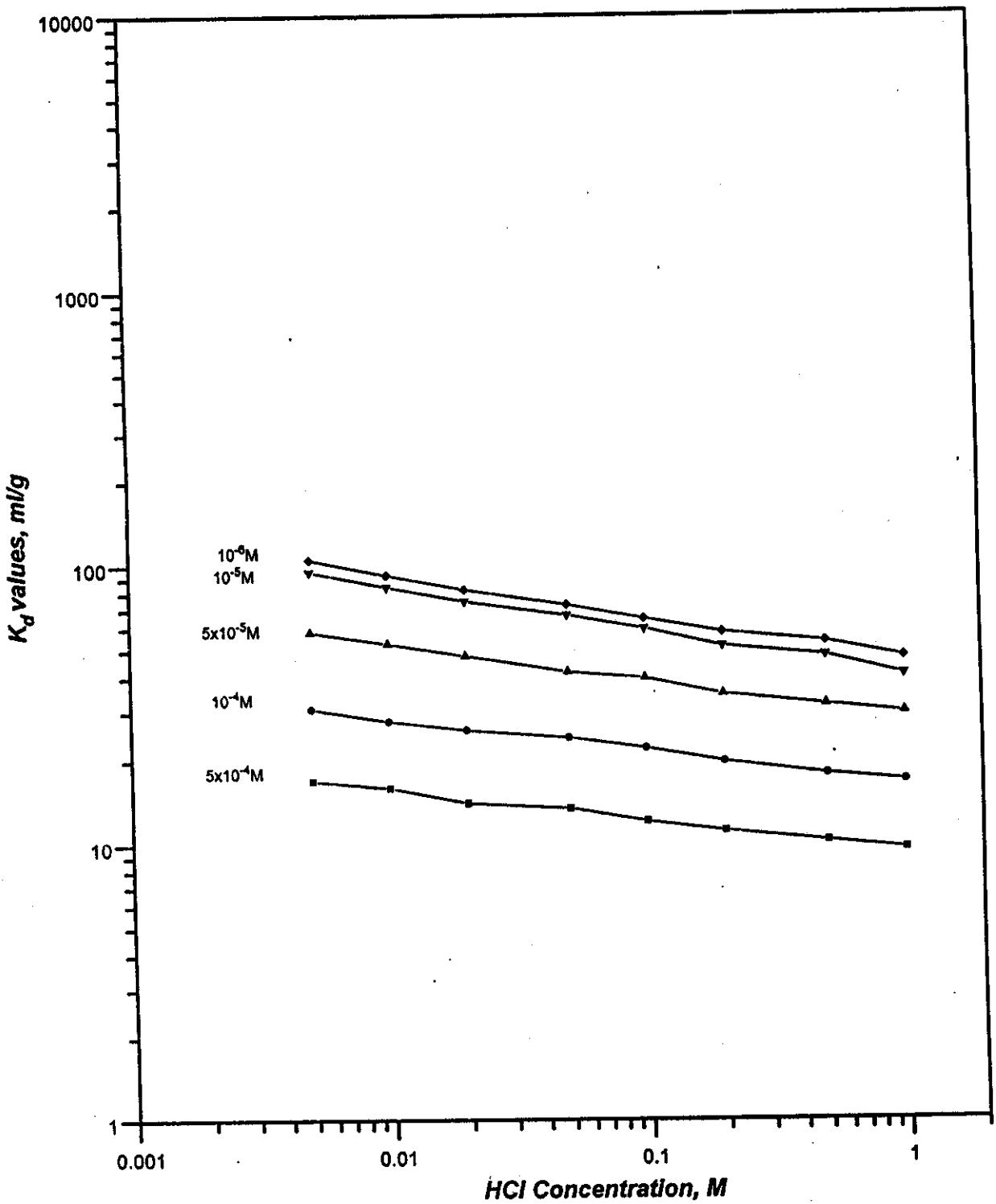

Fig.12. Distribution coefficients (K_d) values of Fe(III) in HNO_3 acid solutions on 12-molybdocerate (IV) at different Fe(III) concentrations(25+1 °C).

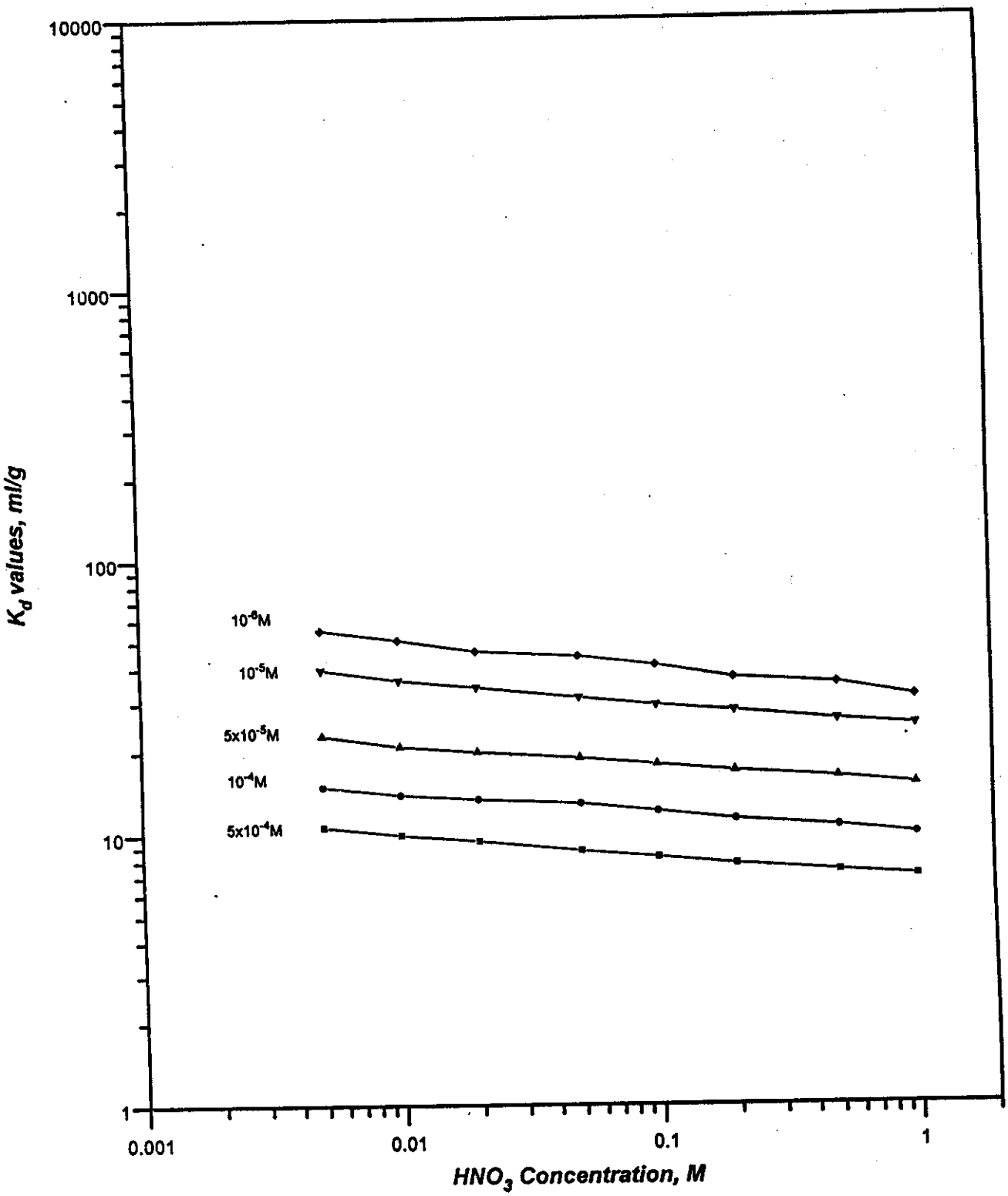

Fig.13. Distribution coefficients(k_d) values of Fe(III) in HCl acid solutions on 12-molybdocerate (IV) at different Fe(III) concentrations(25+1 °C).

50 ml/g and 28 and 40 ml/g at 0.5 M nitric and hydrochloric acid solutions, respectively.

The K_d values in nitric acid are higher than those in hydrochloric acid solutions; under similar experimental conditions. In all cases; the K_d values of both copper and iron are very low compared to the target element and the product radiotracer indicating their tendency to prefer the aqueous phase more than the molybdocerate(IV) matrix. The low K_d values of Cu(II) and Fe(III), even in dilute acid solutions, on 12-molybdocerate(IV), prove that the columns bed will be easily cleaned from its iron(III) and copper(II) contents during any of the following chromatographic column operations; loading or feeding processes, washing and elution steps. The level of both copper (II) and iron (III) radiocontaminants in solutions of the cyclotron irradiated target was always below 5μg/ ml. M.K.Das and N.Ramamoorthy[116] found that iron and copper levels in the etching solution were less than 5μg/ ml. Qaim, Weinrich and ollig[10] also stated that total concentration of the iron and copper in the etching solution were <1μg/ml. Therefore, the contribution of those interfering radiocontiminants to the sorption uptake (i.e uptake capacity of the column matrix); and consequently to the separation process; could be considered negligible.

3.1.1.2 Dynamic Studies

Based on the previously obtained distribution coefficient (K_d) values; the acid concentration of the equilibrating solutions divided into three arbitrary values; high, medium and low acid concentrations; 0.5, 0.05 and 0.005 M HNO_3 and HCl acid. The retention behaviour of 12-molybdocerate (IV) matrix for the respective target and product radiotracer in HNO_3 and HCl acid solutions are investigated using the chromatographic column breakthrough technique. For this purpose,

chromatographic columns (0.6 cm i.d x 3.5 cm) packed each with 1g of 12-molybdocerate(IV) matrix were prepared. Fed solutions of 10^{-5} to $5x10^{-4}$M target radiotracer and 10^{-5} M product radiotracer dissolved in the proper acid solution were continuously passed through individual column beds at a flow rate of 1 ml / min and room temperature (25°C). The column effluents were radiometrically analysed and the counting rates (C_v) of equal volume fractions were compared with standard samples (C_o). Breakthrough curves (C_v/C_o, % vs. effluent volume, ml) for zinc(II) and gallium(III) were withdrawn. Figures 14-16 and 17-19 display the breakthrough behaviour of gallium (III) and zinc(II) radiotracers (10^{-5} M Ga (III) and 10^{-5} to 5 $x10^{-4}$ M Zn (II)) in 0.005, 0.05 and 0.5M HNO_3 and HCl acid solutions, respectively.

3.1.1.2.1 Effect of Concentration of the Radiotracers

Figure 14 shows that at higher concentration of zinc (II) in the feed solution, faster kinetic equilibrium and immediate breakthrough are obtained. Therefore; the positions of 100% zinc(II) and 1% gallium(III) breakthrough can be delayed towards higher effluent volume differences (i.e, higher resolution or separation) at lower concentrations of the target element in the feed solution. Taking into consideration that zinc (II), as the target element, would be present in macro or micro amounts (~$5x10^{-4}$ M Zn(II)) while gallium(III) as the product radiotracer is in trace amounts (<< 10^{-6} M Ga(III)); there will be a target/product wide displacement (i.e, high resolution) between the saturation uptake of 12-molybdocerate(IV) for zinc(II) and 1% breakthrough of the product radiotracer. Hence, small chromatographic columns; packed with small amounts of the molybdate matrix would be sufficient to achieve almost quantitative uptake of the gallium(III) radiotracer product with consequence distinct separation from macro amounts of its zinc(II) target.

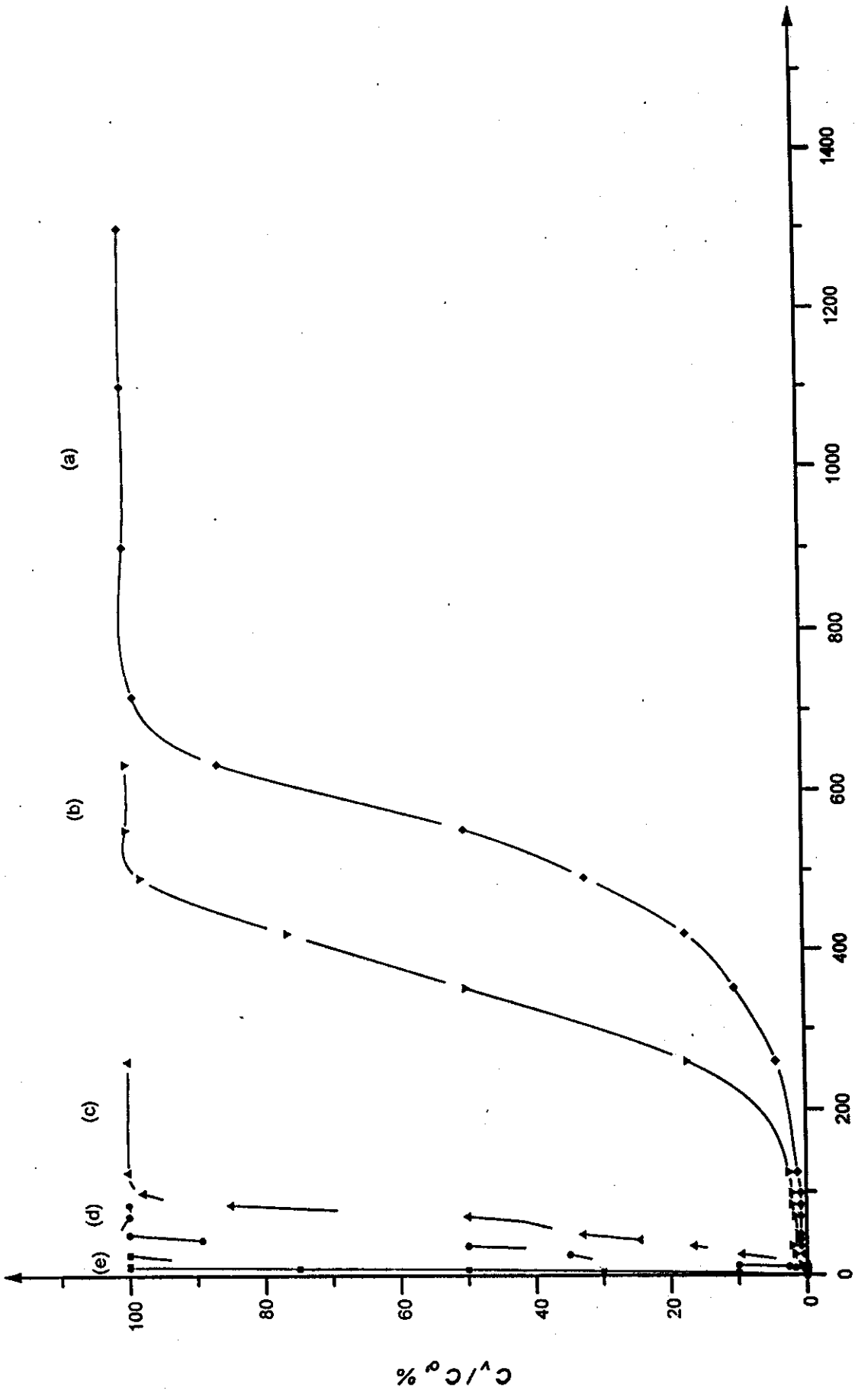

Fig.14. Breakthrough curves of Zn(II) and Ga(III) in 0.005M HNO_3 from 1g 12-molybdocerate(IV) columns (0.6cm i.d x 3.5cm) at a flow rate of 1ml/min at different metal ions concentrations
(a) 10^{-5}M Ga(III) (b)10^{-5}M Zn(II) (c)$5x10^{-5}$M Zn(II) (d)10^{-4}M Zn(II) (e)$5x10^{-4}$M Zn(II)

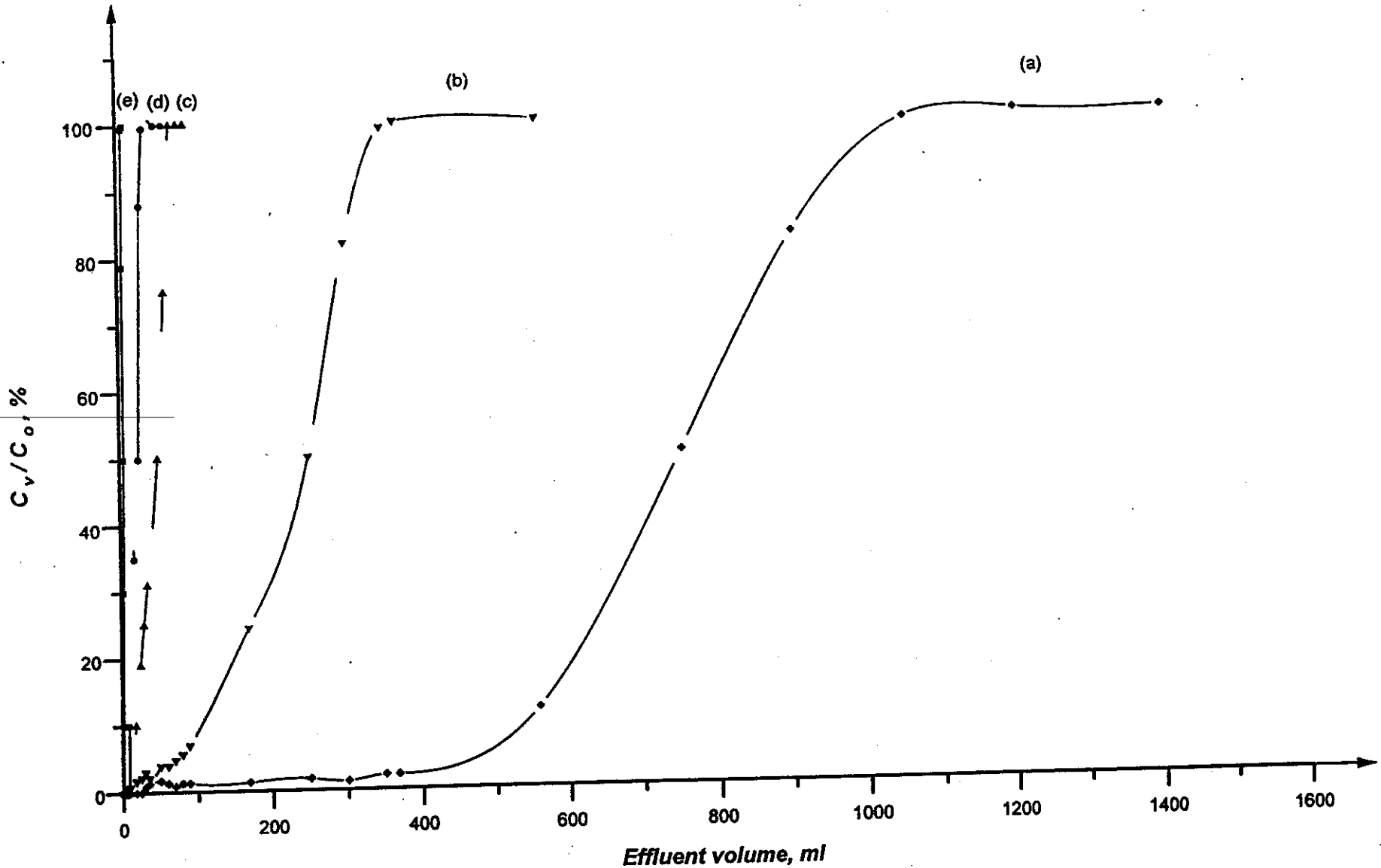

Fig.15. Breakthrough curves of Zn(II) and Ga(III) in 0.05M HNO_3 from 1g 12-molybdocerate(IV) columns (0.6cm i.d x 3.5cm) at a flow rate of 1ml/min as a function of metal ions concentrations. (a) 10^{-5}M Ga(III) (b)10^{-5}M Zn(II) (c)$5x10^{-5}$M Zn(II) (d)10^{-4}M Zn(II) (e)$5x10^{-4}$M Zn(II)

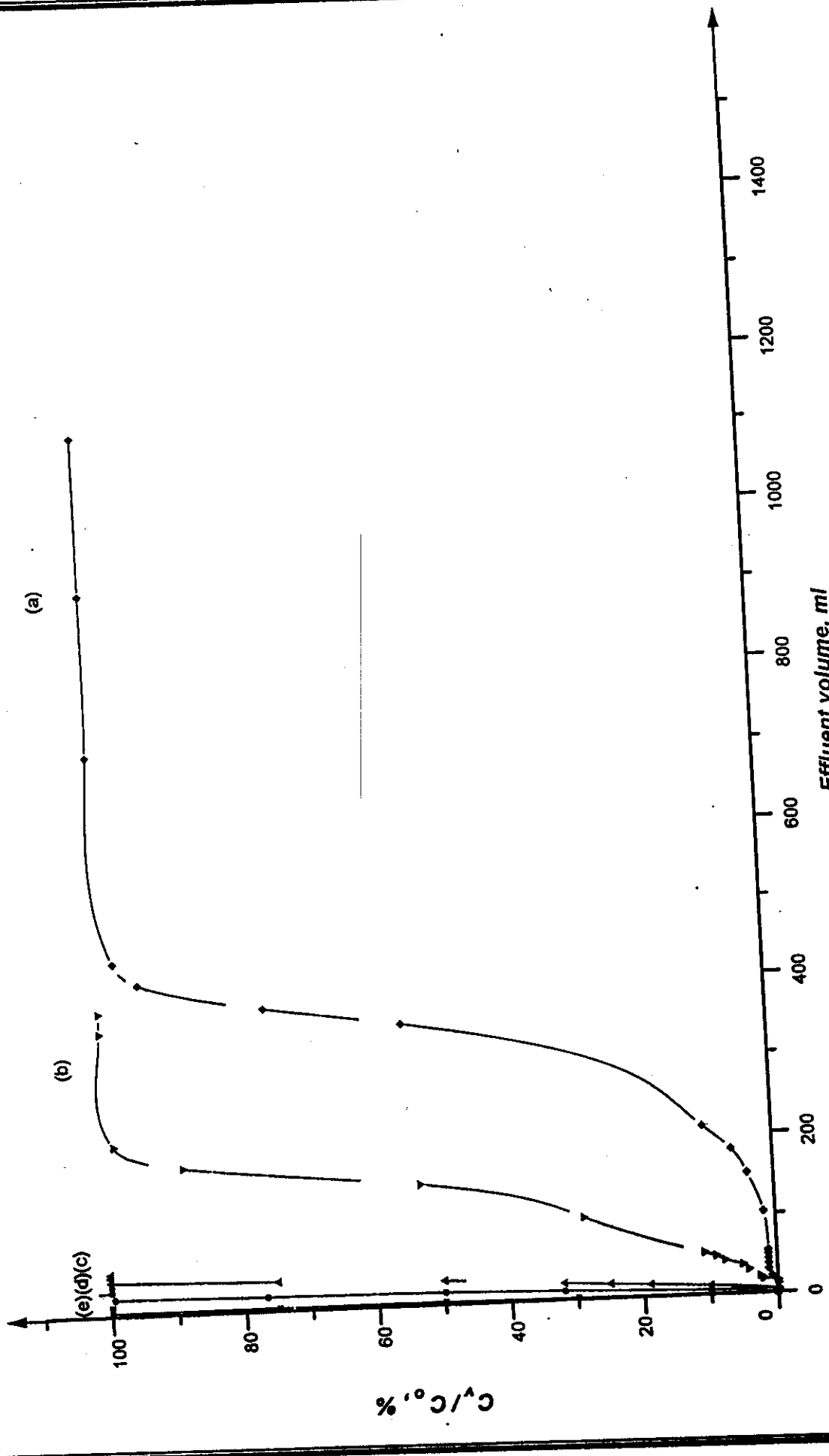

Fig.16. Breakthrough curves of Zn(II) and Ga(III) in 0.5M HNO3 from 1g 12-molybdocerate(IV) columns (0.6cm i.d x 3.5cm) at a flow rate of 1ml/min as a function of metal ions concentrations. (a) 10^{-5}M Ga(III) (b)10^{-5}M Zn(II) (c)$5x10^{-5}$M Zn(II) (d)10^{-4}M Zn(II) (e)$5x10^{-4}$M Zn(II)

Morever, at a constant flow rate, the loading time of the 12-molybdocerate (IV) column bed will decrease with concentration of the target radiotracer in the feed solution.

3.1.1.2.2 Effect of Chemical Composition and Nature of the Feed Solutions

Figures 14 - 16 show the effect of concentration of nitric acid in the feed solutions on the breakthrough behaviour of zinc (II) and gallium (III) from 1g 12-molybdocerate(IV) columns. It is clear that fast breakthrough of zinc(II) attained as the acid concentration was increased from 0.005 to 0.5M HNO_3. Whereas, the breakthrough of Ga(III) is delayed; to higher effluent volumes, as the acid concentration increased from 0.005 to 0.05M HNO_3, i.e; improved resolution. Beyond this value; with acid concentration increasing from 0.05 to 0.5M HNO_3, low Zn(II)-Ga(III) resolution is observed.

Figures 17-19 show that increasing the concentration of hydrochloric acid in the feed solutions have more or less similar breakthrough behaviour trend in accordance with the previously obtained distribution coefficient (K_d) values under comparable conditions. It is distinct from figures 14-19 that the breakthrough of zinc(II) radiotracers is more faster from hydrochloric acid than from nitric acid solutions; at comparable feed conditions. Dilute nitric acid solutions will be more suitable for the column loading and washing processes where higher uptake values and delayed breakthrough of gallium (III) will be favoured in the range of investigation; while concentrated hydrochloric acid is more preferable in the elution process.

3.1.2 Chromatographic Columns Separations

In chromatographic column separations, the constituents of the mixture under consideration are separated from each other, more or less

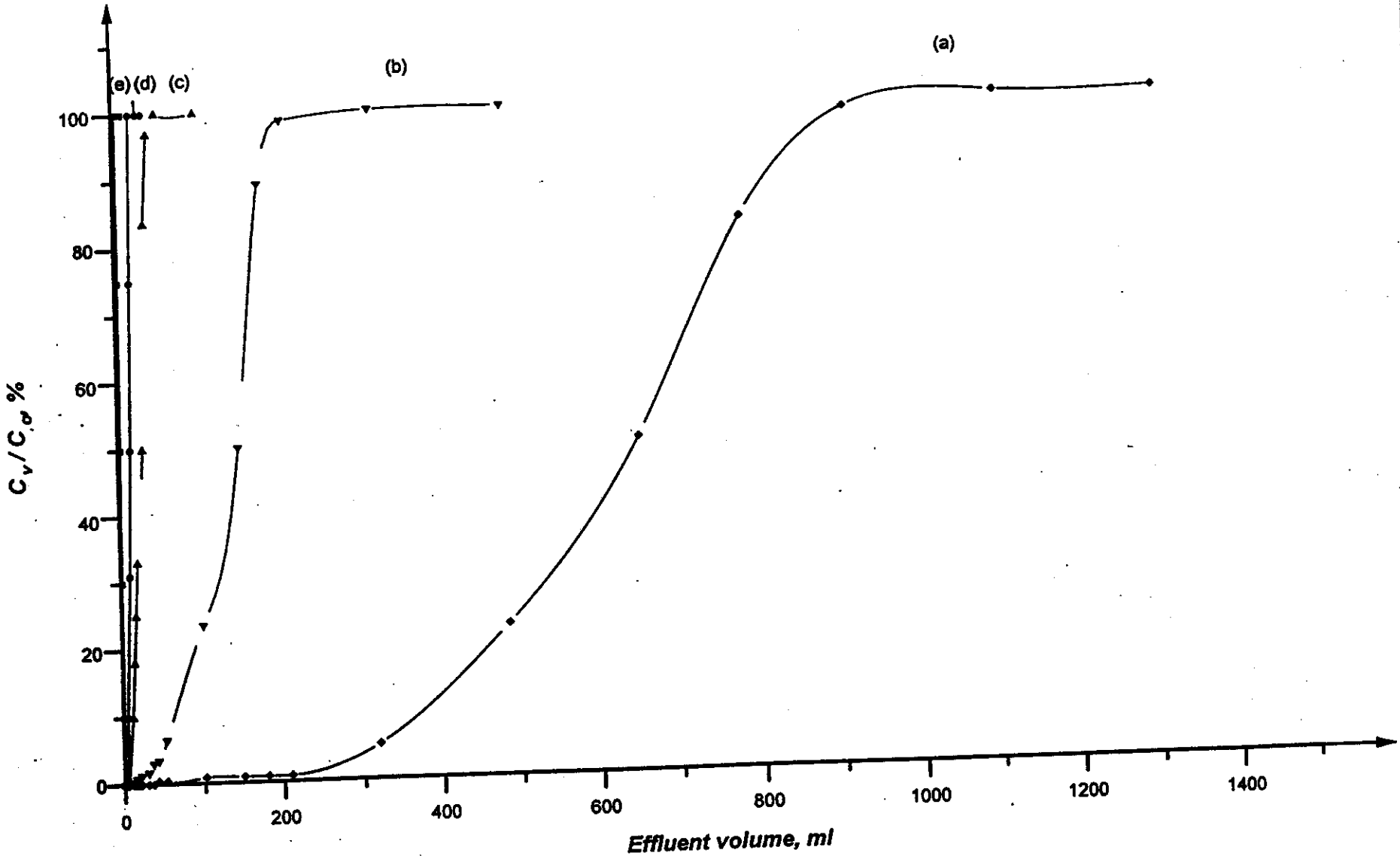

Fig.18. Breakthrough of Zn(II) and Ga(III) in 0.05M HCl from 1g 12-molybdocerate(IV) columns (0.6cm i.d x 3.5cm) at a flow rate of 1ml/min as a function of metal ions concentrations. (a)10^{-5}M Ga(III) (b)10^{-5}M Zn(II) (c)$5x10^{-5}$M Zn(II) (d)10^{-4}M Zn(II) (e)$5x10^{-4}$M Zn(II)

M Zn(II) (d)10^{-4}M Zn(II) (e)$5x10^{-4}$M Zn

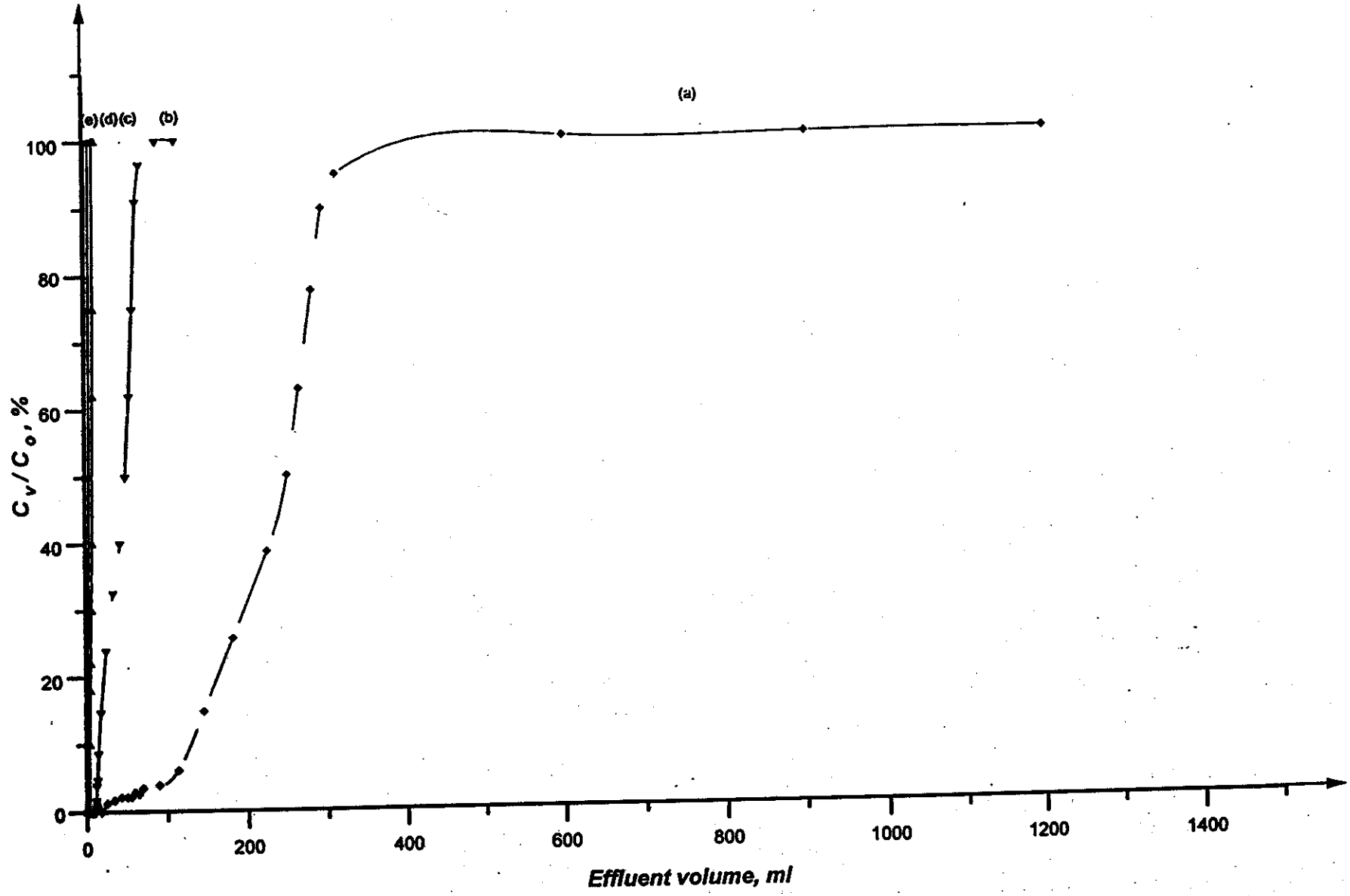

Fig.19. Breakthrough curves of Zn(II) and Ga(III) in 0.5M HCl from 1g 12-molybdocerate(IV) columns (0.6cm i.d x 3.5cm) at a flow rate of 1ml/min as a function of metal ions concentrations. (a)10^{-5}M Zn(II) (e)$5x10^{-4}$M Zn(a)10^{-5}M Ga(III) (b)10^{-5}M Zn(II) (c)$5x10^{-5}$M Zn(II) (d)10^{-4}M Zn(II) (e)$5x10^{-4}$M Zn(II)

completely by virtue of the differences in their distribution ratios between the ion exchanger which form the column stationary phase and the eluent as the mobile phase in intimate contact with each other.

Chromatographic separations can be carried out by elution; frontal and/or displacement techniques. The displacement technique was excluded to avoid the contribution of undesirable chemical contaminates in the separation process; which affect chemical purity of the eluates. Furthermore; displacement development separation may not produce elution bands completely separated from each other i.e bad resolution. Therefore; neither quantitative nor clean separation can be obtained. The optimum conditions for chromatographic separations are those permitting strong retention (or fixation) on the column matrix of one of the radiotracers under consideration; preferably the radiotracer product present in trace amount, and weak retention (i.e easier elution) of the target material present in micro or macro amount together with the other contaminates. These conditions are elucidated from the previously obtained distribution coefficient (K_d) values; the separation factor values of the Zn(II)-Ga(III) couple, as well as from their breakthrough behaviour characteristics.

In elution technique a small amount of the irradiated target solute in dilute acid solution is loaded onto 12-molybdocerate (IV) column matrix. The target and product radiotracers were selectively eluted from the column with passing 0.005 – 0.5 M HNO_3 and HCl acid solutions, as eluents, which have a lower affinity for the sorbent material than the mixture constituents. The mixture components; therefore, move along the column at a slower rate than the eluent in inverse order of their affinities. In frontal separation technique big amounts of the irradiated target material and large volumes of solute in HNO_3 and/or HCl acid are continuously added to the column of 12-molybdocerate (IV) bed. The

target radiotracer, usually having the lower affinity for the sorbent matrix, will pass faster along the column bed while; the strongly sorbed product radiotracer builds up on the column bed.

It is clear from the aforementioned distribution coefficient (K_d) values that gallium (III) ions in dilute and concentrated nitric and hydrochloric acid solutions have marked sorption affinity towards the 12-molybdocerate (IV) matrix; compared to zinc (II) ions which show decreasing sorption affinity with stepwise increasing acid concentration. Table 8 illustrates the gallium (III) / zinc(II) separation factor [α] at different concentrations of hydrochloric and nitric acid solutions. The separation factor [α] values for gallium (III) / zinc (II) in different acid solutions reflect the versatility to achieve their separation from each other onto 12-molybdocerate(IV) chromatographic column by the elution method. It is observed that Ga(III) can be preferably separated from 5 x 10^{-4} M Zn(II) in 0.05M nitric and hydrochloric acid solutions (concentrations at which the Ga(III)/Zn(II) couple has high separation factor [α] values). On the other hand; it is observed that the gallium (III)-zinc (II) separation factors [α]in nitric acid solutions are much greater than in hydrochloric acid solutions under similar conditions. At the other extreme, Table 9 compiles the breakthrough characteristics of Zn(II) and Ga(III) in HCl and HNO_3 acid solutions at different concentrations of acid and metal ions in the feed solution. Therefore; separation of the product gallium (III) from its zinc (II) target is investigated using small chromatographic columns of 12- molybdoceratre (IV) by both elution and frontal separation method.

3.1.2.1 Elution Chromatography

The separation of zinc (II) – gallium (III) couple was conducted using

Table 8. Individual distribution coefficients (K_d) values and separation factors (α) of Zn(II) / Ga(III) couple in HNO_3 and HCl acid solutions on 12-molybdocerate(IV)

Metal ion Concentration: M		Concentration of the equilibrating solutions											
		0.005M HNO_3			0.05M HNO_3			0.5M HNO_3			0.005M HCl			0.05M HCl			0.5M HCl		
		Distribution coefficient (K_d) values, ml/g																	
		Ga^{3+}	Zn^{2+}		Ga^{3+}	Zn^{2+}		Ga^{3+}	Zn^{2+}		Ga^{3+}	Zn^{2+}		Ga^{3+}	Zn^{2+}		Ga^{3+}	Zn^{2+}	
		Separation factor $\alpha = K_d (Ga) / K_d (Zn)$																	
Product Ga^{3+}	Target Zn^{2+}	K_d	K_d	α	K_d	K_d	α	K_d	K_d	α	K_d	K_d	α	K_d	K_d	α	K_d	K_d	α
$5x10^{-4}$	$5x10^{-4}$	50	110	0.45	89	73	1.22	23	50	0.46	18	150	0.12	32	63	0.51	13	50	0.26
10^{-4}		190	110	1.73	290	73	3.97	70	50	1.4	50	150	0.33	105	63	1.67	30	50	0.6
$5x10^{-5}$		290	110	2.64	400	73	5.48	120	50	2.4	95	150	0.63	200	63	3.17	65	50	1.3
10^{-5}		380	110	3.45	550	73	7.53	175	50	3.5	190	150	1.27	300	63	4.76	160	50	3.2
$5x10^{-4}$	10^{-4}	50	175	0.29	89	85	1.05	23	70	0.33	18	175	0.103	32	84	0.38	13	65	0.2
10^{-4}		190	175	1.09	290	85	3.41	70	70	1	50	175	0.29.	105	84	1.25	30	65	0.46
$5x10^{-5}$		290	175	1.66	400	85	4.71	120	70	1.71	95	175	0.54	200	84	2.38	65	65	1
10^{-5}		380	175	2.17	550	85	6.47	175	70	2.5	190	175	1.09	300	84	3.57	160	65	2.46
$5x10^{-4}$	$5x10^{-5}$	50	230	0.22	89	122	0.73	23	90	0.26	18	225	0.08	32	120	0.27	13	90	0.14
10^{-4}		190	230	0.83	290	122	2.38	70	90	0.78	50	225	0.22	105	120	0.88	30	90	0.33
$5x10^{-5}$		290	230	1.26	400	122	3.28	120	90	1.33	95	225	0.42	200	120	1.67	65	90	0.72
10^{-5}		380	230	1.65	500	122	4.09	175	90	1.94	190	225	0.84	300	120	2.5	160	90	1.78
$5x10^{-4}$	10^{-5}	50	280	0.18	89	160	0.56	23	130	0.18	18	260	0.07	32	145	0.22	13	120	0.11
10^{-4}		190	280	0.68	290	160	1.81	70	130	0.54	50	260	0.19	105	145	0.72	30	120	0.25
$5x10^{-5}$		290	280	0.92	400	160	2.5	120	130	0.92	95	260	0.37	200	145	1.38	65	120	0.54
10^{-5}		380	280	1.36	500	160	3.13	175	130	1.35	190	260	0.73	300	145	2.07	160	120	1.33

Table 9. Breakthrough characteristics of Zn(II) and Ga(III) in HCl and HNO_3 acid solutions from 1g 12-molybdocerate(IV) column at a flow rate of 1ml/min

Metal ion conc., M	Character	Concentration of HCl, M						Concentration of HNO_3, M					
		0.005		0.05		0.5		0.005		0.05		0.5	
		Zn	Ga	Zn	Ga	Zn	Ga	Zn	Ga	Zn	Ga	Zn	Ga
10^{-5}	V(1%)	9	21	5	32	2	11	12	26	9	37	5	16
	V(50%)	250	450	150	650	50	250	350	550	250	750	150	350
	V(100%)	350	585	210	910	70	313	490	715	350	1050	210	438
	C, meq/g	$15x10^{-3}$	$1.35x10^{-2}$	$3x10^{-3}$	$1.95x10^{-2}$	$1x10^{-3}$	$7.5x10^{-3}$	$7x10^{-3}$	$1.65x10^{-2}$	$5x10^{-3}$	$2.25x10^{-2}$	$3x10^{-3}$	$1.05x10^{-2}$
$5x10^{-5}$	V(1%)	2	4	1	6	1	3	3	5	2	7	2	3
	V(50%)	50	90	30	130	10	50	70	110	50	150	30	70
	V(100%)	70	117	42	182	14	63	98	143	70	210	42	88
	C, meq/g	$5x10^{-3}$	$1.35x10^{-2}$	$3x10^{-3}$	$195x10^{-2}$	$1x10^{-3}$	$7.5x10^{-3}$	$7x10^{-3}$	$1.65x10^{-2}$	$5x10^{-3}$	$2.25x10^{-2}$	$3x10^{-3}$	$1.05x10^{-2}$
10^{-4}	V(1%)	1	2	1	3	1	2	2	3	1	4	1	2
	V(50%)	25	45	15	65	5	25	35	55	25	75	15	35
	V(100%)	35	59	21	91	7	31	49	72	35	105	21	44
	C, meq/g	$5x10^{-3}$	$1.35x10^{-2}$	$3x10^{-3}$	$1.95x10^{-2}$	$1x10^{-3}$	$7.5x10^{-3}$	$7x10^{-3}$	$1.65x10^{-2}$	$5x10^{-3}$	$2.25x10^{-2}$	$3x10^{-3}$	$1.05x10^{-2}$
$5x10^{-4}$	V(1%)	1	1	1	1	1	1	1	1	1	1	1	1
	V(50%)	5	9	3	13	1	5	7	11	5	15	3	7
	V(100%)	7	12	4	18	2	6	10	15	7	21	4	9
	C, meq/g	$5x10^{-3}$	$1.35x10^{-2}$	$3x10^{-3}$	$1.95x10^{-2}$	$1x10^{-3}$	$7.5x10^{-3}$	$7x10^{-3}$	$1.65x10^{-2}$	$5x10^{-3}$	$2.25x10^{-2}$	$3x10^{-3}$	$1.05x10^{-2}$

chromatographic columns of (0.6 cm i.d x 3.5 cm) packed each with 1g of the 12-molybdocerate (IV) matrix loaded with 5 ml mixture solution which consists of 2.5 ml $5x\ 10^{-4}$ M zinc (II) and 2.5 ml 10^{-5} M gallium (III) at flow rate of 0.5, 1 and/or 2 ml/min.

3.1.2.1.1 Effect of Nature and Concentration of the Eluent

Figure 20 displays the effect of concentration of hydrochloric acid solutions (0.5; 0.05 and 0.005 M); as eluents, on the elution profiles and yield of the Zn(II) – Ga(III) couple from 1g 12-molybdocerate (IV) columns at a flow rate of 0.5 ml/min. It is clear from Figure 20(curve a) that Zn(II) and Ga(III) are eluted in sharp elution peaks with 2ml and 8ml 0.5M HCl acid solution, respectively. Zinc(II) is readly eluted and concentrated in smaller eluate volumes as the acid concentration increased from 0.005M to 0.5M HCl as shown in Figure 20(curves c, b and a). On the other hand, Figure 20(curves b and c) show diffuse-tailed and broad-tailed elution profile for Ga(III) with 0.05 and 0.005M HCl acid solution, as eluents, respectively. It found that about 92% of the loaded zinc (II) radioactivity was eluted in the first 2 ml 0.5M hydrochloric acid eluate whereas; 89% and 85% of the loaded zinc (II) were eluted with 0.05 and 0.005 M HCl acid eluate; respectively. On the other hand; about 95%; 8.5% and 53% of the eluted gallium(III) radioactivity are concentrated in the eluate volume fraction of 6-11ml 0.5; 0.05 and 0.005 M HCl acid; respectively. The elution profiles of the respective radiotracers with 0.5; 0.05 and 0.005 M nitric acid, Figure 21, have more or less similar behaviour as in Figure 20. However; the positions of the maximum elution peaks are displaced to higher eluate volumes with nitric acid solutions than with hydrochloric acid solutions under comparable conditions in agreement with the previously obtained batch distribution and dynamic behaviour studies.

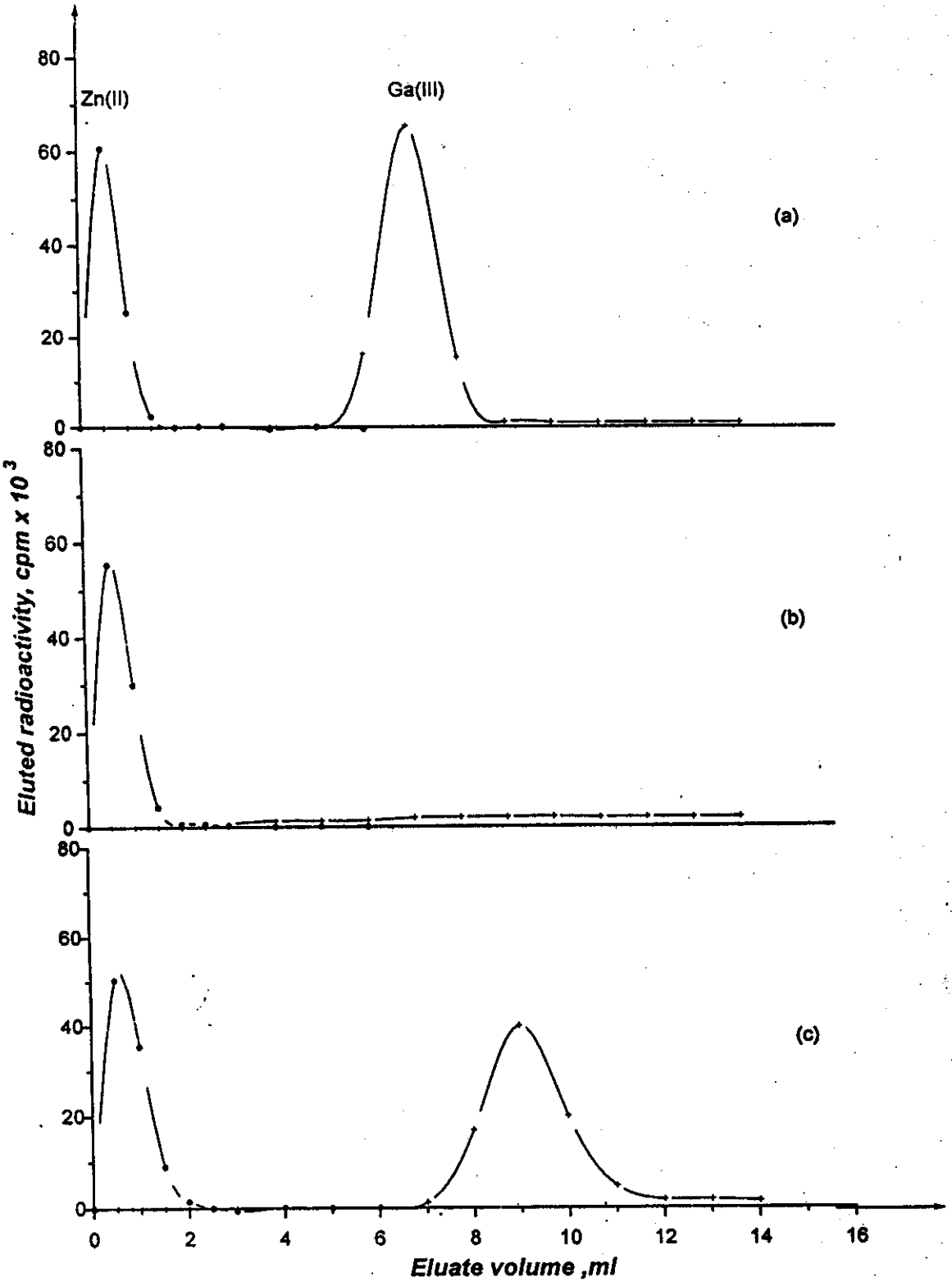

Fig.20. Elution curves of Zn(II) from Ga(III) onto 1g 12-molybdocerate(IV) columns (0.6cm i.d x 3.5cm) with (a)0.5 (b)0.05 (c)0.005M HCl acid solutions at a flow rate of 0.5ml/min.

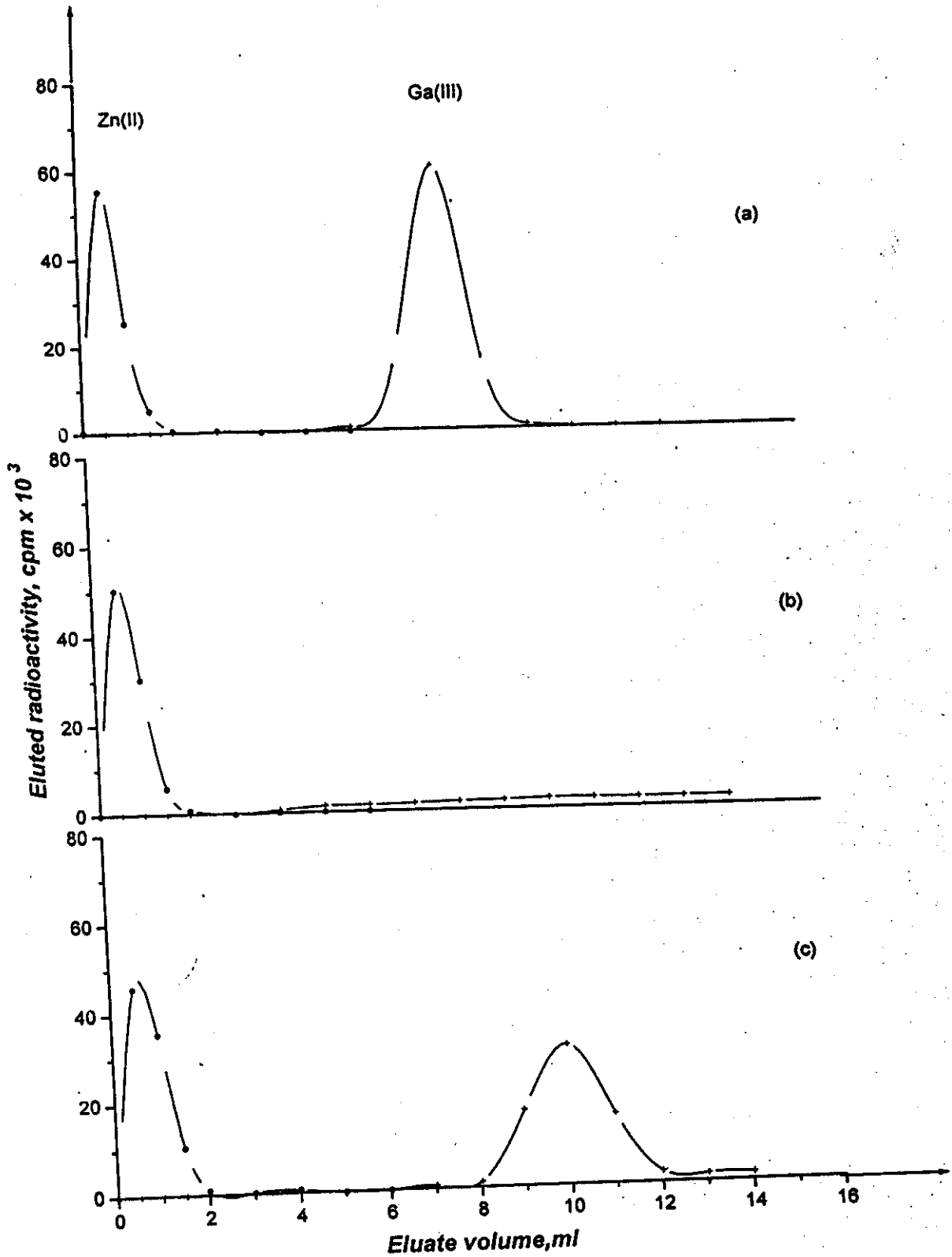

Fig.21. Elution curves of Zn(II) from Ga(III) onto 1g 12-molybdocerate(IV) columns (0.6cm i.d x3.5cm) with (a)0.5 (b)0.05 (c)0.005M HNO_3 acid solutions at flow rate of 0.5 ml/min.

3.1.2.1.2 Effect of Flow Rate of the Eluent

Figures 22, 23 and 24 display the elution profiles of gallium (III) and zinc(II) radiotracers from 1g 12-molybdocerate (IV) columns with hydrochloric acid solutions (0.5; 0.05 and 0.005 M acid) at flow rates of 0.5, 1.0 and 2.0 ml / min; respectively. It is distinct that the positions of the maximum elution peaks are displaced to higher eluate volumes with increasing the flow rate of the eluent. The obtained broad and tailed elution profiles with increasing the flow rate may be due to slow sorption / desorption kinetics of the gallium (III) and zinc (II) radiotracers retained on the surface of the molybdocerate (IV) matrix to the eluent [slow diffusion mechanisms]. Figures 25-27 show that the elution profiles of the respective radiotracers with nitric acid solutions at comparable flow rates have more or less similar elution behaviour trend. It is found that about 88%, 76% and 55% of the zinc (II) radioactivity was eluted in the first 2ml 0.005 M hydrochloric acid at flow rates of 0.5, 1 and 2 ml/min.; respectively. On the other hand; about 83%; 78% and 72% of the eluted gallium (III) radioactivity were obtained in the eluate volume fraction of 9-12ml at flow rates of 0.5, 1 and 2 ml/min; respectively.

In all cases; 4 and 14 ml of hydrochloric and nitric acid solutions are sufficient for complete elution of zinc(II) and gallium (III) radiotracers from 1g 12-molybdocerate column under the investigated conditions.

3.1.2.1.3 Recommended Procedure for Elution Separation of the Zinc (II) - Gallium (III) Couple

In the case of small amounts of the target material (i.e, ≤15% of the total sorption capacity of the 12-molybdocerate (IV) bed matrix) and small volume of solute, the chromatographic column elution mode is recommended for radiochemical separation of the zinc (II) – gallium (III)

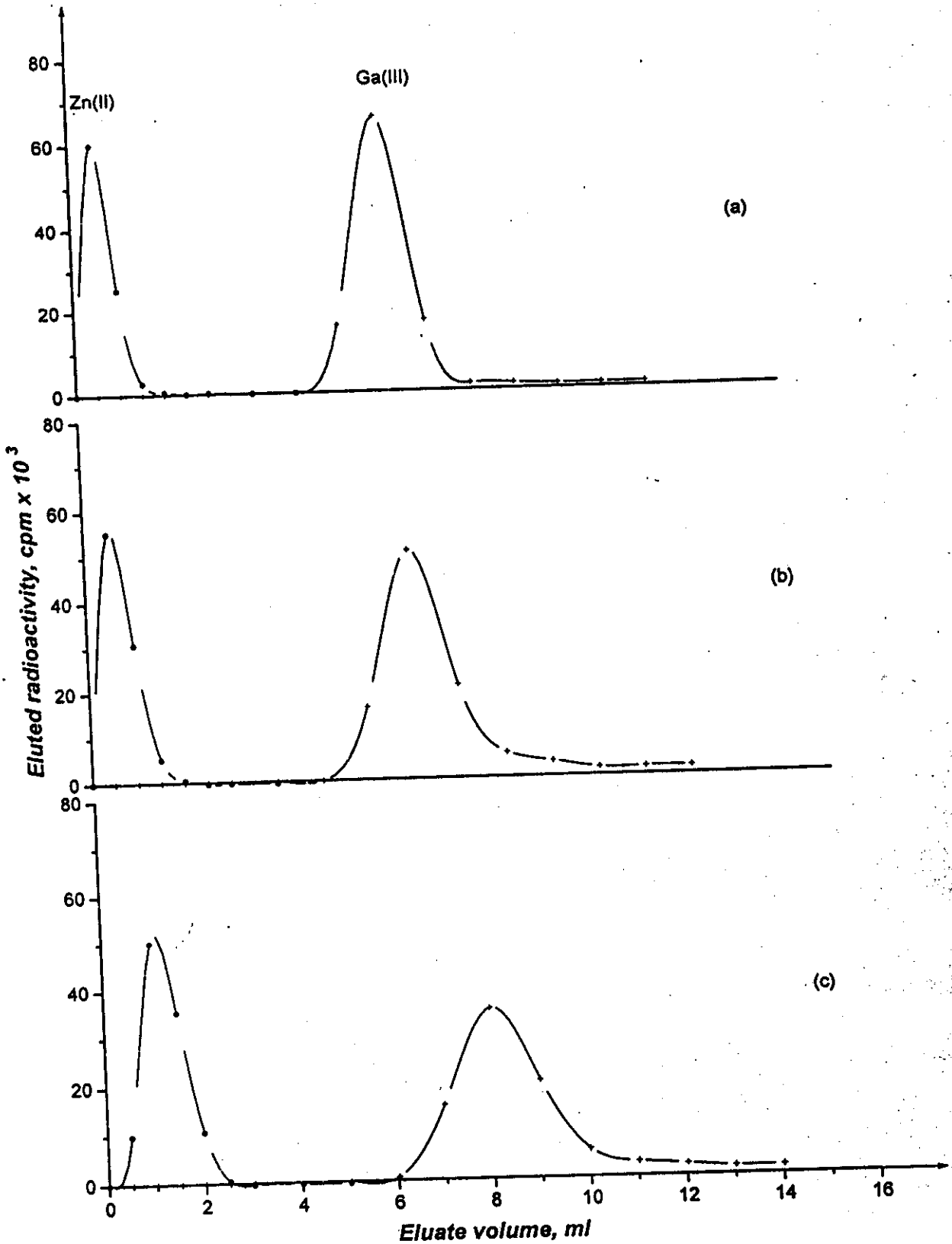

Fig.22. Elution curves of Zn(II) from Ga(III) onto 1g12-molybdocerate(IV) columns (0.6cm i.d x3.5cm) with 0.5M HCl acid solution at a flow rate of (a)0.5ml/min (b)1.0ml/min (c)2.0ml/min.

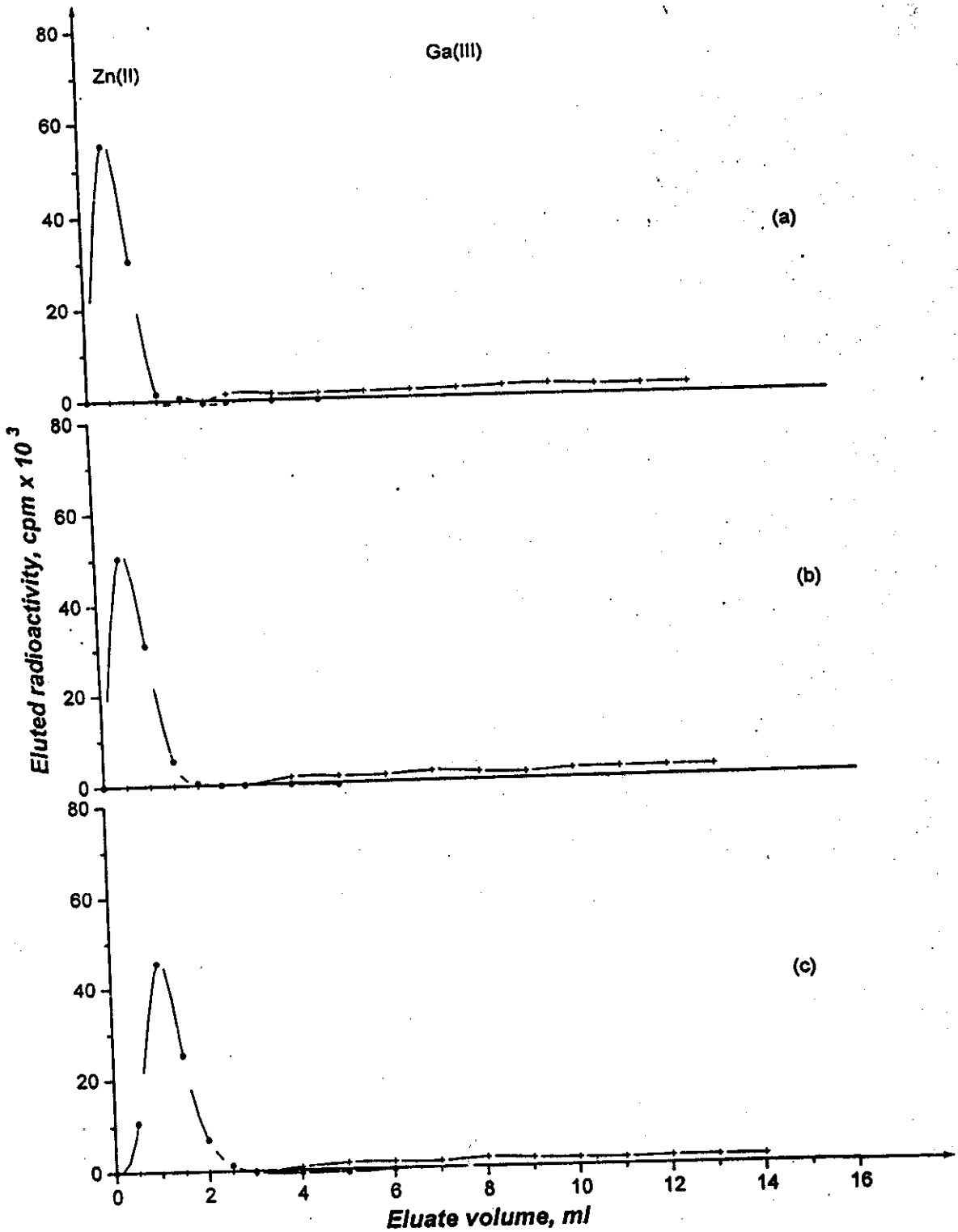

Fig.23. Elution curves of Zn(II) from Ga(III) onto 1g 12-molybdocerate(IV) columns (0.6cm i.d x3.5cm) with 0.05M HCl at a flow rate of (a)0.5ml/min (b)1.0ml/min (c)2.0ml/min.

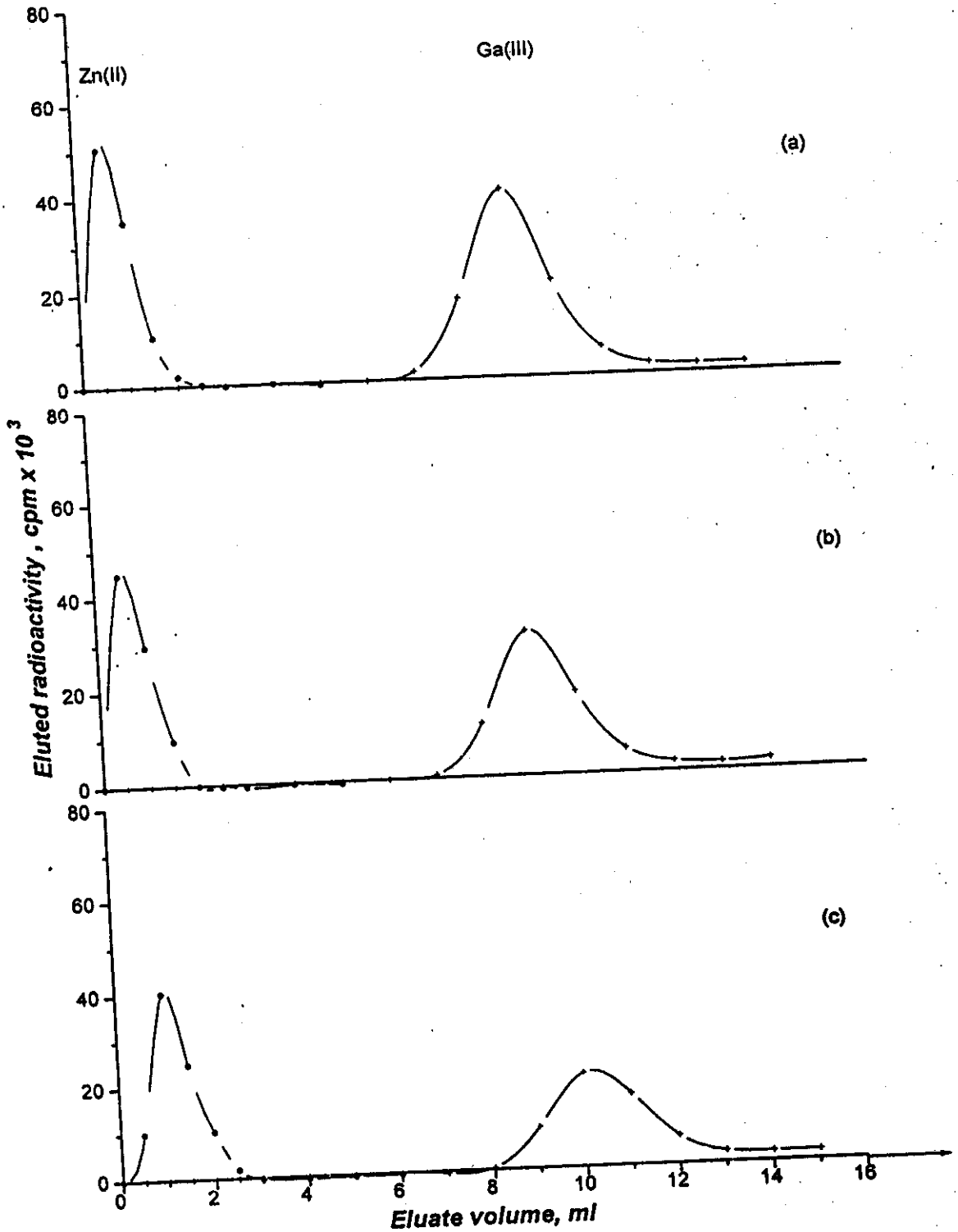

Fig.24. Elution curves of Zn(II) from Ga(III) onto 1g 12-molybdocerate(IV) columns (0.6cm.i.d x3.5Cm) with0.005M HCl at a flow rate of (a)0.5ml/min (b)1.0ml/min (c)2.0ml/min.

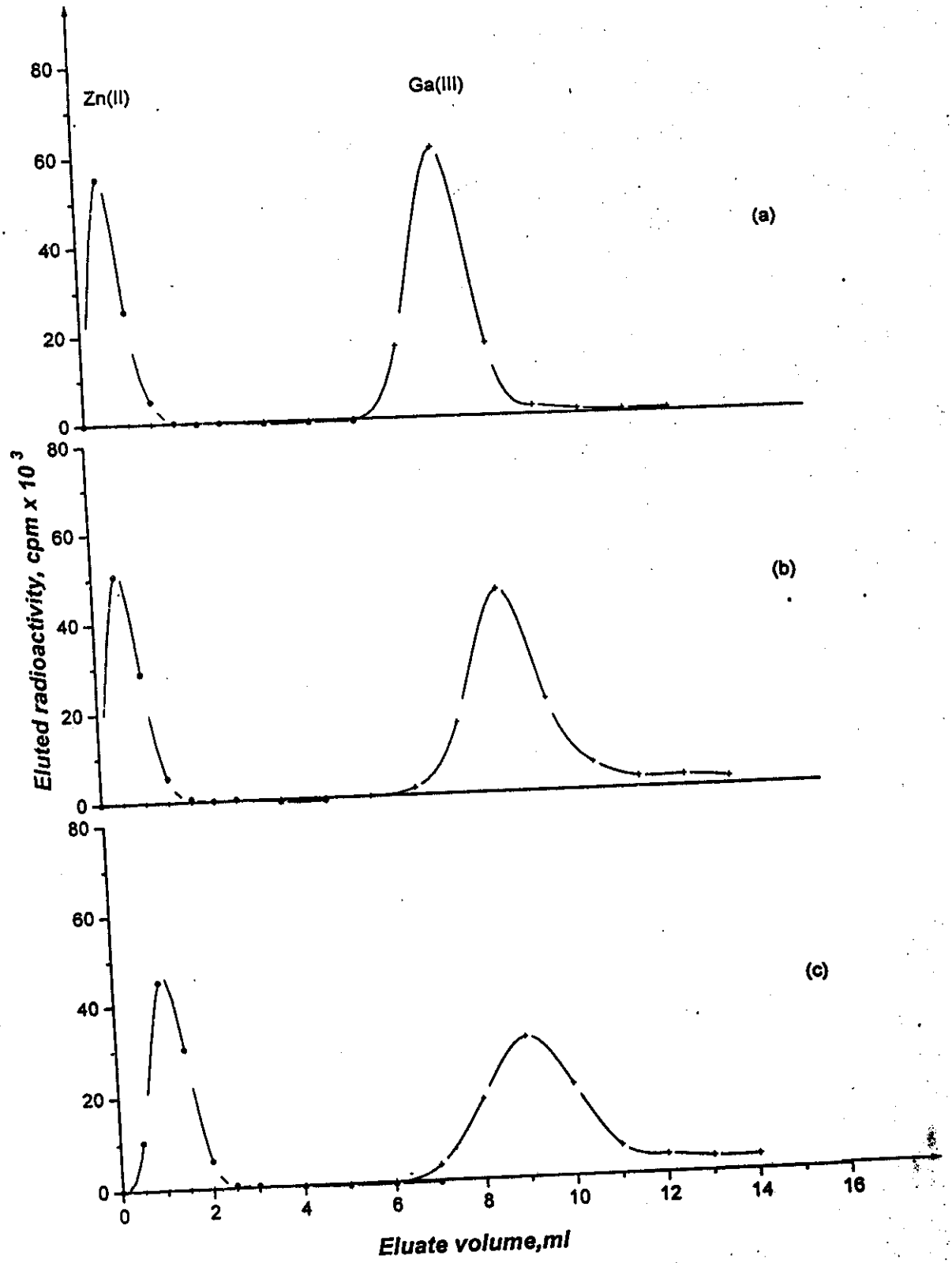

Fig.25. Elution curves of Zn(II) from Ga(III) onto1g 12-molybdocerate(IV) columns (0.6cmx3.5cm) with 0.5M HNO_3 at a flow rate of (a)0.5ml/min (b)1.0ml/min (c)2.0ml/min.

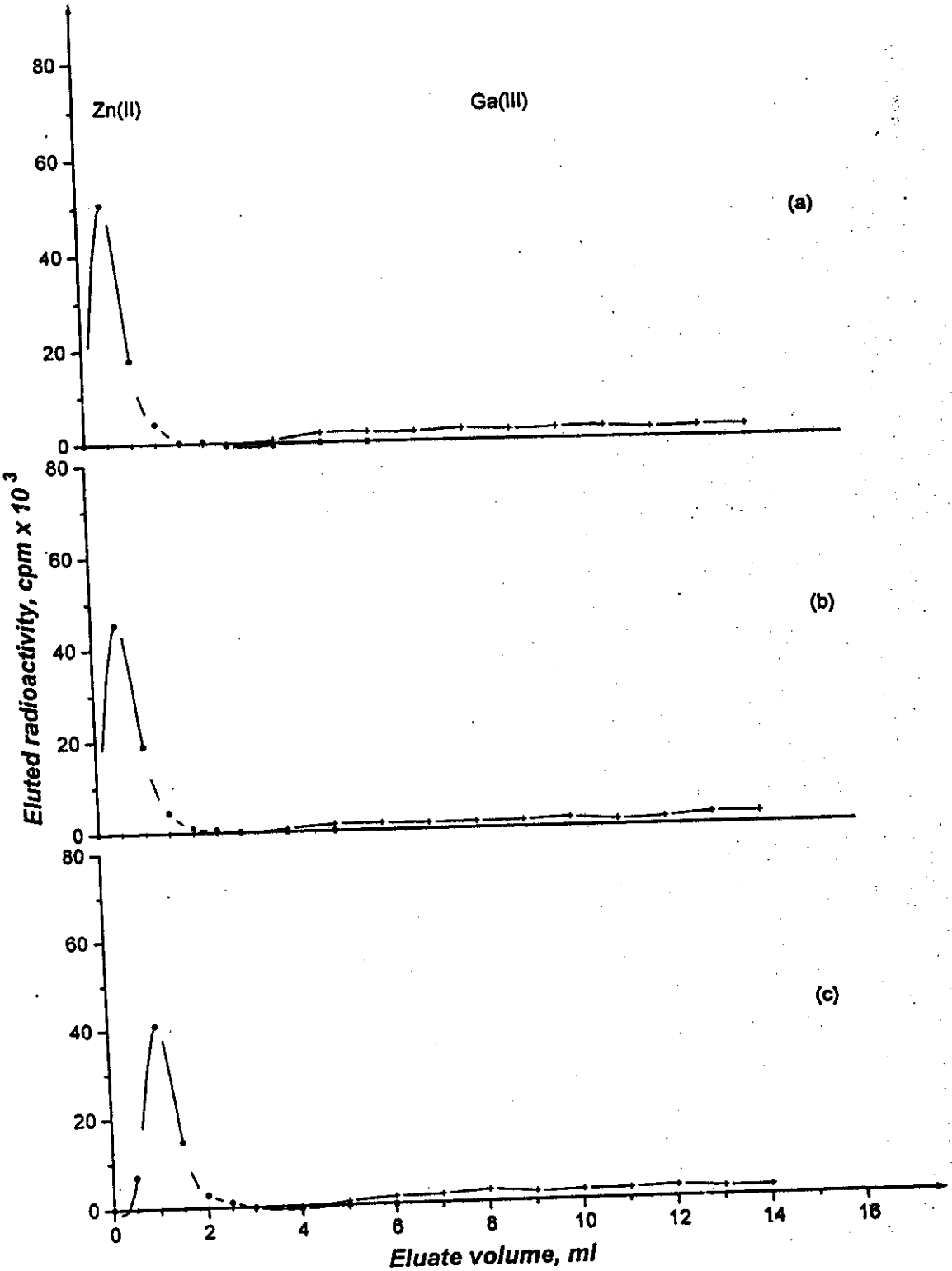

Fig.26. Elition curves of Zn(II) from Ga(III) onto 1g 12-molybdocerate(IV) columns(0.6cm i.d x3.5cm) with 0.05M HNO_3 at a flow rate of (a)0.5ml/min (b)1.0ml/min (c)2.0ml/min.

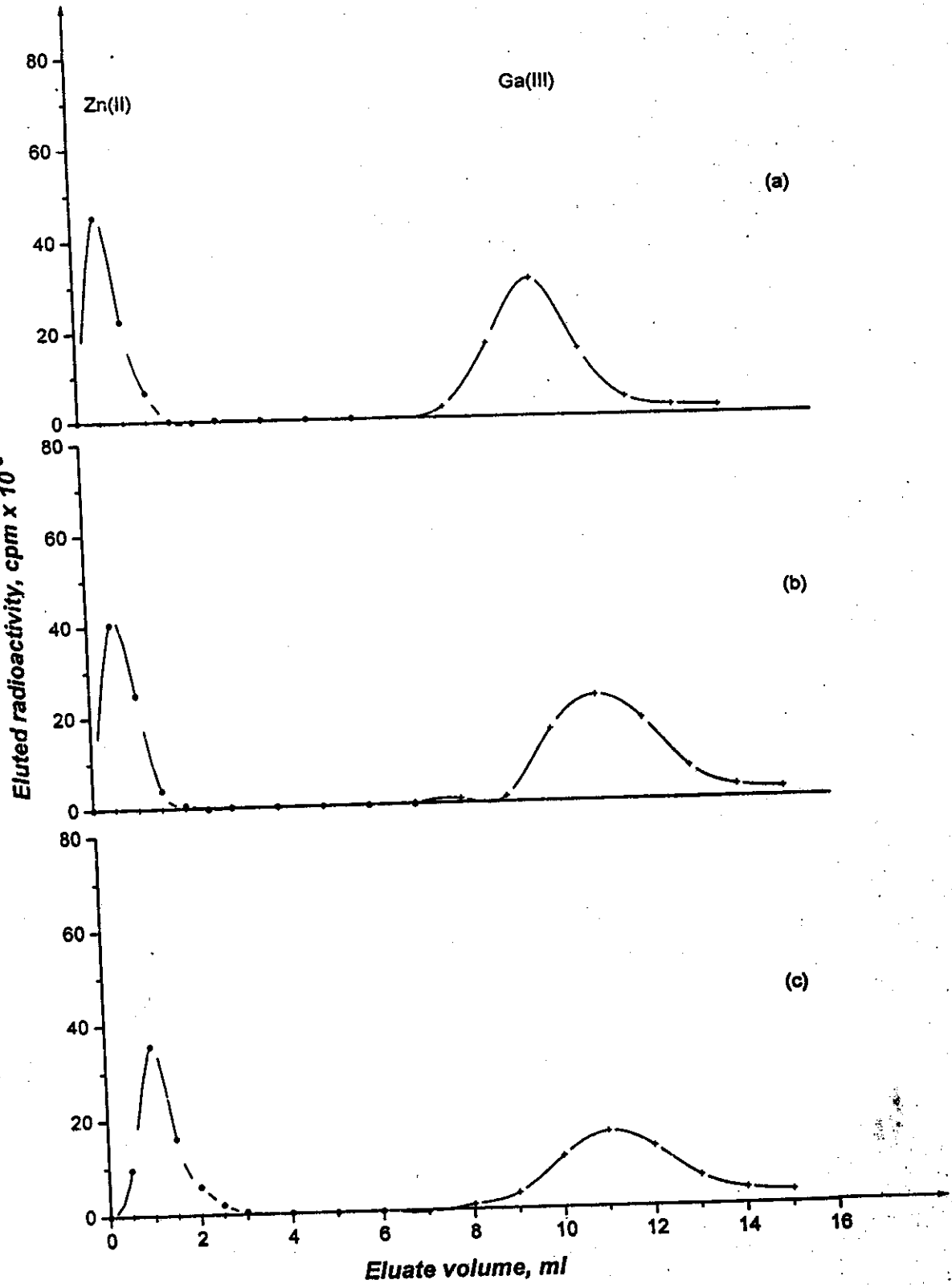

Fig.27. Elution curves of Zn(II) from Ga(III) onto 1g 12-molybdocerate(IV) columns(0.6cm i.d x3.5cm) with 0.005M HNO_3 at a flow rate of (a)0.5ml/min (b)1.0ml/min (c)2.0ml/min.

couple. In this process mixture solution consists of 2.5ml of $5x10^{-4}$M zinc (II) and 2.5ml of 10^{-5}M gallium (III) radiotracer in 0.05M HNO_3 acid solution was loaded onto 1g 12-molybdocerate (IV) column. Zn(II) and Ga(III) were sorbed quantitatively onto the column matrix as verified by radiometric measurements of the column effluents. Elution and purification of the bed matrix from retained Zn(II) is carried out with 3ml 0.05M HNO_3 acid solution at a flow rate of 0.5ml/min. Further purification and conditioning of the column matrix from any residual Zn(II) retained onto the MoCe(IV) is carried out with passing 1ml 0.05M HCl at same flow rate. Thereafter, the strongly retained Ga(III) is eluted with 6ml 0.5M HCl acid solution at flow rate of 1ml/min. It is observed from Figure 28 and radiometric analysis measurements indicate that about 92 % of the loaded zinc (II) radioactivity were eluted and concentrated in the first 3 ml of the eluate; whereas about 98 % of the eluted gallium (III) radioactivity were concentrated in the 5-10 ml fraction of the eluate. The elution yield of gallium (III) was found to be about 94.7% of the total radioactivity present on the column. The obtained elution yield is comparable with those obtained from other cation exchange columns; Dowex 50 x 8; 100-200 mesh and Dowex 50 W x 2; 100-200 mesh (i.e., 85and 81%), respectively[69,70,116]. Figure 29 demonstrates a schematic diagram for proposed separation of carrier-free Ga(III) from its Zn(II) target by chromatographic column elution method.

3.1.2.2 Frontal Chromatography

In cyclotron-produced radioisotopes; the target material and the product radiotracers are usually present in high solution volumes of about 70ml of the etching solution. Therefore; the continuous separation technique is of great importance in practice compared to the elution

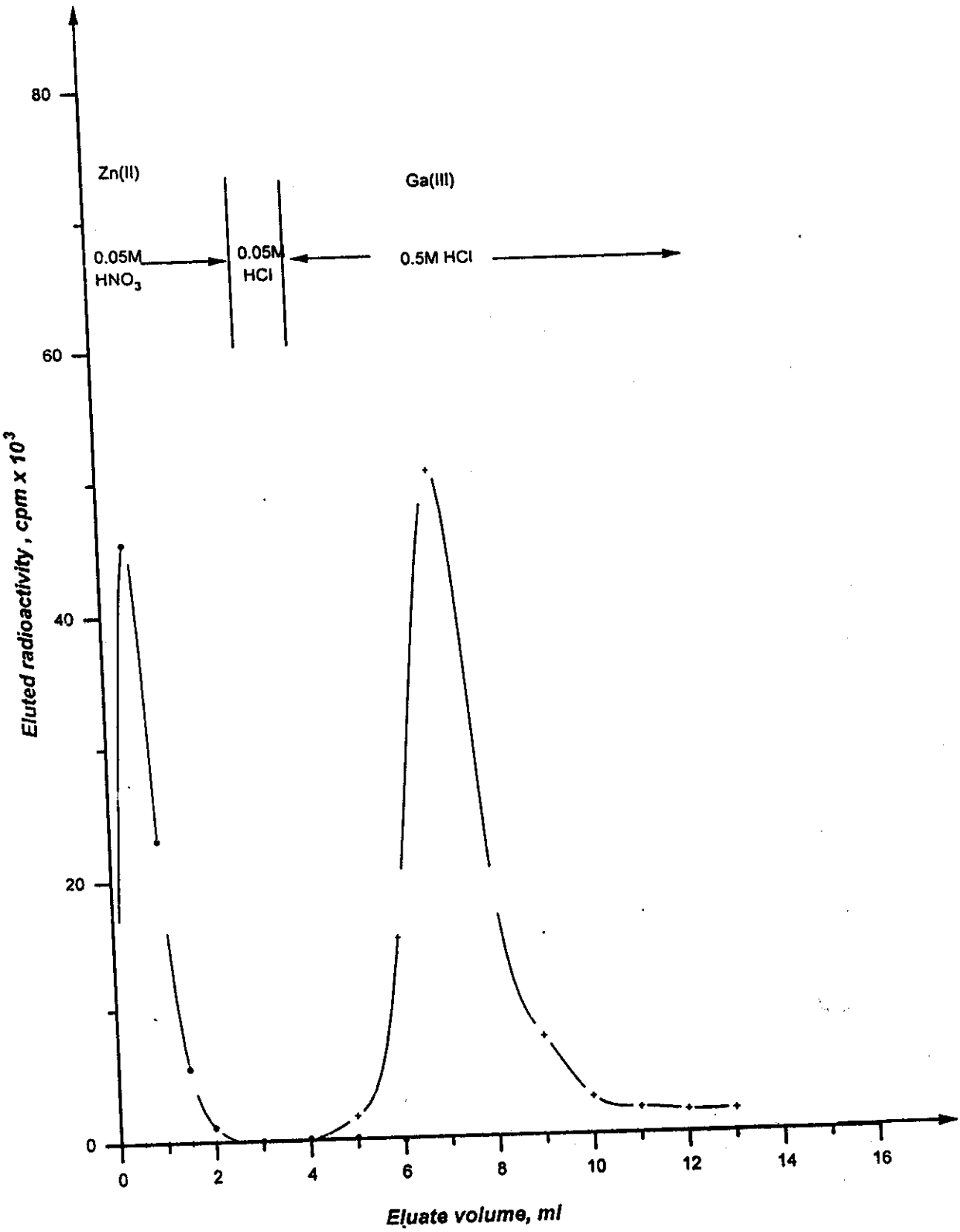

Fig.28. Typical elution profile of Ga(III) from Zn(II) onto 1g 12-molybdocerate(IV) column (0.6cm i.d x 3.5cm) with HNO_3 and HCl acid solutions at a flow rate of 1ml/min.

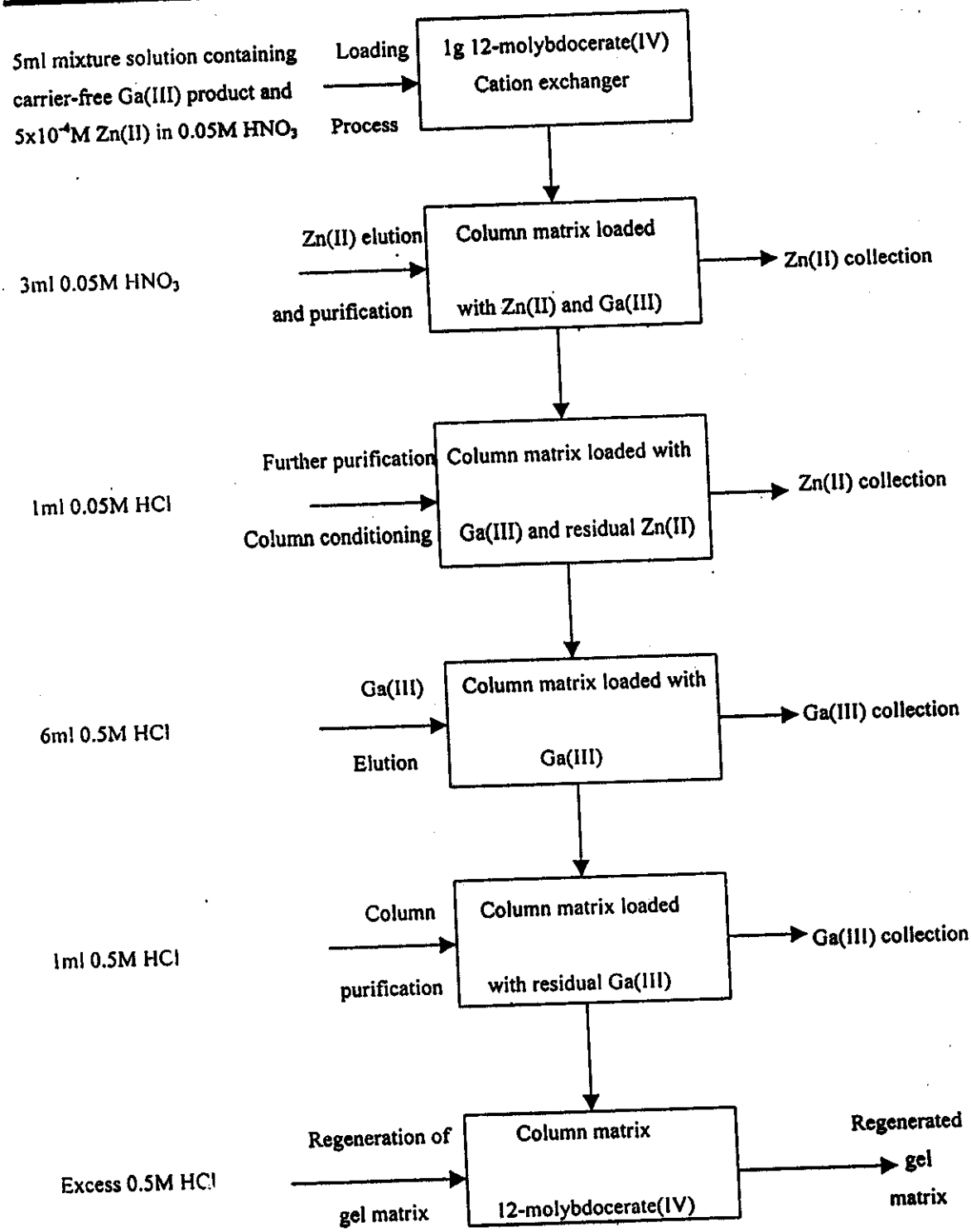

Fig.29. Proposed schematic diagram for separation of carrier-free Ga(III) from cyclotron irradiated Zn(III) targets by chromatographic column elution method.

method. In this technique; Zn(II)-Ga(III) separation can be achieved by continuously adding of a mixture solution (~35 ml) consists of 5 x 10^{-4} M zinc (II) and 10^{-5}M gallium (III) in 0.05M HNO_3 acid solution to small chromatographic column packed with 1g 12-molybdocerate (IV) matrix (0.6cm i.d x 3.5cm) at a flow rate of 1ml/min.

3.1.2.2.1 Recommended Procedure for Frontal Separation of the Zinc(II)-Gallium (III) Couple

The previous studies of breakthrough and elution profiles indicated that the optimum operating conditions for the separation of carrier free ^{67}Ga from bulk amounts of zinc (II) targets can be achieved by using small chromatographic columns each of 1g amounts 12-molybdocerate (IV) gel material (0.6cm i.d x 3.5cm). Figure 30 display that zinc(II)-gallium(III) separation can be achieved by passing 35ml mixture solution consisting of $\geq$ 5 x 10^{-4} M zinc (II) and $\leq 10^{-5}$ M Ga (III) [in real cases; gallium (III) is present in the trace concentration] in 0.05 M nitric acid through the column bed at a flow rate of 1 ml/min (~25 ^{0}C). The relative rates of migration through the column bed are determined by their interactions with the sorbent material and the eluents. It is observed that the zinc (II) constituent; with the least affinity for the molybdate gel, was immediately passed along the column. The strongly sorbed gallium (III) radiotracer is build up onto the sorbent matrix of the column. The retained Zn(II) contaminent was eluted and purified from the column with 3ml 0.05M HNO_3 acid solution at flow rate of 0.5ml/min. further purification of the bed matrix from any remaining Zn(II) and column conditioning carried out with passing 1ml 0.05M HCl at the same flow rate.

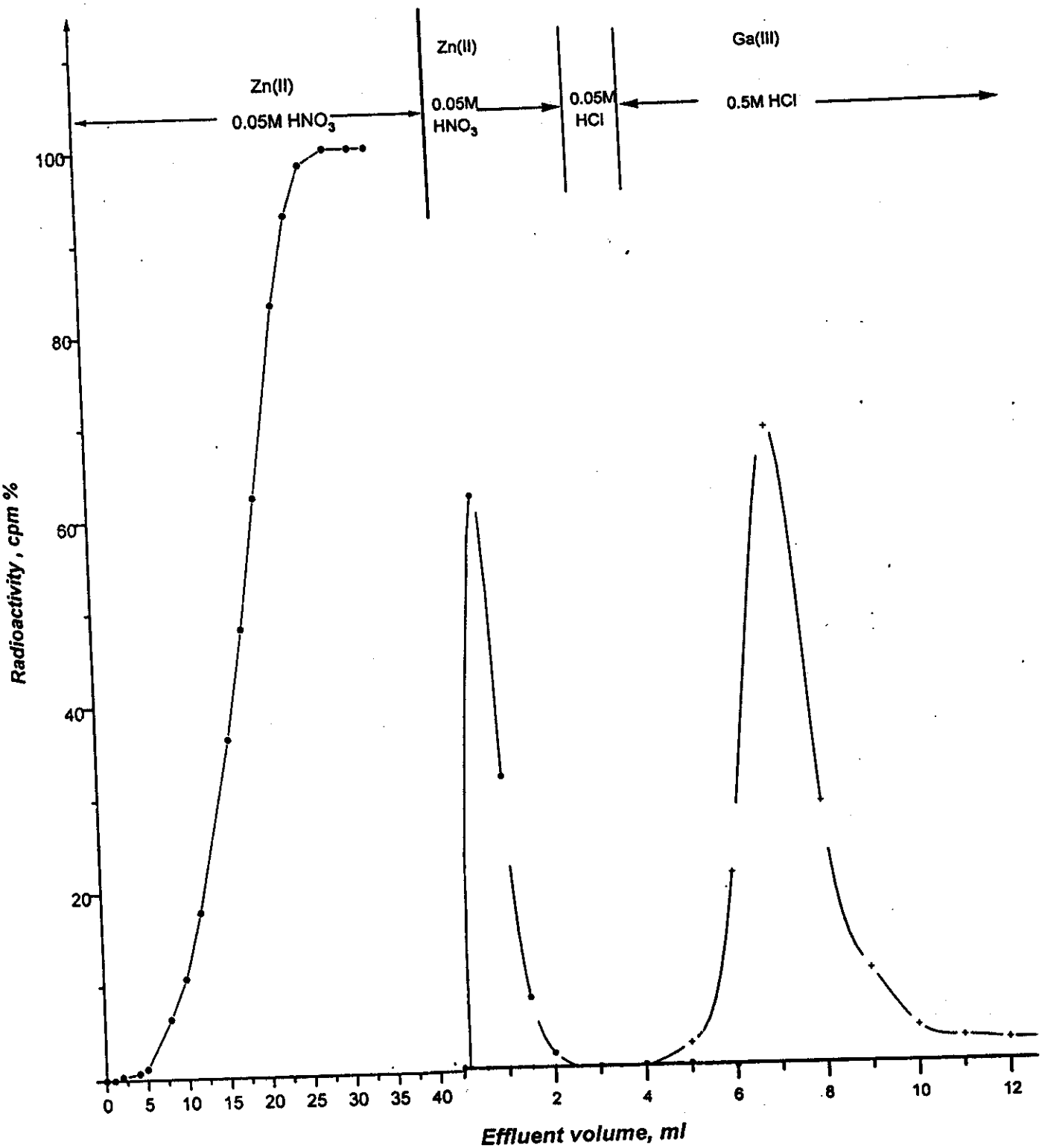

Fig.30. Frontal separation of a mixture solution containing 10^{-5}M Ga(III) and $5x10^{-4}$M Zn(II) from 12-molybdocerate(IV) columns (0.6cm i.d x 3.5cm) with HNO_3 and HCl acid solutions.

Thereafter, Ga(III) is eluted and purified with 7ml 0.5M HCl acid solution at flow rate of 1ml/min. Figure 31 displays the proposed schematic diagram for separation of carrier-free Ga(III) from its Zn(II) target by chromatographic column frontal method. The exchange capability of an ion in solution (solution phase ion) is dependent on the affinity of the ion for the resin. When the affinity of the solution phase ion is greater than that of the counter ion, which is initially present in the ion-exchange resin (resin phase ion), exchange occurs. When the ion initially in solution diffuses into the resin, the exchanged ion migrates out of the resin into the solution. In this work, hydrogen ion was chosen as the counter ion initially present on the 12-molybdocerate (IV) gel, because the hydrogen from resin has an advantage in developing an elution process using hydrochloric and nitric acids. The affinity sequence of the ion analyzed in this work for the resin is in the following order:

$$H^+ < Zn^{2+} < Ga^{3+}$$

Following the normal affinity sequence of the ions. The mechanisms of ion exchange reactions between the 12-molybdocerate (IV) resin and the solution phase ions can be expressed by consequent ion exchange equilibrium equations:

$\overline{HR} + [Ga]_S \leftrightarrow \overline{[Ga]\,R} + [H^+]_S.$

$\overline{HR} + [Zn]_S \leftrightarrow \overline{[Zn]\,R} + [H^+]_S.$

$\overline{HR} + [Zn,Ga]_S \leftrightarrow \overline{[Zn,Ga]\,R} + [H^+]_S.$

$\overline{ZnR} + [Ga]_S \leftrightarrow \overline{[Ga]\,R} + [Zn^{2+}]_S$

Where;

$\overline{HR}$ = 12- Molybdocerate (IV) gel matrix

Subscript *S* =Solution phase

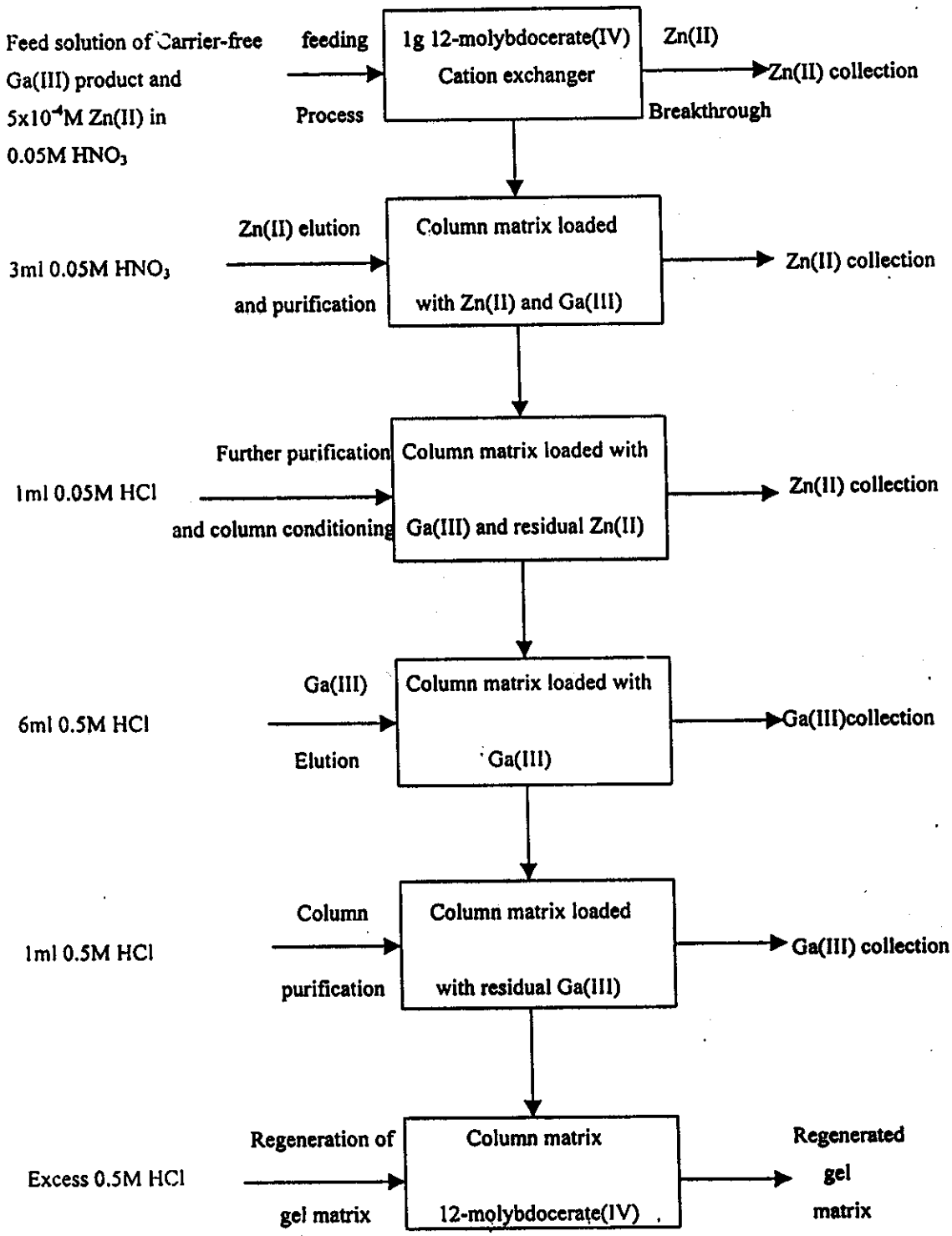

Fig.31. Proposed schematic diagram for separation of carrier-free Ga(III) from cyclotron irradiated Zn(II) targets by chromatographic column frontal method.

Initially, When the 12-molybdocerate (IV) resin comes into contact with the radiotracer solution, the ion exchange reactions move to the right. As the MoCe(IV) gel sorbes the Zn^{2+} and Ga^{3+} and the resin phase ions increase, a reversible ion exchange occurs and finally equilibrium between the two phases is reached . Since Ga^{3+} has the strong affinity, the resin phase, Zn^{2+} may be replaced by Ga^{3+} as noted in equations. The overall ion-exchange process is composed of two steps. The first step is a loading process in which the solution phase ion is exchanged onto the resin. In the second step, or the elution process, the ion previously loaded on the resin is eluted by using other ions. In the loading process, the hydrogen form resin is used and the H^+ on the resin is exchanged for the solution phase ions Zn^{2+} and Ga^{3+} according to equations. The exchange process continues until an equilibrium state between the resin and solution phases is reached. After loading, the process is initiated to elute the resin phase ions. Since ion exchange is reversible process, the eluent of either nitric or hydrochloric acid solution can elute the solid phase ions by the law of mass action to regenerate the resin to its original hydrogen ion form. This elution process is achieved by forcing the loading equations to move to the left by using a sufficient high concentration of the hydrogen from eluent.

3.1.3 Regeneration of the Column Matrix

When a cation in solution is being exchanged for an ion of different valency; the relative affinity of lower valent ion increases in direct proportion to the concentration. Therefore; to replace an ion of higher valency on the exchanger by one of lower valency; the conversion is assisted by using a relative concentrated solution of the replacing cation. And hence; the conversion of the bed matrix to the H^+-form was carried out with passing sufficient volume (about 30 times the matrix bed

volume) of 0.5 M nitric or hydrochloric acid solutions at a flow rate of 0.5 ml / min to insure that the resin was completely converted to the H^+-form. After completion of the conversion process the sorbent matrix become ready for further usage.

3.1.4 Quality Control Tests

3.1.4.1 Chemical Purity of the Gallium (III) Eluates

Presence of any chemical impurities in the gallium (III) eluate; originating from either the back of the target holder; the 12-molybdocerate (IV) bed or at least, from the eluents, will markedly affect the use of the gallium(III) eluate for clinical applications[35,41]. Since the used chemicals are of analytical reagent grade; its contribution as chemical impurities was eliminated. The gallium(III) eluates were analyzed spectrophotometrically[75,159] for the presence of molybdenum and cerium as chemical contaminants originating from the sorbent matrix. It was found that the concentration of cerium and molybdenum in the eluates were under the detection limit of the method (i.e, 1.0μg Ce / ml) and in the range of 1-2μg Mo / ml in 0.05M acid. Molybdenium concentration in the eluates are below the restricted limit for nuclear medicine applications. The solubility of molybdenum and cerium are dependent on the acid concentration as well as the temperature. Since the concentration of the acid media was ranging from 0.005M up to 0.5M and the working temperature at the ambient room temperature (~27°C); the contribution of molydenum and cerium in the eluates would be very small and could be neglected in nuclear medicine applications[32,37].

3.1.4.2 Radionuclidic Purity of the Gallium (III) Eluates

The radionuclidic purity of gallium(III) eluates is defined as the fraction of the gallium(III) radionuclide to the total eluate

radioactivity. The presence of any other radionuclidic contaminants e.g ^{65}Zn and ^{64}Cu; of longer half-lives; higher radiation energies and / or undesirable mode of decay, may affect the quality of the diagnostic pictures and cause high radiation doses to the patient[32,35,43]. Therefore; the radionuclidic purity of $^{72}Ga(III)$ [$T_{1/2}$ =14 h] eluates in hydrochloric acid solutions were confirmed by high-resolution gamma ray spectroscopy using high purity germanium (HPGe) detector coupled to multichannel analyzer. Figure 32 shows a typical gamma spectra of gallium(III) eluates measured immediately after separation. It is observed that only the photo peaks [629.86 and 834.98 keV] corresponding to ^{72}Ga are the main detected γ-energies. If it is assumed that the sum of the total residual activities corresponds to radionuclide impurities; the corresponding radionuclidic purity was found ≥ 99.9%. The obtained eluate was further identified by its 14h half-life corresponding to $^{72}Ga(III)$ radionuclide, as shown from the decay curve in Figure 33. If the residual radioactivity after 168h decay period is the radionuclidic impurities, the calculated radionuclidic purity of the eluate was found to be greater than 99.9%. This value is suitable for human administration according to the standard requirements for $^{67}Ga(III)$ application in nuclear medicine[32,33,38,43,45].

3.1.4.3 Radiochemical Purity of the Gallium (III) Eluates

The radiochemical purity is defined as the percent of the gallium(III) radioactivity in the desired chemical form to the total radioactivity. The presence of different radiochemical forms give poor quality images due to poor localization in the organ of interest and the high background from the surrounding tissues[32,43]. The radiochemical purity of gallium(III) eluates was assessed by ascending paper chromatography; using stripes of Whatman No.1 filter paper in a mixture

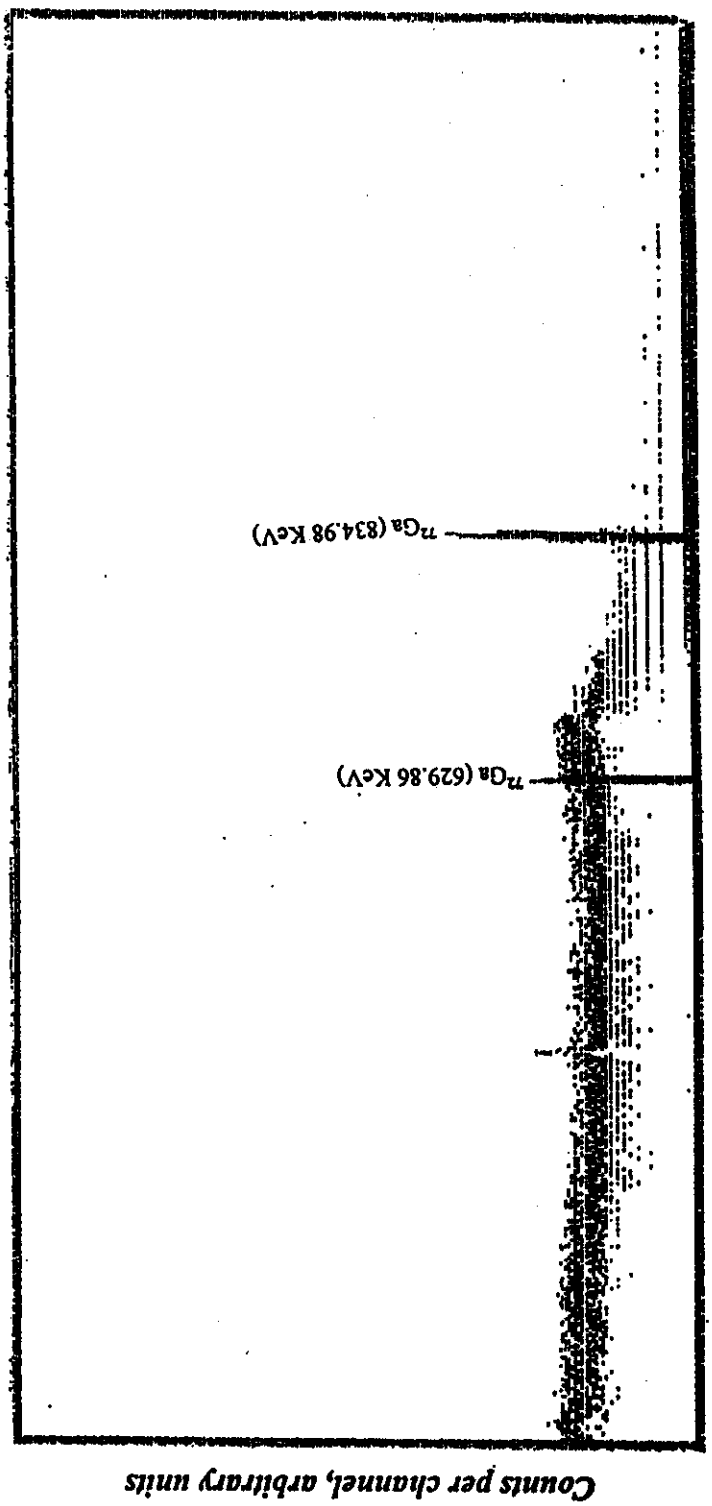

Fig.32.Gamma spectra of gallium eluates from12-molybdocerate(IV) matrix.

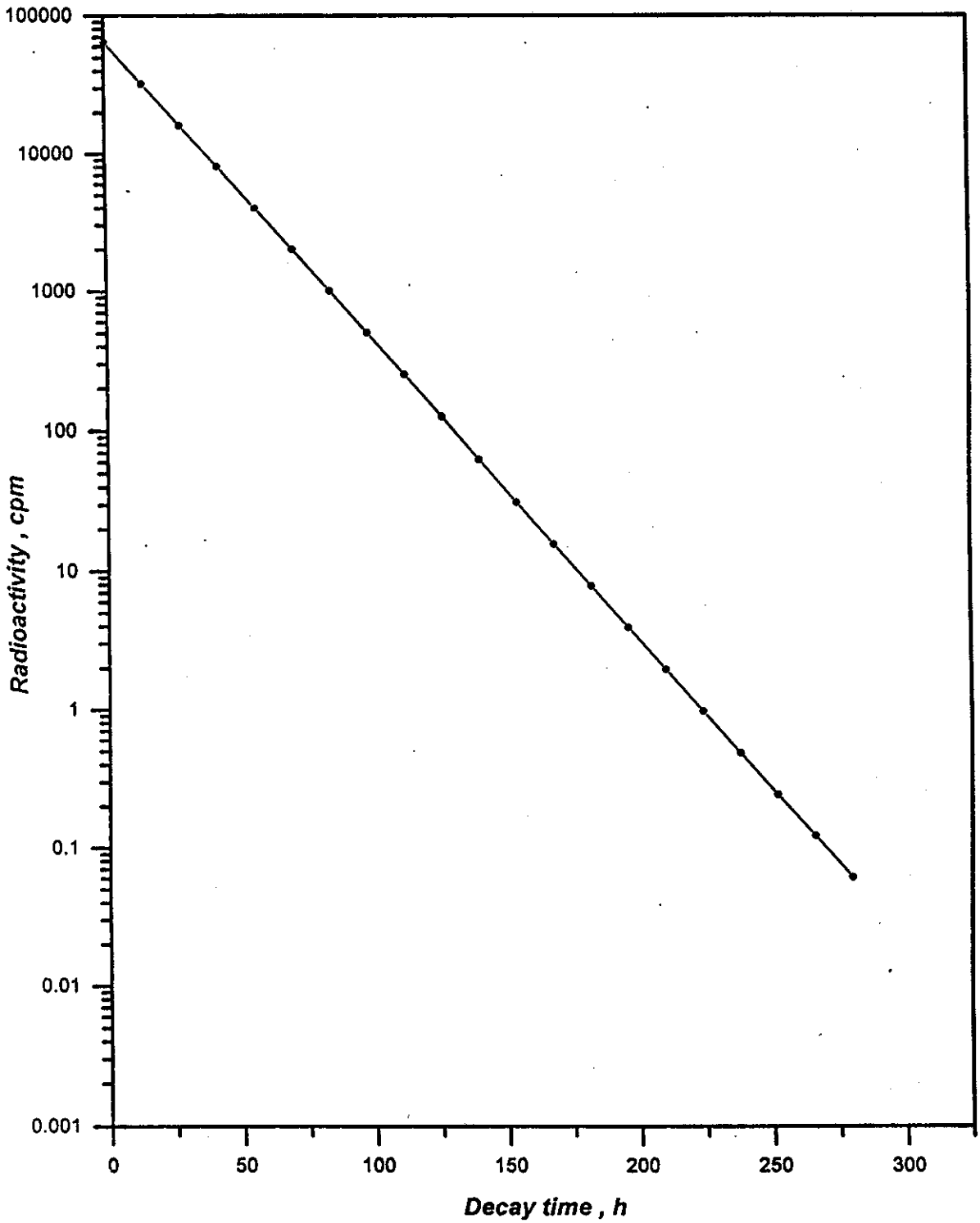

Fig.33. Decay curve of gallium(İİİ) eluates from 12-molybdocerate(IV) columnn matrix.

of water: methanol in 4:2 volume ratio as a developing solvent[74,116]. Figure 34 display a typical radiochromatogram of gallium(III) eluates from 12-molybdocerate column matrix. The radiochromatogram shows one only peak localized at R_f=0.6. Whereas; the retardation factor (R_f) represents the traveled distance from the base line to the peak position divided by the distance from the base line to the solvent front. The obtained R_f value may be due to gallium chloride; $GaCl_3$, radiotacer[70,116]. The corresponding radiochemical purity was found to be about 95%. This value is in agreement with the recommended specifications for use of gallium(III) for therapeutic and diagnostic purposes in nuclear medicine[83,41,45].

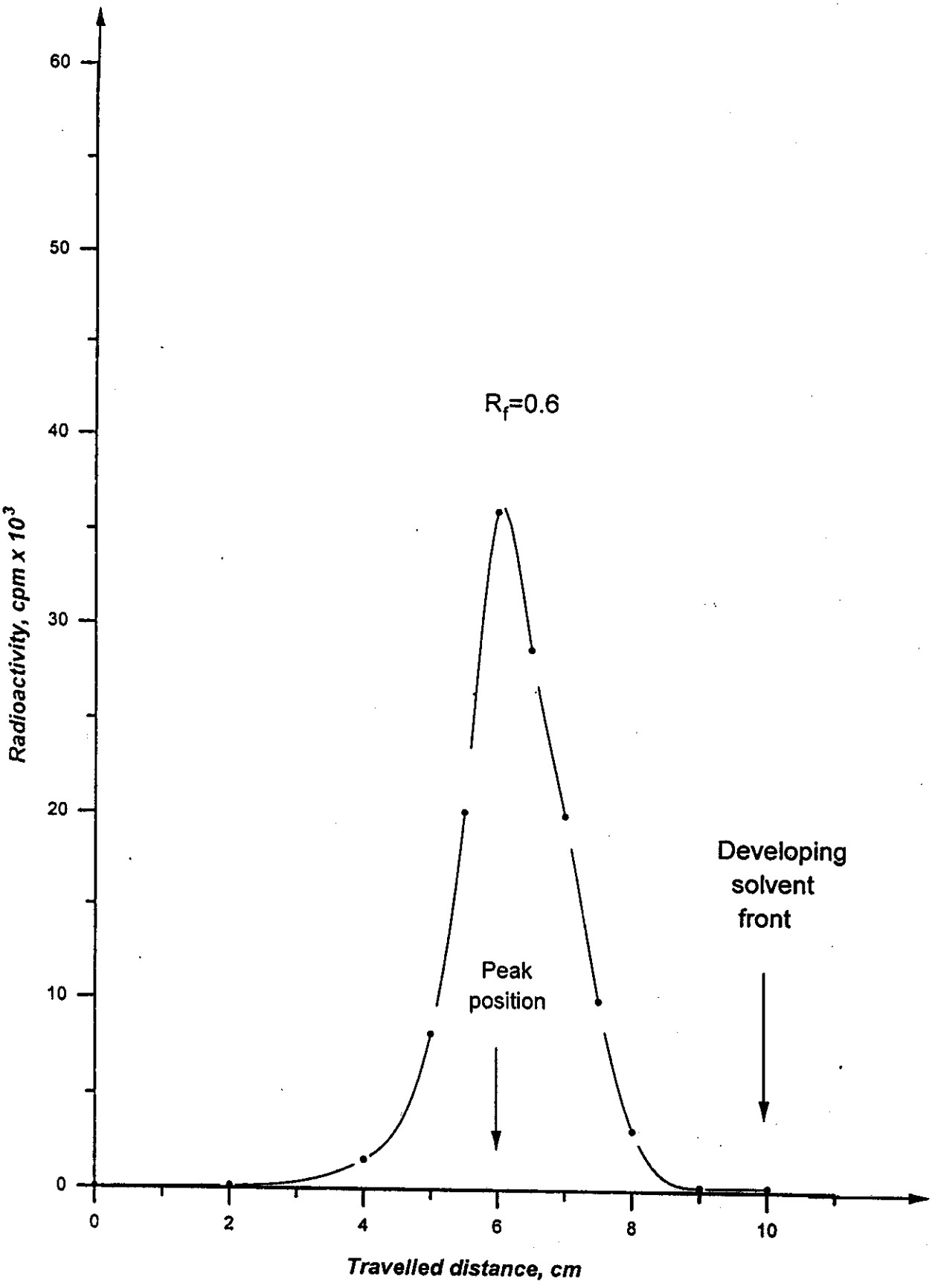

Fig.34. Radiochromatogram of gallium(III) eluates from 12-molybdocerate(IV) column matrix.

3.2 Cadmium (II) – Indium (III) Couple

3.2.1 Distribution Behaviour Investigations

3.2.1.1 Static Studies

The distribution behaviours of the radiotracers of cadmium (II) and indium (III) in 0.005-0.5M nitric and hydrochloric acid solutions on 12-molybdocerate (IV) matrix were individually investigated by the batch equilibration method in a shaker thermostat adjusted at 25 ±1°C.

3.2.1.1.1 Effect of H^+-ion Concentration

Figure 35 shows that the distribution behaviour of 10^{-6}M cadmium (II) in nitric acid solutions on 12-molybdocerate(IV) gel is characterized by a high distribution coefficient value of around 750 ml/g at 0.005M HNO_3 acid. Thereafter, the K_d values decrease markedly with increasing the acid concentration up to 0.15M HNO_3 (K_d=18ml/g). At low acid concentrations Cd(II) has a great tendency to form hydrolyzed cationic and neutral species of $[Cd_2(OH)_2]^{2+}$, $[Cd_2(OH)]^{3+}$, $[Cd(OH)]^+$and $[Cd(OH)_2]^o$ [23,25]. So, the corresponding increase in the retention behaviour of cadmium (II) with decreasing the acid concentration may be attributed to cation exchange and / or hydrolytic sorption and precipitation mechanisms of polynuclear hydrolyzed species of cadmium(II) from solution onto the surface of the 12-molybdocerate(IV) gel. The predominance of weakly sorbable mononuclear species of $[Cd(OH)_2]$, $[Cd(OH)]^+$ and $[Cd(OH)(NO_3)]$ may contribute to the obtained decrease in the corresponding K_d values with increasing the acid concentration. In solutions ≥ 0.15M nitric acid, the obtained increase in the amount of retained Cd (II) may be due to simple cation exchange of unhydrolyzed Cd^{2+} and $[Cd(NO_3)]^+$ species with the counter H^+-ions on the surface of the molybdate matrix.

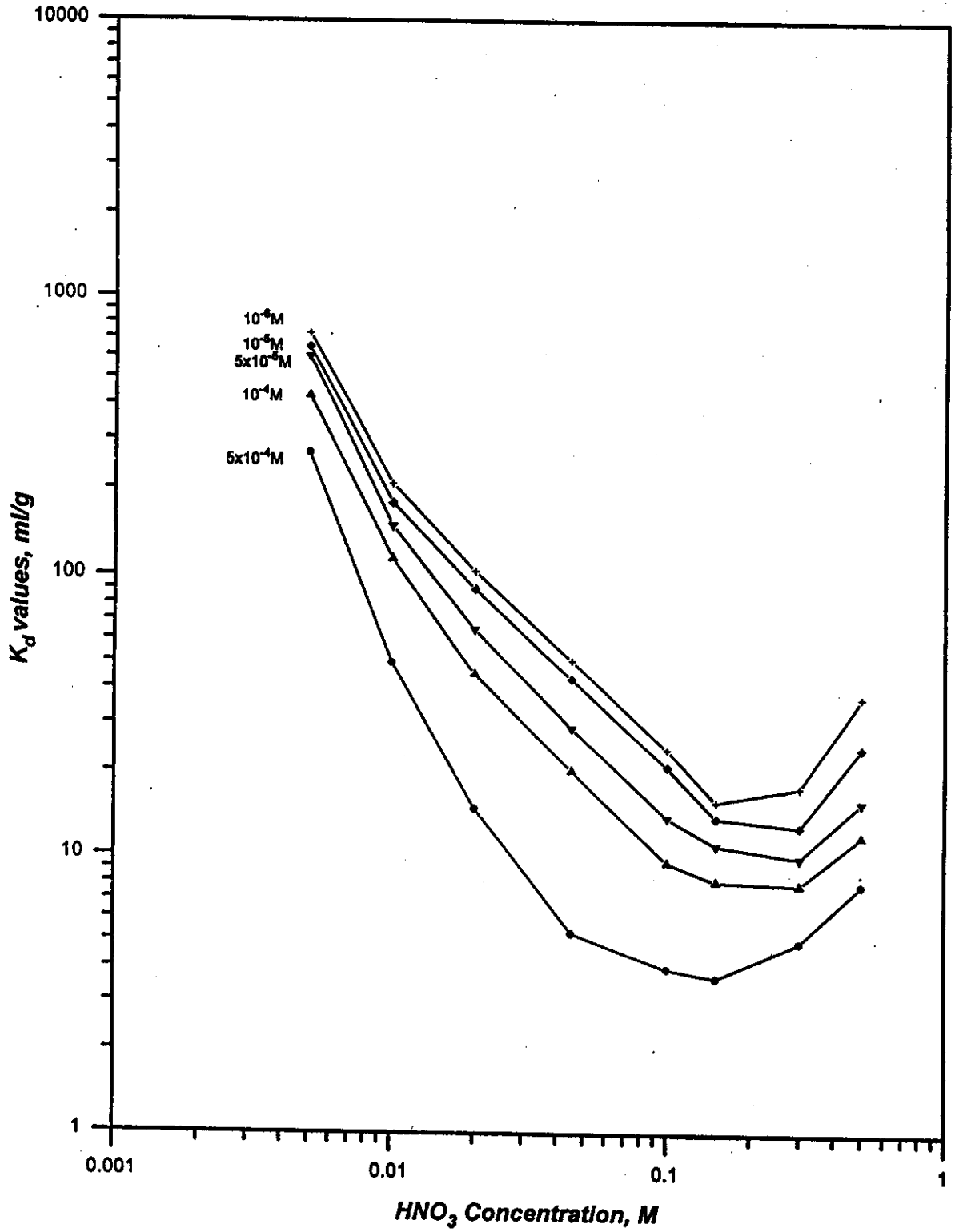

Fig.35. Distribution coefficient (K_d) values of Cd(II) in HNO_3 acid solutions on 12-molybdocerate(IV) at different Cd(II) concentrations(25±1°C)

Therefore; it may be deduced that cation exchange mechanism is the main ruling reaction process in 0.15-0.5M HNO_3 solutions (K_d=18-43ml/g).

Figure 36 shows the distribution behaviour of 10^{-6}M indium (III) in nitric acid solutions on 12-molybdocerate (IV) gel in the acid concentration range 0.005- 0.5M at 25±1°C. Increasing the nitric acid concentration up to 0.05M HNO_3, a sorption maximum plateau with almost constant K_d values of about 364 ml/g is obtained. The observed high K_d values of In(III) in dilute nitric acid solutions presumably attribute to predominance of In(III) cationic species such as : $[In(OH)_2]^+$, $[In(OH)]^{2+}$, In^{3+}, $[In(NO_3)]^{2+}$ and $[In(NO_3)_2]^+$[23,24] which are strongly retained onto the molybdate matrix by cation exchange and / or hydrolytic sorption mechanisms. In concentrated nitric acid solutions; the K_d values of indium(III) decrease with increasing the acid concentration upto 0.5M acid (K_d=31 ml/g). This behaviour may be attributed to the predominance of molecular $[In(NO_3)_3]$ species as well as anionic species of indium(III): $[In(NO_3)_4]^-$ and $[In(NO_3)_5]^{2-}$ at higher acid concentrations[24,25,155].

It is obvious that the retention behaviour of Cd(II) and In(III) on the MoCe(IV) matrix follows more than one reaction mechanism, cation exchange, hydrolytic sorption and complex formation(i.e., precipitation). Inorganic ion exchangers are usually not very good in the ion exchange stoichiometry because of the inorganic nature of the matrix, they show other uptake phenomenon in addition to the normal ion exchange process on the surface. The ongoing cation exchange, hydrolytic sorption and hydrolytic precipitation mechanisms of the In(III)species under consideration on the 12-molybdocerate(IV) matrix ($H_nMoCe(OH)_m$) can be illustrated with the following equations;

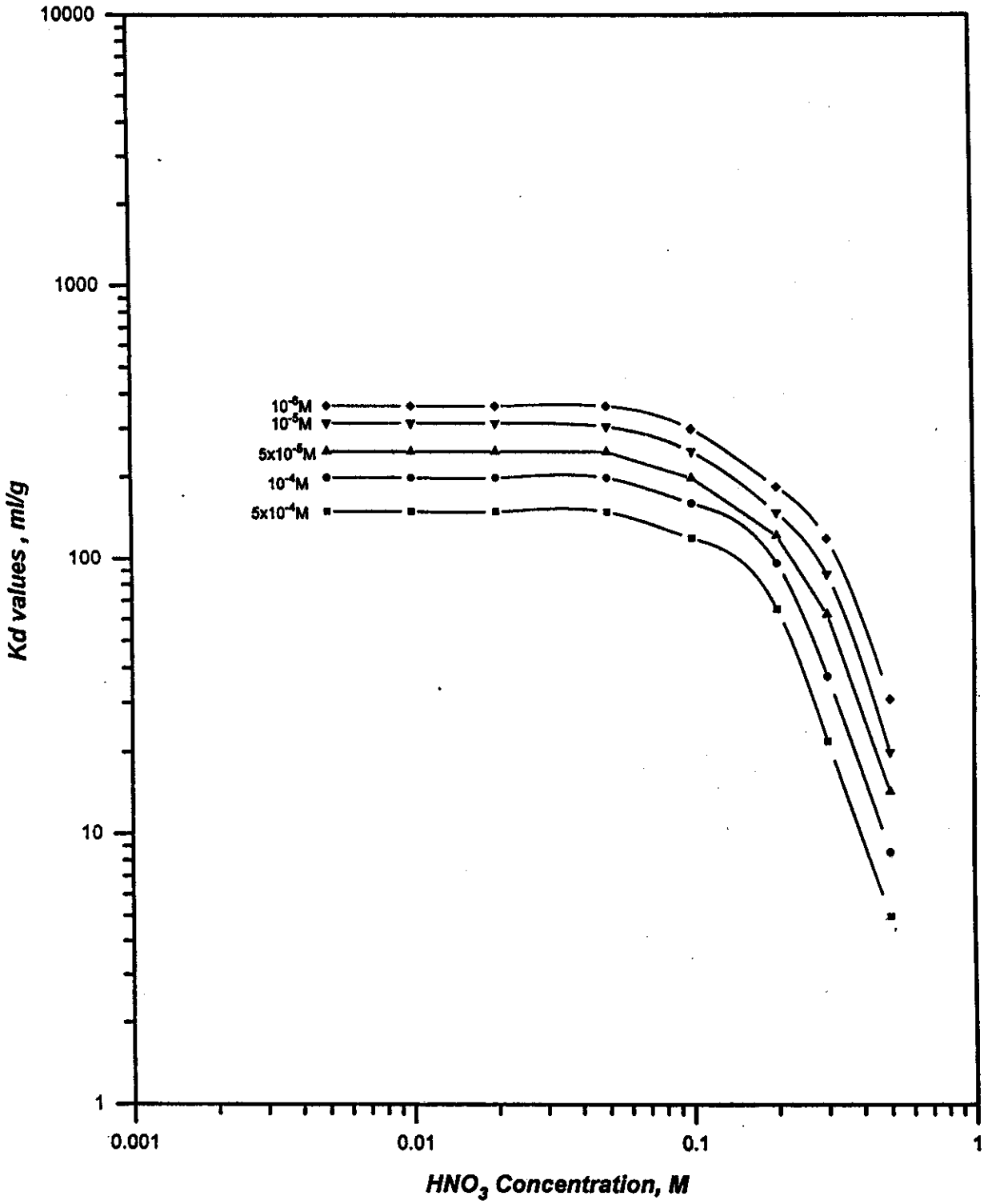

Fig.36. Distribution coefficient (k_d) values of In(III) in HNO_3 acid solutions on12-molybdocerate(IV) at different In(III) concentrations(25±1°C)

Cation exchange reaction of unhydrolysed cationic species:

$$H_nMoCe(OH)_m + M^{x+} \rightleftharpoons H_{(n-x)}MoCe(OH)_mM + xH^+$$

Hydrolytic sorption reaction of hydrolyzed cationic species:

$$H_nMoCe(OH)_m + M(OH)_y^{(x-y)+} \rightleftharpoons H_{n-(x-y)}\ MoCe(OH)_{m-y}O_yM + (x-y)H^+ + yH_2O$$

Where $x \geq y$

Hydrolytic precipitation of molecular species:

$$H_nMoCe(OH)_m + M(OH)_x \longrightarrow H_{n-m}MoCe(OH)_{m-x}O_xM + xH_2O$$

Where $m \geq x$

3.2.1.1.2 Effect of the acid Anion

Figure 37 depicts the sorption behaviour of 10^{-6}M cadmium (II) in 0.005-0.8M hydrochloric acid solutions on 12-molybdocerate (IV) gel. It is obvious that the K_d values of Cd(II) is high at low HCl acid concentration (550ml/g in 0.005M acid) and decreases with increasing the acid concentration to K_d=22ml/g at 0.1M HCl. At low acid concentrations cadmium (II) has a great tendency to form cationic species of $[Cd_2(OH)_2]^{2+}$ and $[Cd_2(OH)]^{3+}$ and neutral molecules of $[Cd(OH)_2]^0$ which are strongly retained onto the surface of the sorbent matrix[24,26,155]. As mentioned before, the sorption behaviour of Cd(II) at low acid concentrations can be explained on the basis of cation exchange, hydrolytic sorption and precipitation reaction mechanisms. The gradual decrease in K_d values with increasing the acid concentration may be attributed to the predominance of molecular $[Cd(OH)(Cl)]^0$ species. Above 0.2M HCl acid (K_d=17ml/g), the formation of $[Cd(Cl)]^+$ and Cd^{2+} species may lead to the observed increase in the K_d values(20ml/g at 0.8M acid).

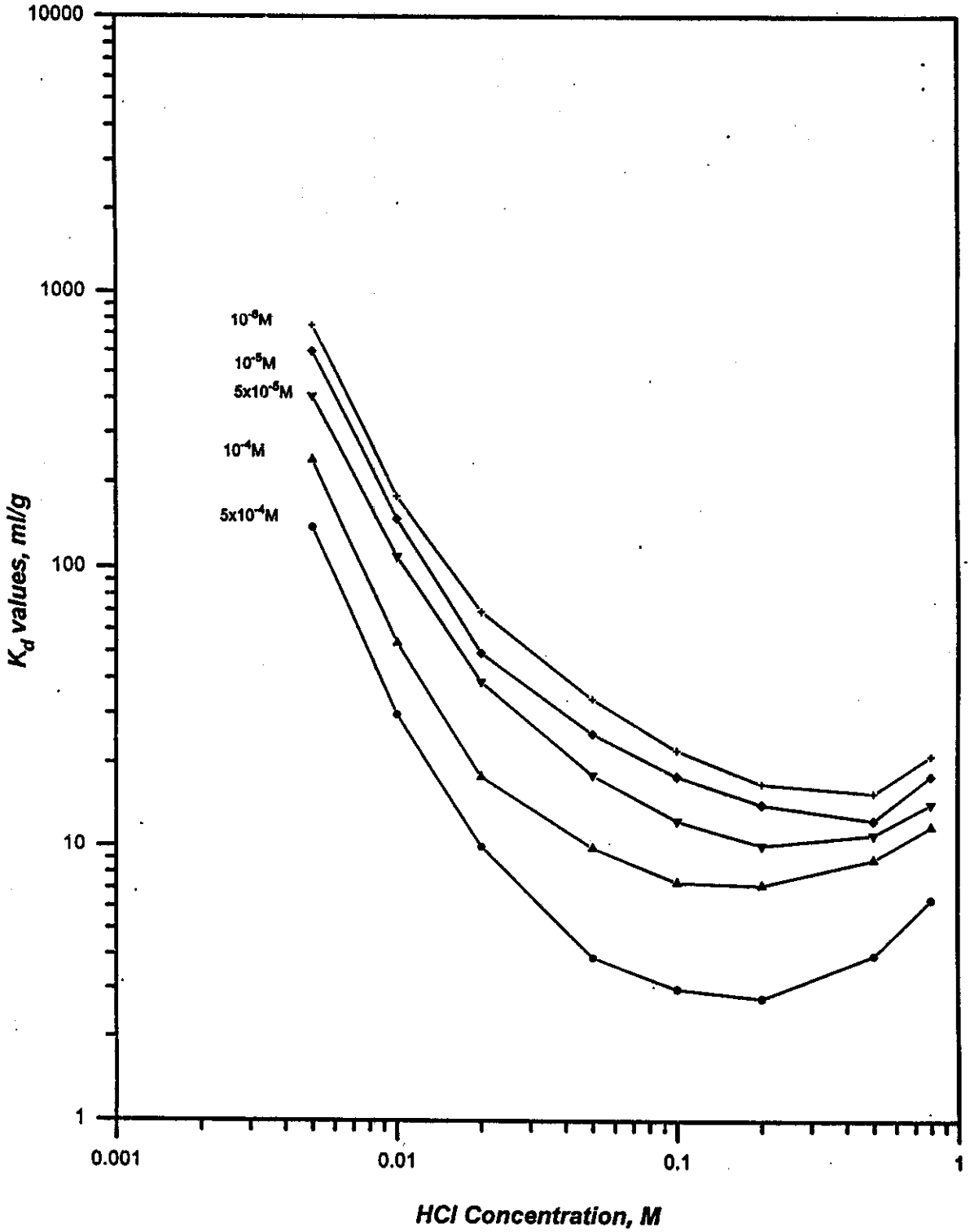

Fig.37. Distribution coefficient(K_d) values of Cd(II) in HCl acid solutions on 12-molybdocerate (IV) at different Cd(II) concentrations(25±1 °C).

Figures 36 and 38 show that the K_d values of cadmium (II) in hydrochloric acid media are somewhat lower than those from nitric acid solutions; at comparable conditions. This behaviour may be attributed to different association affinity of the NO_3^- and Cl^- anions with cadmium (II) in HNO_3 and HCl acid solutions to form weakly sorbed stable complexes. As well as, figures 36 and 38 show that the sorption behaviour of indium (III) is improved in nitric acid solutions than in hydrochloric acid media, where the K_d values of indium (III) in hydrochloric acid solutions are lower than that in nitric acid solutions at comparable experimental conditions. This observation is in accordance with the high association affinity of indium (III) towards Cl^- anions than NO_3^- anions to form more stable chloride complexes [24,25,156].

3.2.1.1.3 Effect of Concentration of the Radiotracers

Figures (35 and 36) and (37 and 38) illusterate the distribution behaviours of cadmium (II) and indium (III) at different metal ions concentrations [from 10^{-6} to $5x10^{-4}$M] in nitric and hydrochloric acid solutions on 12-molybdocerate (IV) gel; respectively. It is obvious that K_d values of the respective metal ions increase with decreasing the concentration of the radiotracer in the reaction medium. Usually, cadmium (II) ions are less retained onto the 12-molybdocerate(IV) gel than indium (III) ions in acid solutions $\geq$ 0.01M at comparable concentrations. In practice, cadmium is present in macro or micro amounts in the processing solution [say $\geq 5x10^{-4}$M Cd(II)] and indium (III) as the irradiation product of the Cd target is present in trace amounts as carrier-free In(III)($<< 10^{-6}$M). The obtained data is promising and meet with the actual conditions for separation of cyclotron produced indium(III) radiotracer from its cadmium (II) target.

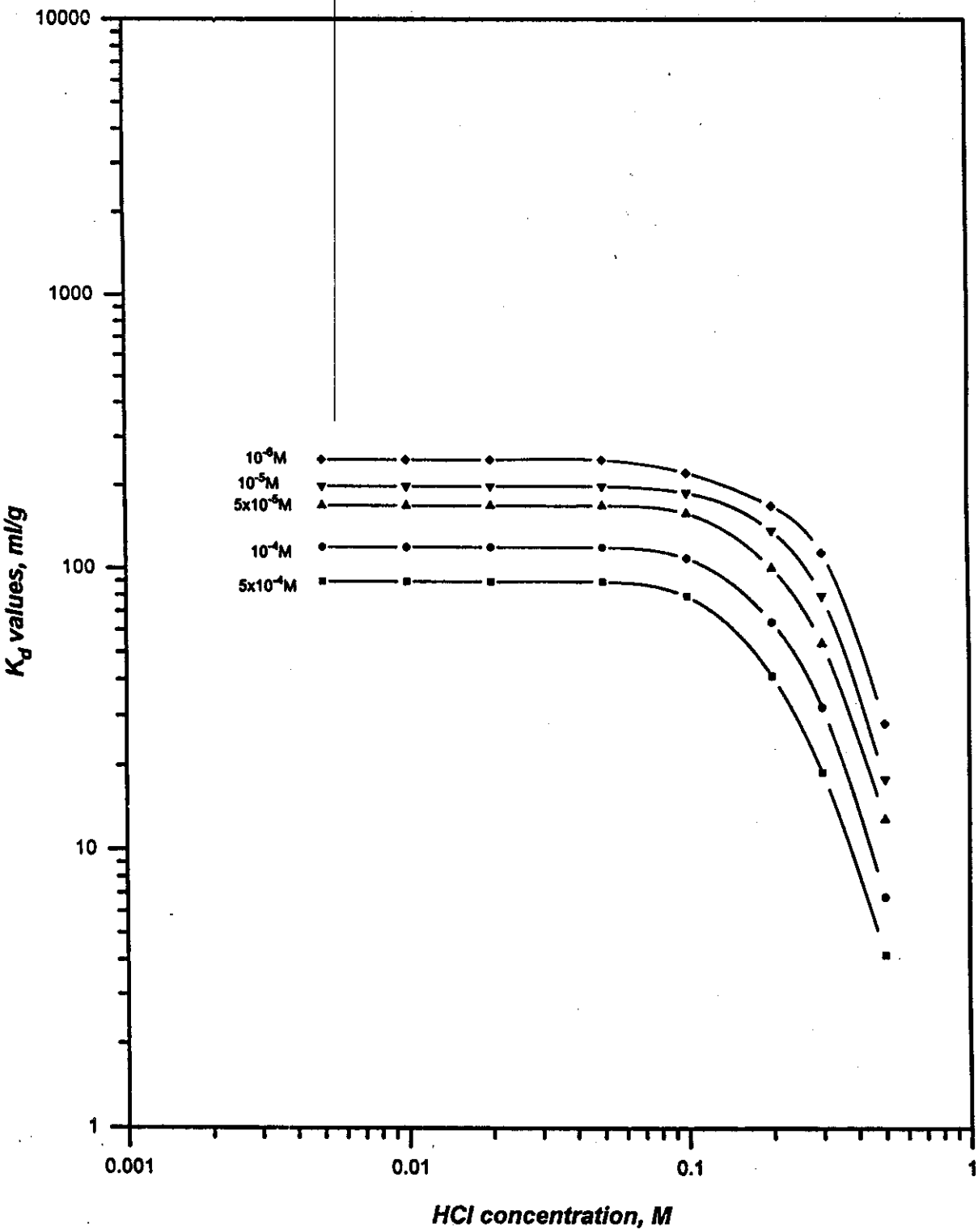

Fig.38. Distribution coefficient (K_d) values of In(III) in HCl acid solutions on 12-molybdocerate(IV) at different In(III) concentrations(25±1°C)

3.2.1.2 Dynamic Studies

The breakthrough behaviour of cadmium(II) and indium(III) radiotracers from 1g 12-molybdocerate(IV) columns has been individually investigated at different concentrations of the respective radiotracers ranging from 10^{-5} to $5x10^{-4}$M Cd(II) and 10^{-5}M In(II) in 0.01 and 0.05M nitric and hydrochloric acid solutions, respectively. The feed solution was continuously passed through the column bed at a flow rate of 1ml/min and room temperature (25°C). The column effluents were collected in equal volume fractions for radiometric analysis and the counting rates(C_V) of equal volume fractions were compared with standard samples (C_o). The obtained results were drawn in the form of breakthrough curves (C_V/C_o, % vs. effluent volume, ml).

3.2.1.2.1 Effect of Concentration of the Radiotracers

Figure 39 (curves a,b,c,d and e) shows the breakthrough profiles of 10^{-5}M In(III) and 10^{-5}, $5x10^{-5}$, 10^{-4} and $5x10^{-4}$MCd(II) in 0.01M HNO_3 from 1g MoCe(IV) columns. Comparison of the plots of Figure 39 (curves b,c,d and e) show that faster breakthrough kinetic equilibrium of cadmium(II) in 0.01M HNO_3 acid is established at higher cadmium (II) concentration in the feed solution. Therefore, increasing the concentration of Cd(II) in the feed solution markedly decreases the loading time in the Cd(II)-In(III) radiochemical separation step. Furthermore, the breakthrough saturation positions of Cd(II) [C_v/C_o=100%] will be displaced towards lower effluent volumes with increasing the target concentration in the feed solution. Regarding Figure 39.curve a, improved Cd(II)-In(III) separation resolution could be achieved at higher Cd(II) concentrations.

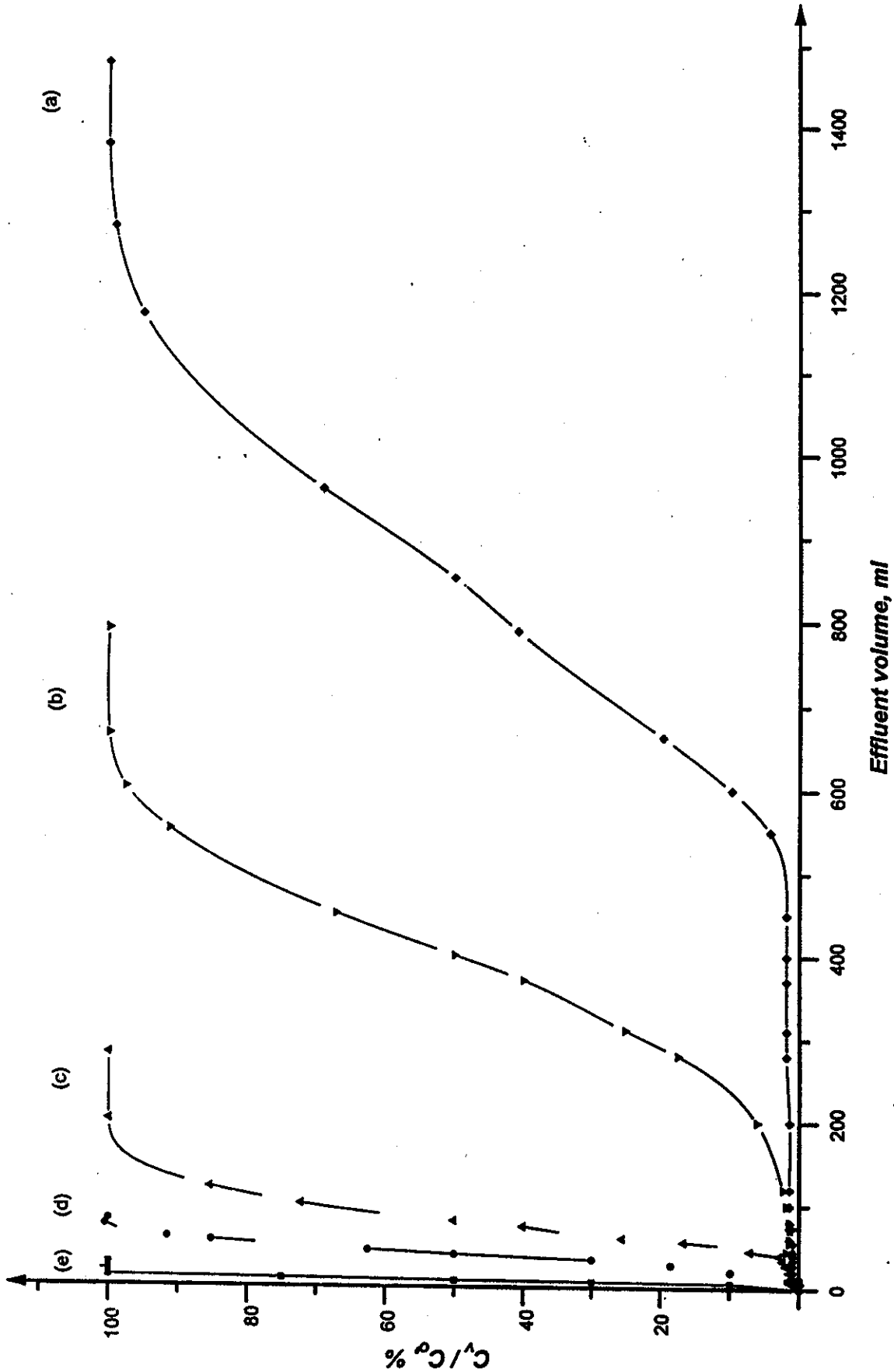

Fig.39. Breakthrough curves of Cd(II) and In(III) in 0.01M HNO_3 from 1g 12-molybdocerate(IV) columns (0.6cmi.dx3.5cm) at flow rate of 1ml/min as a function of metal ions concentrations. (a)10^{-5}MIn(III) (b) 10^{-5}M Cd(II) (c)$5x10^{-5}$M Cd(II) (d)10^{-4}M Cd(II) (e)$5x10^{-4}$M Cd(II)

In practice, the product indium (III) would be present in trace amounts [<< 10^{-6}M In(III)] and cadmium(II) is present in macro or micro amounts according to its weight and volume of the processing solute. So, chromatographic columns packed with adequate amounts of the molybdocerate matrix would be ultimately sufficient for approximately quantitative retention of In(III) with distinct separation from its cadmium (II) content.

3.2.1.2.2 Effect of Chemical Composition and Nature of the Feed Solution

Figure 40 depicts the effect of 0.05M nitric acid on the individual breakthrough behaviour of cadmium (II) and indium(III) from 1g 12-molybdocerate(IV) columns. From Figures 39 and 40, it is obvious that fast breakthrough for both Cd(II) and In(III) had been attainded with increasing the acid concentration from 0.01 to 0.05M acid.

Figures 41 and 42, show that Cd(II) and In(III) have more or less similar breakthrough behaviour trends in hydrochloric and HNO_3 acid solutions. It is obvious that the breakthrough of Cd (II) and In(III) in hydrochloric acid solutions is more faster than in nitric acid solutions at comparable feeding conditions, in agreement with the previously obtained K_d values.

Therefore; dilute nitric acid solutions would be more suitable for the column loading and washing processes; to achieve high uptake and delayed breakthrough of indium (III). On the other hand; relatively concentrated hydrochloric acid solutions (> 0.05M) would be preferable in the elution process of retained In(III).

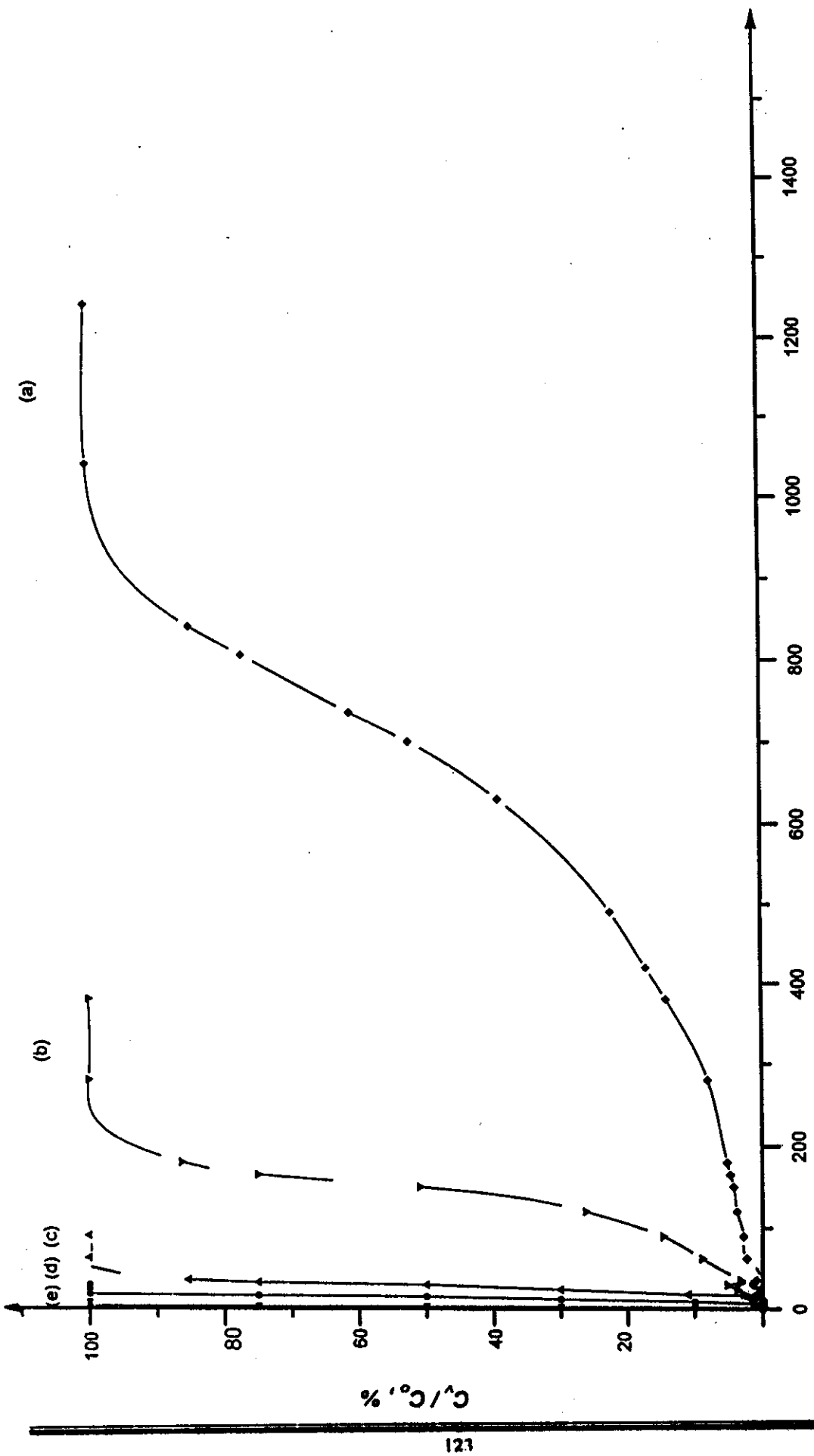

Fig.40. Breakthrough curves of Cd(II) and In(IIII) in 0.05M HNO_3 from 1g 12-molybdocerate(IV) columns(0.6cmi.d x 3.5cm) at flow rate of 1ml/min as a function of metal ions concentrations. (a)10^{-5}M In(III) (b) 10^{-5}M Cd(II) (c) $5x10^{-5}$M Cd(II) (d) 10^{-4}M Cd(II) (e)$5x10^{-4}$M Cd(II)

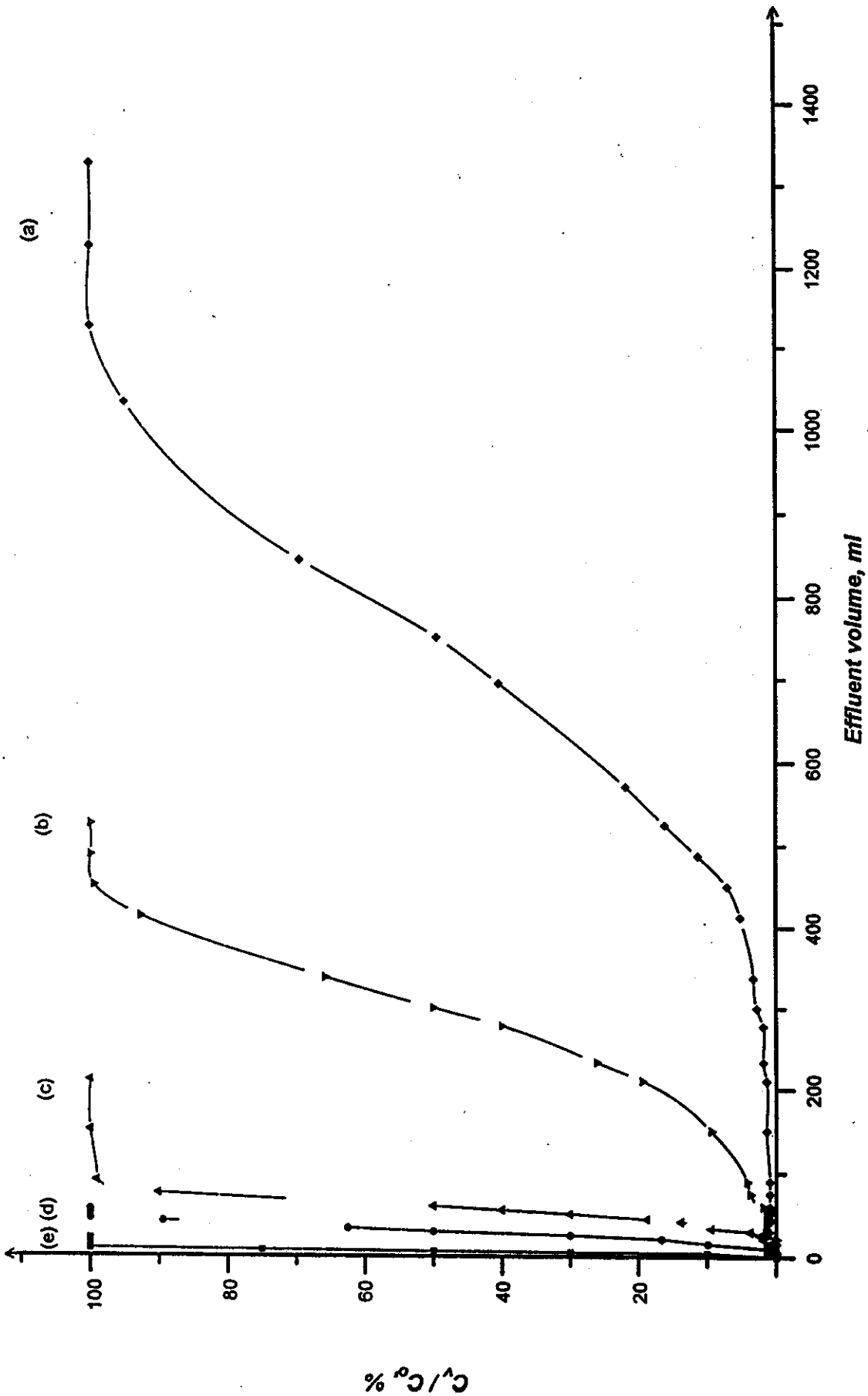

Fig.41. Breakthrough curves of Cd(II) and In(III) in 0.01M HCl from 1g 12-molybdocerate(IV) columns (0.6cm i.dx3.5cm) at flow rate of 1ml/min as a function of metal ions concentrations. (a)10^{-5}M In(III) (b)10^{-5}M Cd(II) (c)$5x10^{-5}$M Cd(II) (d)10^{-4}M Cd(II) (e)$5x10^{-4}$M Cd(II)

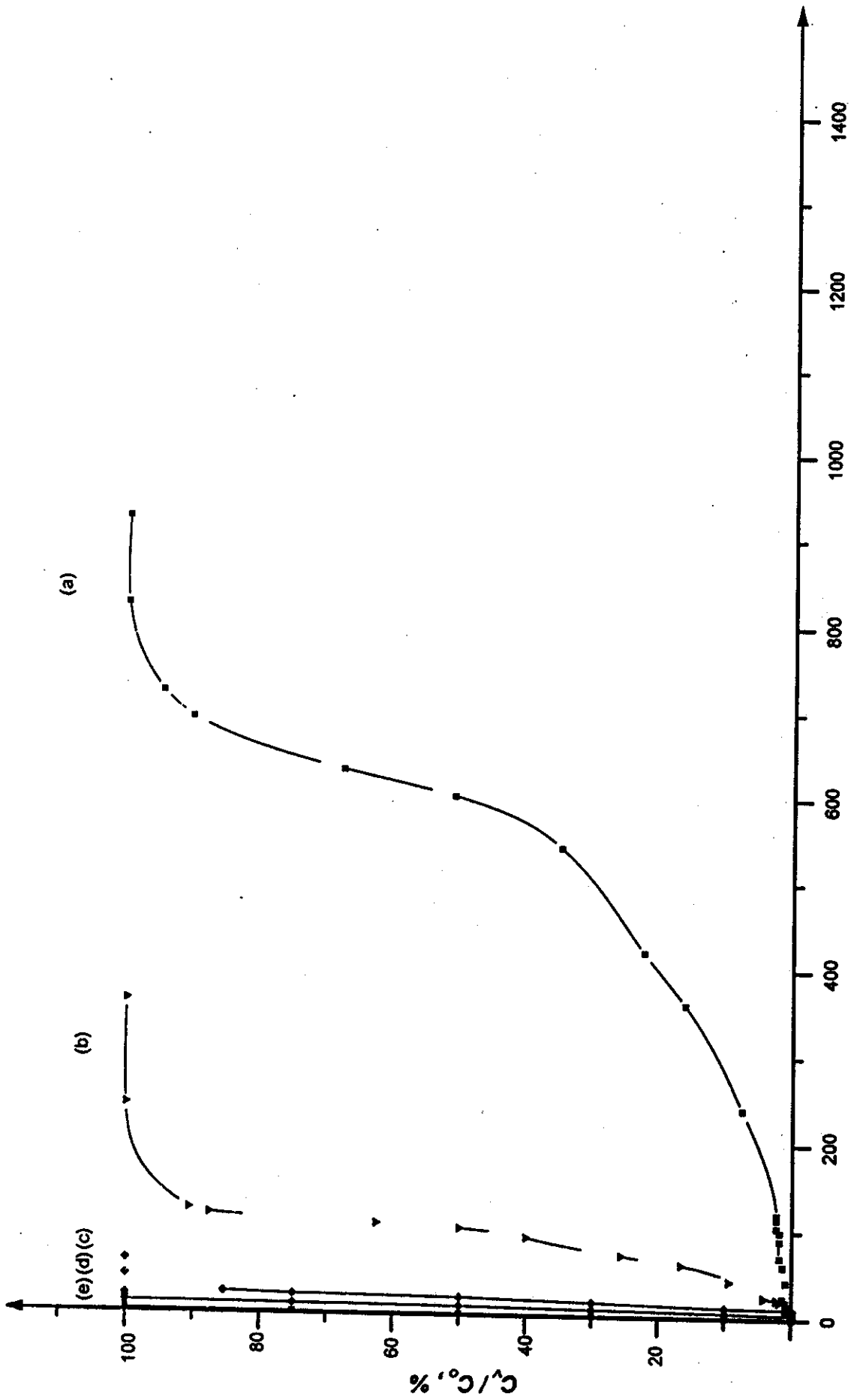

Fig.42. Breakthrough curves of Cd(II) and In(III) in 0.05M HCl from 1g 12-molybdocerate(IV) columns (0.6cmi.d x 3.5cm) at flow rate of 1ml/min as a function of metals ions concentrations (a)10^{-5}M In(III) (b)10^{-5}MCd(II) (c)$5x10^{-5}$M Cd(II) (d)10^{-4}M Cd(II) (e)$5x10^{-4}$M Cd(II)

3.2.2 Chromatographic Column Separations

It is obvious from the previously obtained distribution coefficient values that indium (III), particularly, in 0.01-0.05M nitric and hydrochloric acid solutions show higher affinity towards the molybdate matrix than cadmium (II) under comparable conditions. Table 10 compiles the separation factor [α] values of indium (III) from cadmium(II) at different metal ions concentrations in nitric and hydrochloric acid solutions. It is observed that mixture solutions of In(III)-Cd(II) containing $\leq 10^{-5}$M indium (III) and $\geq 5 \times 10^{-4}$ M cadmium (II) in 0.01 and 0.05M nitric and hydrochloric acid solutions show high separation factors. Furthermore; the separation factors for the indium (III) – cadmium(II) couple in hydrochloric acid solutions are greater than those in nitric acid solutions and 0.05M acid > 0.01M acid. On the other hand, Table 11 compiles the breakthrough characteristics of Cd(II) and In(III) in HCl and HNO_3 acid solutions at different concentrations of acid and metal ions. Micro or trace concentrations of In(III) in the feed solutions would achieve good separation resolution from the bulk amounts of Cd(II) target. Retention of In(III) is better in dilute acid (HNO_3 > HCl) solutions than in concentrated acid($\geq$0.05M). Accordingly, separation of indium (III) - cadmium(III) radiotracers from each other has been investigated by both elution and frontal chromatographic methods using 12-molybdocerate (IV) columns fed with small and large volumes of the Cd(II)-In(III) mixture solute, respectively.

3.2.2.1 Elution Chromatography

Elution performance of the cadmium(II) – indium(III) couple has been investigated by feeding chromatographic columns of 1g 12-molybdocerate (IV) with 5ml mixture solutions consisting of 5×10^{-4}M cadmium(II) and 10^{-5}M indium(III) in dilute acid solutions.

Table 10. Individual distribution coefficient (K_d)values and separation factores (α) of In(III) Cd(II) couple in HNO_3 and HCl acid solutions on 12-molybdocerate(IV)

Metal ion Concentration; M		Concentration of the equilibrating solutions											
		0.01M HNO_3			0.05M HNO_3			0.01M HCl			0.05M HCl		
		Distribution coefficient (K_d) values, ml/g											
		In^{3+}	Cd^{2}		In^{3+}	Cd^{2+}		In^{3+}	Cd^{2}		In^{3+}	Cd^{2+}	
Product In^{3+}	Target Cd^{2+}	Separation factor $\alpha=K_d(In) / K_d(Cd)$											
		K_d	K_d	α	K_d	K_d	α	K_d	K_d	α	K_d	K_d	α
$5x10^{-4}$	$5x10^{-4}$	150	50	3	150	5	30	90	31	2.9	90	4	22.5
10^{-4}		200	50	4	200	5	40	120	31	3.87	120	4	30
$5x10^{-5}$		249	50	4.98	249	5	49.8	170	31	5.48	170	4	42.5
10^{-5}		307	50	6.14	307	5	61.4	200	31	6.45	200	4	50
$5x10^{-4}$	10^{-4}	150	120	1.25	150	18	8.33	90	55	1.64	90	10	9
10^{-4}		200	120	1.67	200	18	11.1	120	55	2.18	120	10	12
$5x10^{-5}$		249	120	2.08	249	18	13.8	170	55	3.09	170	10	17
10^{-5}		307	120	2.56	307	18	17.1	200	55	3.64	200	10	20
$5x10^{-4}$	$5x10^{-5}$	150	150	1	150	24	6.25	90	115	0.78	90	18	5
10^{-4}		200	150	1.3	200	24	8.33	120	115	1.04	120	18	6.67
$5x10^{-5}$		249	150	1.66	249	24	10.4	170	115	1.48	170	18	9.44
10^{-5}		307	150	2.05	307	24	12.8	200	115	1.74	200	18	11.1
$5x10^{-4}$	10^{-5}	150	180	0.83	150	36	4.17	90	160	0.56	90	27	3.33
10^{-4}		200	180	1.11	200	36	5.56	120	160	0.75	120	27	4.44
$5x10^{-5}$		249	180	1.38	249	36	6.92	170	160	1.06	170	27	6.29
10^{-5}		307	180	1.71	307	36	8.53	200	160	1.25	200	27	7.41

Table 11. Breakthrough characteristics of Cd(II) and In(III) in HCl and HNO_3 acid solutions from 1g 12-molybdocerate(IV) columns at a flow rate of 1ml/min

Metal ion conc., M	Character	Concentration of HCl, M				Concentration of HNO_3, M			
		0.01		0.05		0.01		0.05	
		Cd	In	Cd	In	Cd	In	Cd	In
10^{-5}	V(1%)	15	50	4	25	20	56	6	35
	V(50%)	300	750	100	600	400	850	150	700
	V(100%)	450	1125	120	810	600	1275	180	945
	C, meq/g	$6x10^{-3}$	$2.3x10^{-2}$	$2x10^{-3}$	$1.8x10^{-2}$	$8x10^{-3}$	$2.6x10^{-2}$	$3x10^{-3}$	$2.1x10^{-2}$
$5x10^{-5}$	V(1%)	3	10	1	5	4	11	1	7
	V(50%)	60	150	20	120	80	170	30	140
	V(100%)	90	225	24	162	120	255	36	189
	C, meq/g	$6x10^{-3}$	$2.3x10^{-2}$	$2x10^{-3}$	$1.8x10^{-2}$	$8x10^{-3}$	$2.6x10^{-2}$	$3x10^{-3}$	$2.1x10^{-2}$
10^{-4}	V(1%)	2	5	1	3	2	6	1	4
	V(50%)	30	75	10	60	40	85	15	70
	V(100%)	45	112	12	81	60	128	18	94
	C, meq/g	$6x10^{-3}$	$2.3x10^{-2}$	$2x10^{-3}$	$1.8x10^{-2}$	$8x10^{-3}$	$2.6x10^{-2}$	$3x10^{-3}$	$2.1x10^{-2}$
$5x10^{-4}$	V(1%)	1	1	1	1	1	1	1	1
	V(50%)	6	15	2	12	8	17	3	14
	V(100%)	9	23	3	16	12	26	4	19
	C, meq/g	$6x10^{-3}$	$2.3x10^{-2}$	$2x10^{-3}$	$1.8x10^{-2}$	$8x10^{-3}$	$2.6x10^{-2}$	$3x10^{-3}$	$2.1x10^{-2}$

3.2.2.1.1 Effect of Nature and Concentration of the Eluent

Cadmium (II) and indium (III) elution performances were investigated as a function of kind and concentration of the acid eluents. Figure 43 depicts the effect of 0.05 and 0.01M nitric acid solutions, as eluents, on the elution profiles and yields of the cadmium (II) – indium (III) couple from 1 g 12-molybdocerate (IV) columns at a flow rate of 0.5 ml/min. It is distinct that Cd(II) is readily eluted in the first 1ml eluate 0.01 and 0.05M HNO_3 acid solution as an eluents. Elution of In(III) is achieved in the form of a sharp elution profile in the 2-4ml 0.05MHNO_3 acid solution. While, a diffuse-tailed elution curve characteristic for In(III) elution behaviour with low acid concentration (0.01M acid) is obtained. It was found that as the acid concentration increases; the corresponding elution efficiency (i.e., elution yield) increases and distribution of the eluted radioactivity is concentrated in smaller eluate volumes. Whereas; 96.3% and 81.4% of the Cd (II) radioactivity is eluted in the first 1ml; 34.75% and 6.4% of the indium (III) radioactivity is concentrated in the 2-4ml eluates of 0.05 and 0.01 M HNO_3 acid; respectively.

Figure 44 shows the elution profiles of the respective radiotracers with 0.05 and 0.01M hydrochloric acid. More or less similar elution profiles of Cd(II) and In(III) with nitric and hydrochloric acid solutions have been obtained. It was found that about 98.6% and 89.3% of the Cd(II) radioactivity is eluted in the first 1ml of the HCl acid eluates; whereas; 62.3% and 9.3% of the indium(III) radioactivity is eluted in the 2-4ml eluate fraction of 0.05 and 0.01M HCl acid, respectively. It is distinct from figures 43 and 44 that the positions of the maximum elution peaks of In(III) are displaced to higher eluate volumes (and lower elution yields were obtained) when nitric acid solutions were used as eluents in agreement with its batch distribution and dynamic behaviour data.

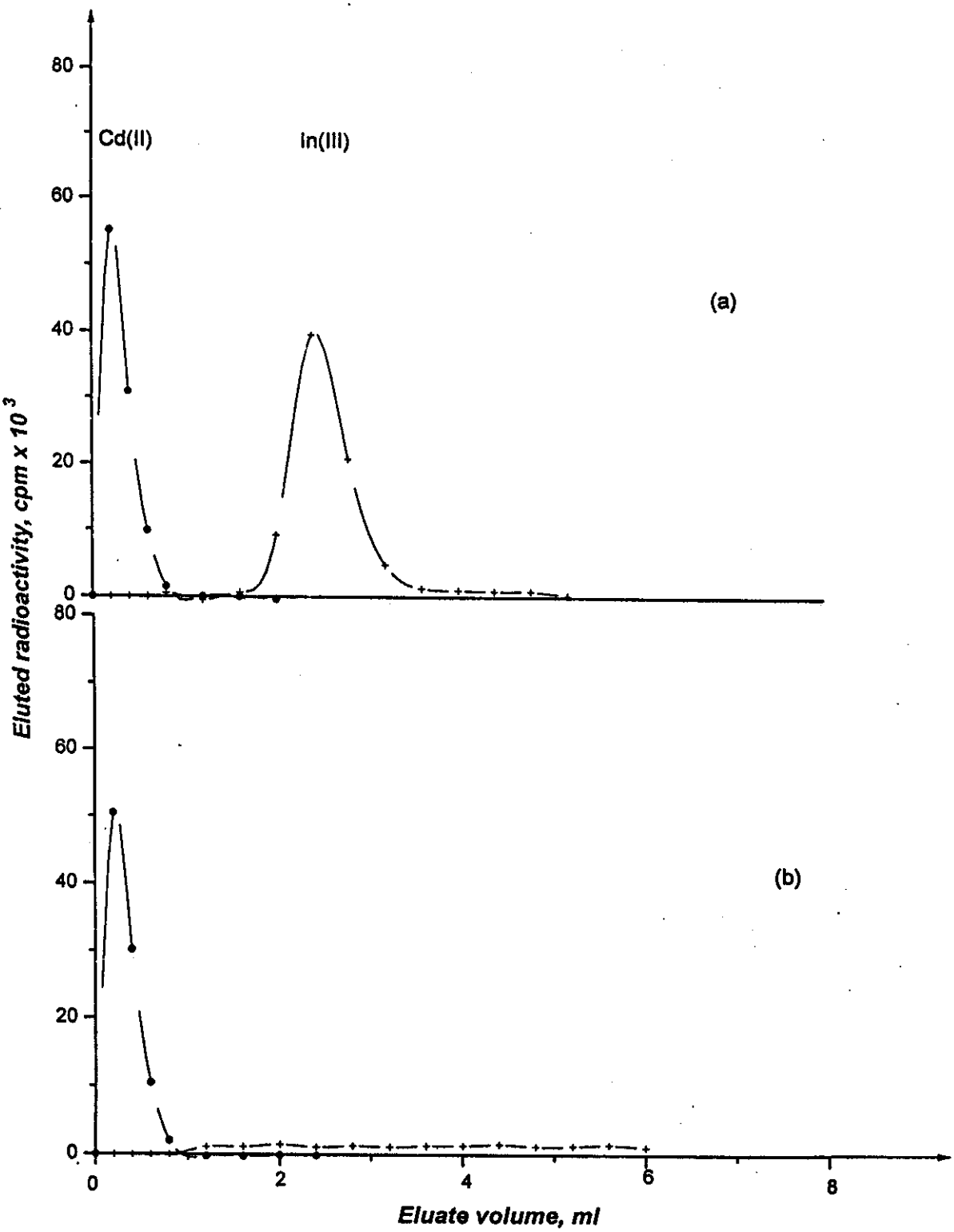

Fig.43.Elution curves of Cd(II) from In(III) onto 1g 12-molybdocerate(IV) columns(0.6cmx3.5cm) with (a)0.05 (b)0.01M HNO_3 acid solutions at flow rate of 0.5ml/min.

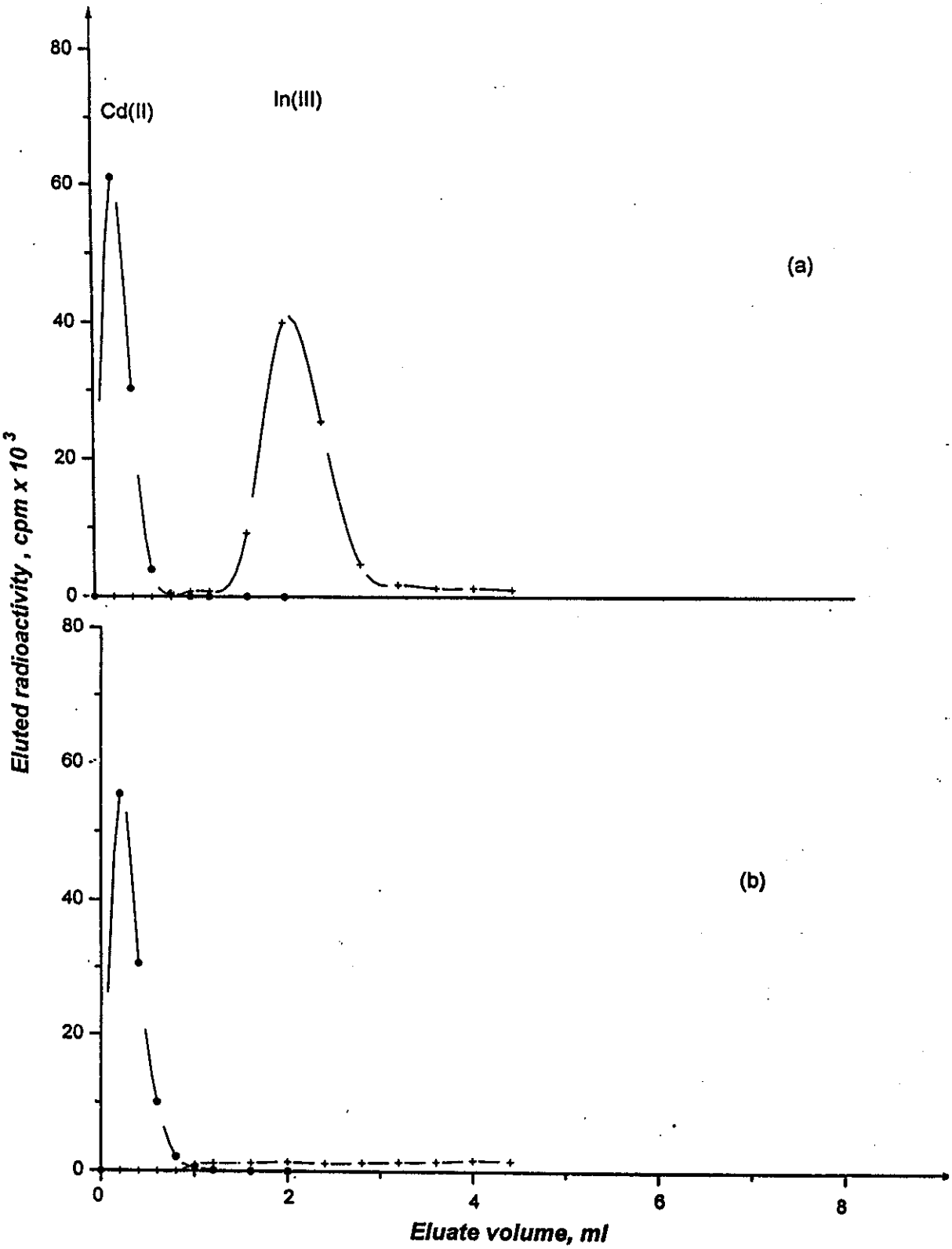

Fig.44. Elution curves of Cd(II) from In(III) onto 1g 12-molybdocerate(IV) columns (0.6cm i.d x3.5cm) with (a)0.05 (b) 0.01M HCl acid solutions at flow rate of 0.5ml/min.

3.2.2.1.2 Effect of Flow Rate of the Eluent

Figures 45 and 46 (curves a,b and c) display the elution profiles of indium (III) and cadmium (II) radiotracers from 1g 12-molybdocerate (IV) columns with 0.05 and 0.01 M hydrochloric acid solutions at flow rates of 0.5; 1 and 2 ml/min; respectively. It is observed that the positions of the maximum elution peaks are displaced to higher eluate volumes with decreasing the acid concentrations and / or increasing the flow rates of the eluent. The obtained broad elution profiles with somewhat diffused fore- and aft-boundaries with increasing the eluent flow rates may be attributed to slow sorption / desorption kinetics of the indium (III) and cadmium (II) radiotracers onto the surface of the sorbent matrix to the eluent [i.e.slow diffusion mechanism].

Figures 47 and 48 show that the elution behaviour of Cd(II) and In(III) with nitric acid solutions; have more or less similar elution profiles as mentioned above. It was found that about 96.3% , 82.5% and 74.1% of Cd (II) radioactivity are obtained in the first 1ml 0.05HNO_3 acid solution about 34.75%; 21% and 7.6% of indium (III) radioactivity are obtained in the eluate fractions of 1-3, 2-5 and 2-7 ml at flow rates of 0.5, 1 and 2 ml/min; respectively. It is obvious that the elution yield of In(III) is relatively low in dilute acid eluents ($\leq$ 0.05M acid).

3.2.2.1.3 Recommended Procedure for Elution separation of the Cadmium (II) – Indium (III) Couple

In case of small amounts of the cadmium(II) target not exceeding fifteen percent of the total sorption capacity of the 12-molybdocerate (IV) bed matrix in small volume of solute, the chromatographic column elution mode is recommended for radiochemical separation of the product In (III) radiotracer.

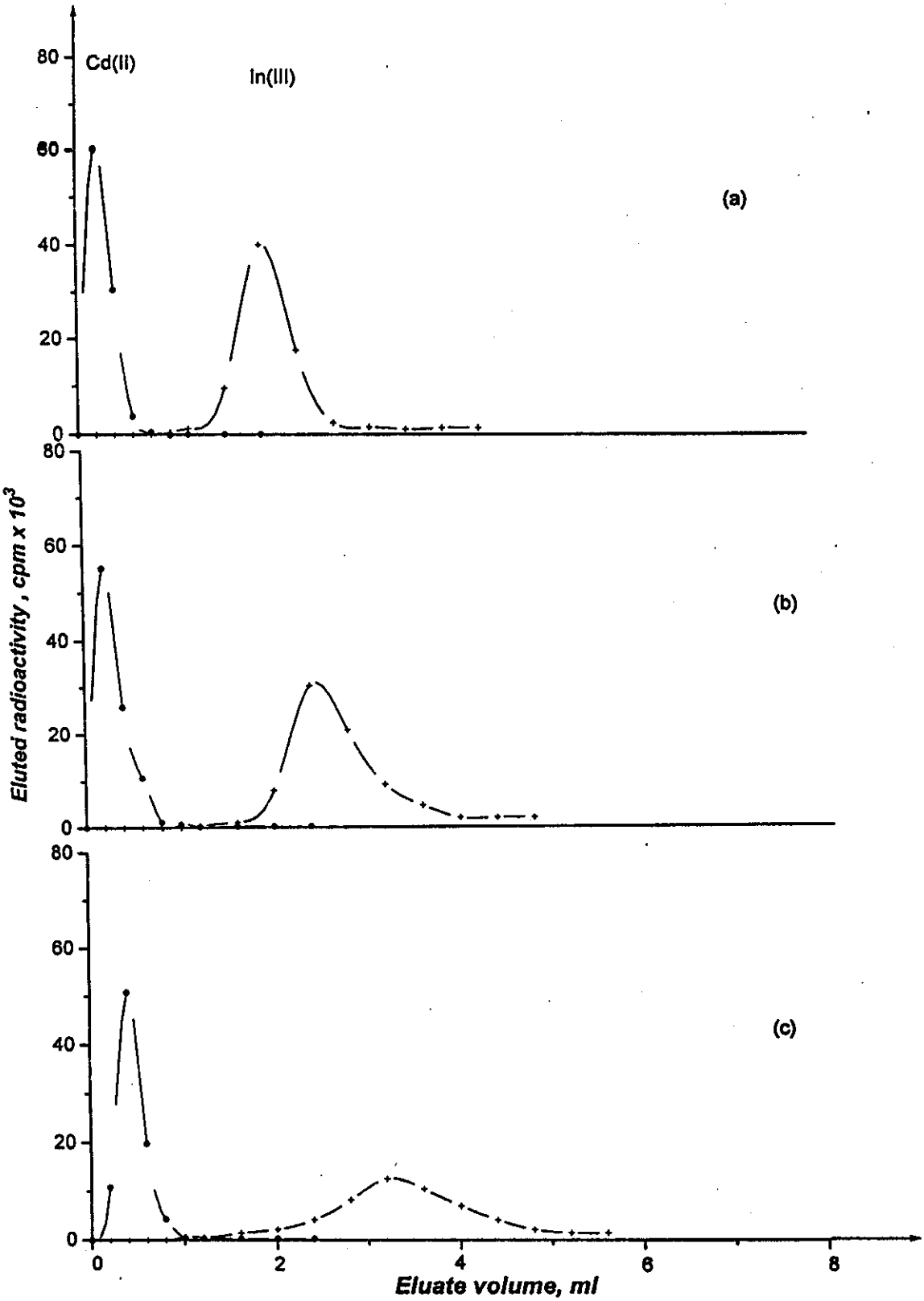

Fig.45. Elution curves of Cd(II) from In(III) onto 1g 12-molybdocerate columns (0.6cm i.d x 3.5cm) with 0.05M HCl at a flow rate of (a)0.5ml/min (b)1.0ml/min (c)2.0ml/min

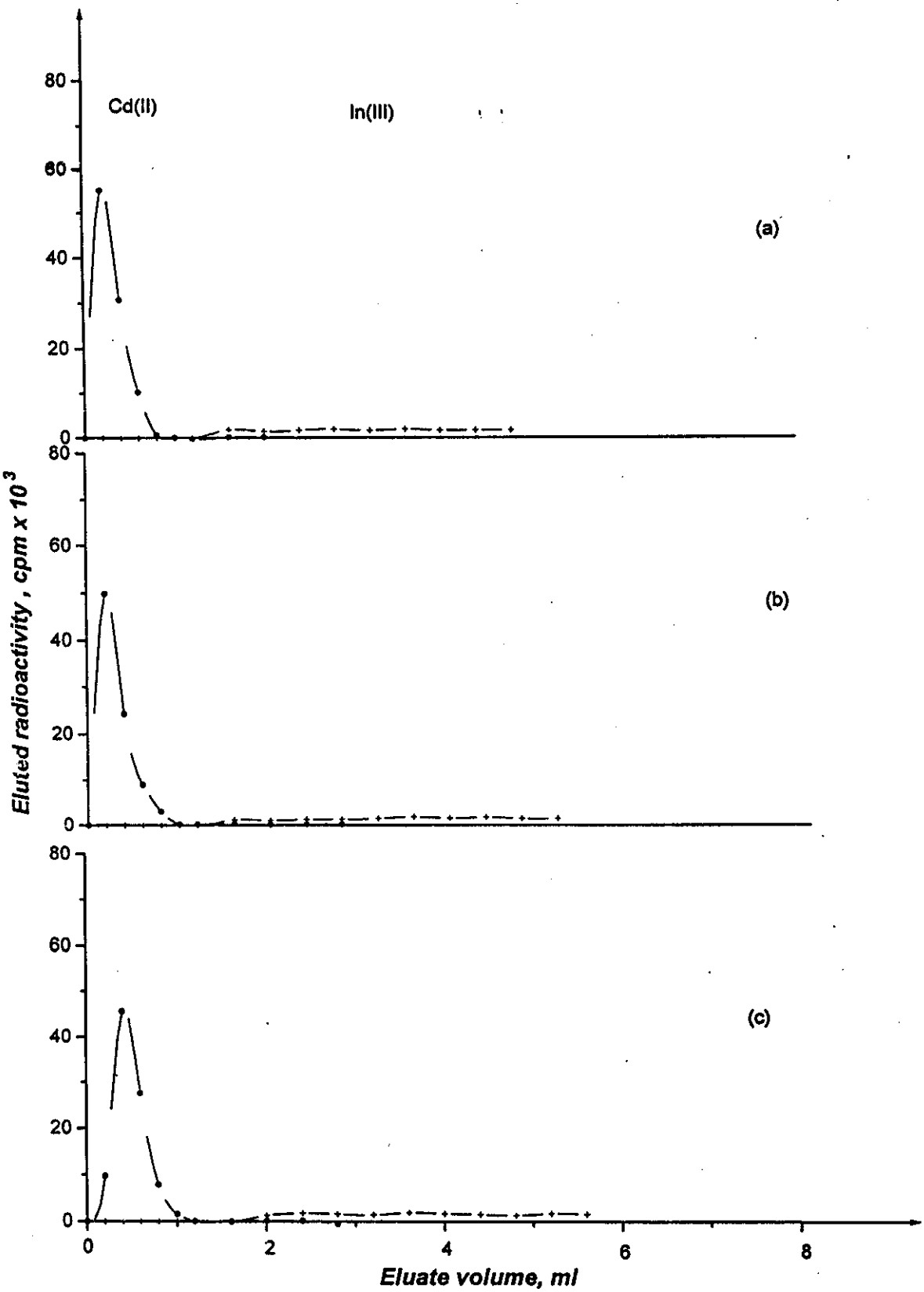

Fig.46. Elution curves of Cd(II) from In(III) onto 1g 12-molybdocerate columns (0.6cm i.d x 3.5cm) with 0.01M HCl at a flow rate of (a)0.5ml/min (b)1.0ml/min (c)2.0ml/min

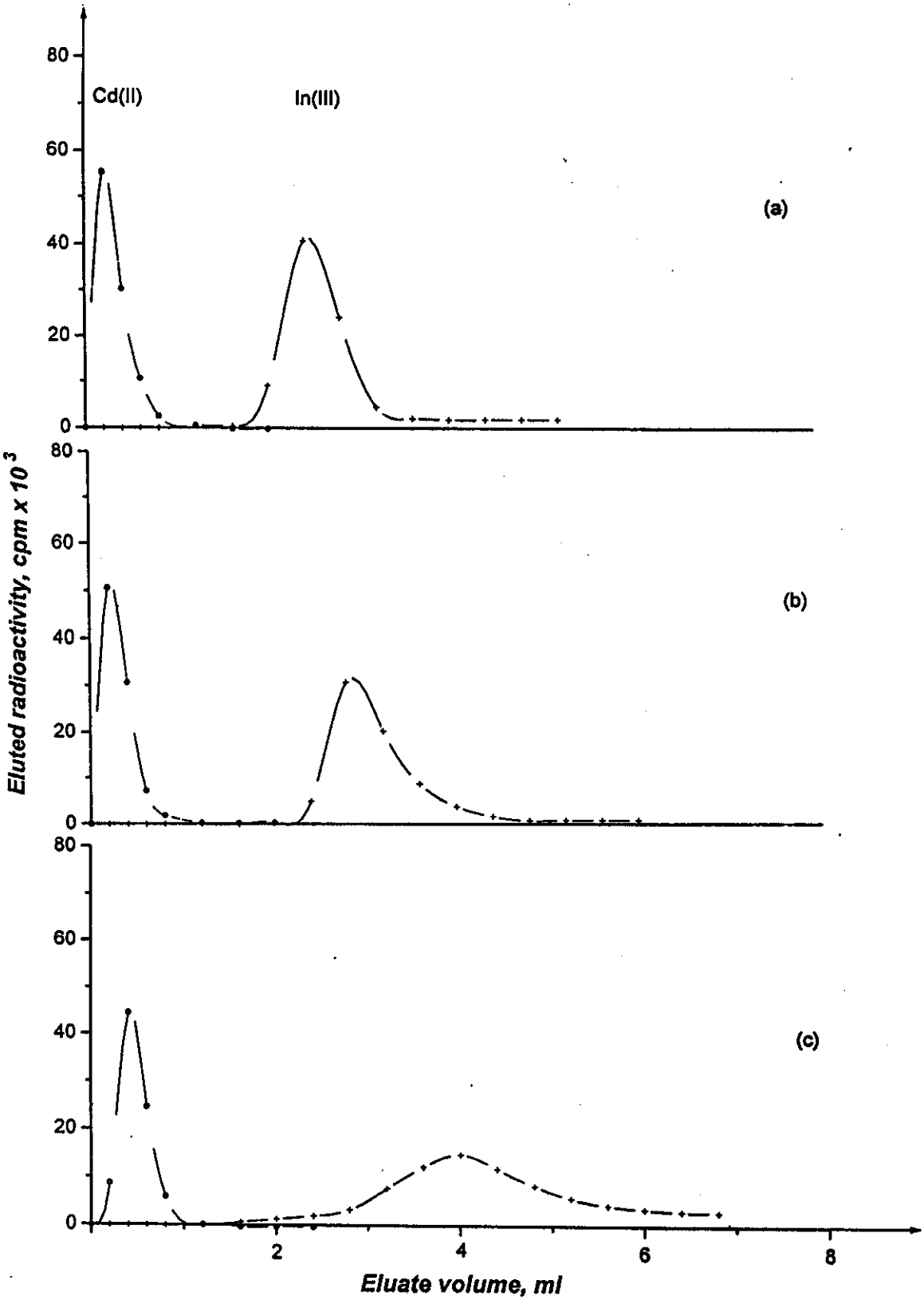

Fig.47. Elution curves of Cd(II) from In(III) onto 1g 12-molybdocerate columns (0.6cm i.d x 3.5cm) with 0.05M HNO_3 at a flow rate of
(a)0.5ml/min (b)1.0ml/min (c)2.0ml/min

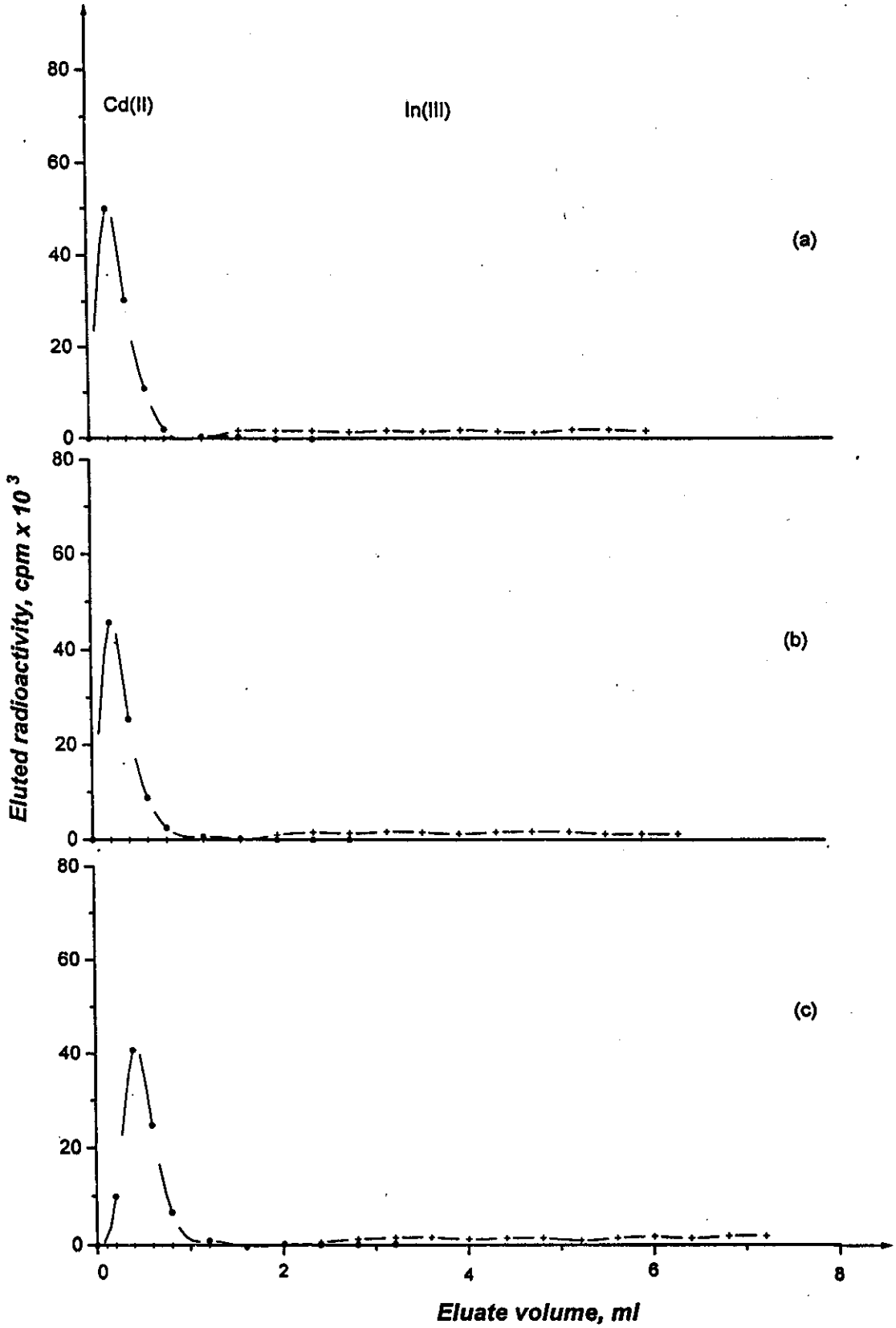

Fig.48. ELution curves of Cd(II) from In(III) onto 1g 12-molybdocerate columns (0.6cm i.d x 3.5cm) with 0.01M HNO_3 at a flow rate of (a)0.5ml/min (b)1.0ml/min (c)2.0ml/min

In this process 5ml of the mixture solution [<< 10^{-5}M In(III) and ~ 5x 10^{-4}M Cd(II)] in 0.01M HNO_3 acid is loaded onto 1g 12-molybdocerate(IV) column. Elution and purification of the bed matrix from retained Cd(II) is carried out successively with passing 5ml 0.01M HNO_3 acid and 2ml 0.05M HCl acid solutions at a flow rate of 0.5ml/min. Thereafter, In(III) is eluted with passing 10ml 0.1M HCl acid solution at flow rate of 1ml/min as shown in figure 49. The elution yield was found to be about 97.3% of indium (III) radioactivity loaded onto the column high concentration radioactivity of In(III) is collected in the first 5ml eluate. The obtained elution yield is comparable with those obtained from cation exchange resins such as AG 50W – X8;50-100 mesh and Dowex 50WX8. 200-400 mesh (i.e., 95 and 89%) respectively[86,82]. Figure 50 shows the proposed schematic diagram for separation of carrier-free In(III) from its bulk Cd(II) target by the chromatographic column elution method.

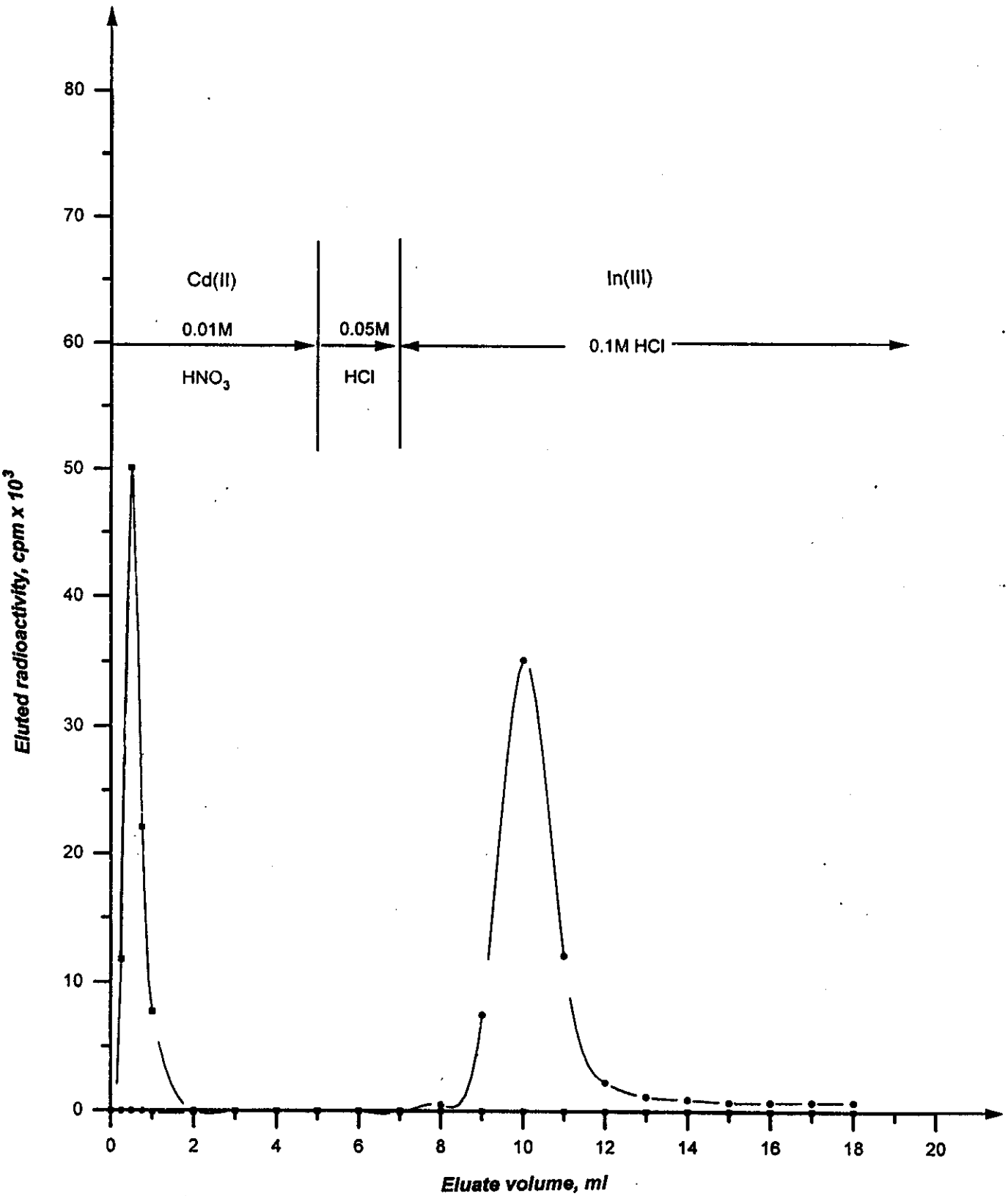

Fig.49. Typical elution profile of In(III) from Cd(II) onto 1g 12-molybdocerate(IV) column (0.6cm i.d x 3.5cm) with HNO_3 and HCl acid solutions at a flow rate of 1ml/min.

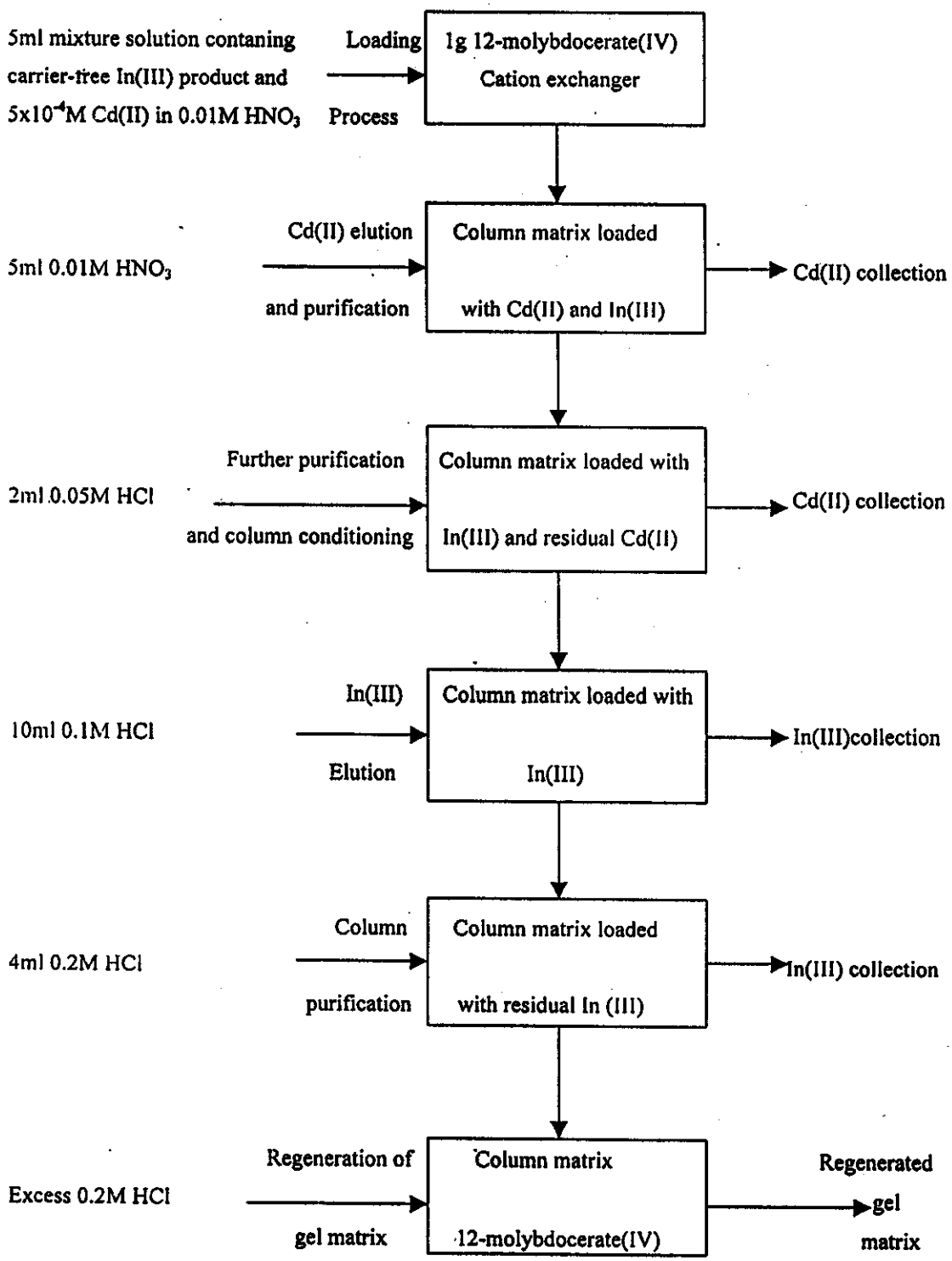

Fig.50. Proposed schematic diagram for separation of carrier-free In(III) from cyclotron irradiated Cd(II) targets by chromatographic column elution method.

3.2.2.2 Frontal Chromatography

In cyclotron produced radioisotopes; the target material and the product radiotracer are usually present in about 80 ml of the etching solution[82,83]. Hence; use of the frontal method for Cd (II) – In (III) separation is of great importance in practice compared to the elution method. In this process Cd(II)-In(III) separation can be achieved by passing 40ml of a mixture solution consists of $5x10^{-4}$M Cd(II) and In(III) radiotracers in 0.01M HNO_3 acid solution through a small chromatographic column packed with 1g 12-molybdocerate(IV) matrix (0.6 cm i.d x 3.5cm)at a flow rate of 1ml/min.

3.2.2.2.1 Recommended Procedure for Frontal Separation of the Cadmium (II)–Indium (III) Couple

The optimum operating conditions for the separation of indium(III) radiotracer from a bulk amount of cadmium(II) target solute could be elucidated from the previously obtained breakthrough behaviour characteristics as well as the elution profiles data. Figure 51 shows a typical frontal separation profiles of 60ml $5x10^{-4}$M Cd(II) - 10^{-5}M In(III) mixture in 0.01M nitric acid solution using 1 g 12-molybdocerate (IV) matrix at a flow rate of 1 ml / min. It is obvious that Cd (II), with the lowest tendency for the sorbent matrix, immediately migrates along the column bed, while indium (III) with the highest tendency for the molybdate gel in the identified and concentration value accumulates onto the sorbent matrix. Therefore the retained Cd(II) was washed out off the column with 5ml 0.05M HNO_3 acid solution at flow rate 0.5ml/min. Further, purification and conditioning of the bed matrix is carried out with passing 2ml 0.05M HCl at the same flow rate. Thereafter; In(III) is eluted with 10ml 0.1M HCl acid solution at flow rate of 1ml/min.

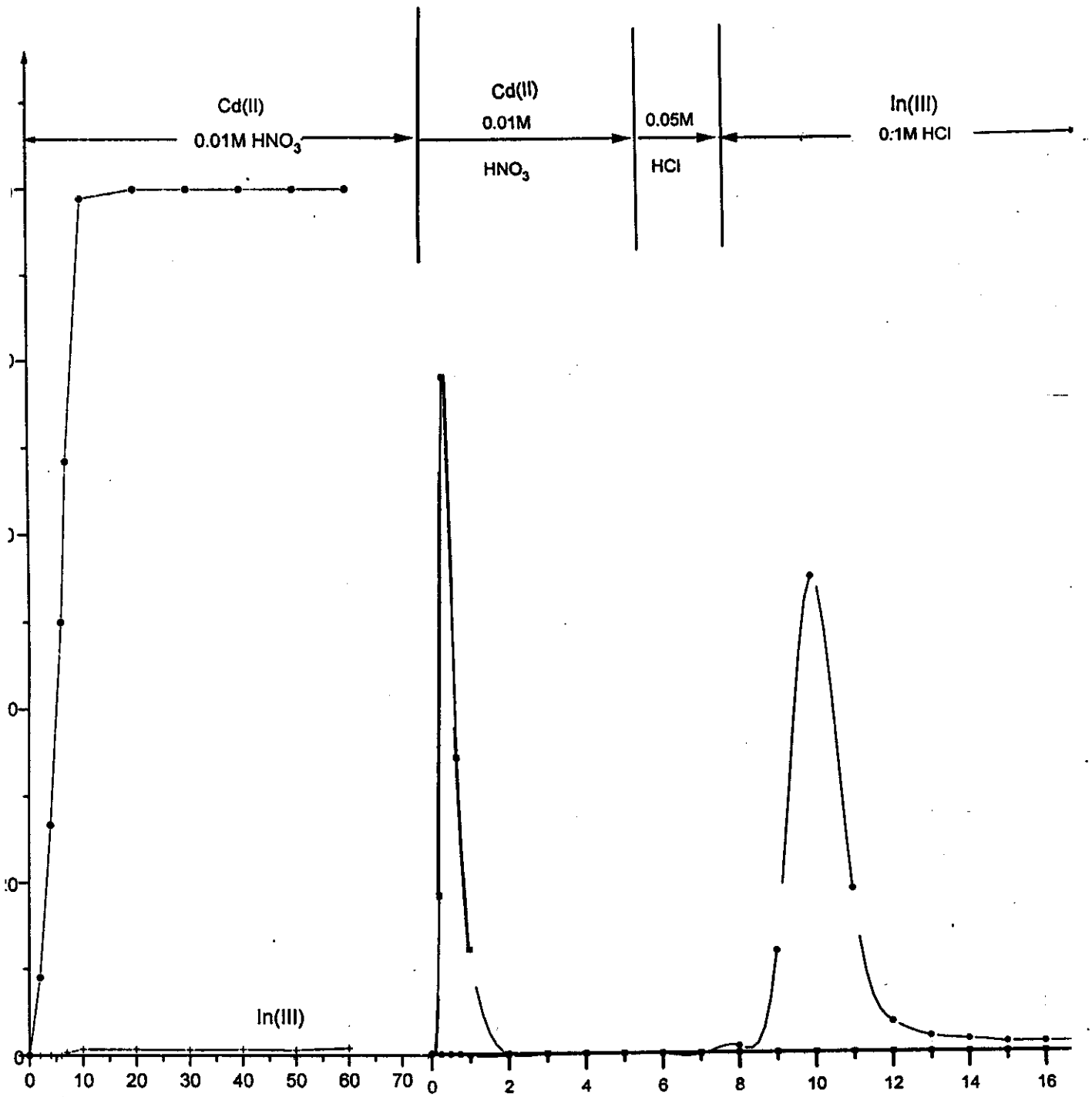

Fig.51. Frontal separation of a mixture solution containing $5x10^{-4}$M Cd(II) and 10^{-5}M In(III) from 1g 12-molybdocerate(IV) columns (0.6cm i.d x 3.5cm) with HNO_3 and HCl acid solutions.

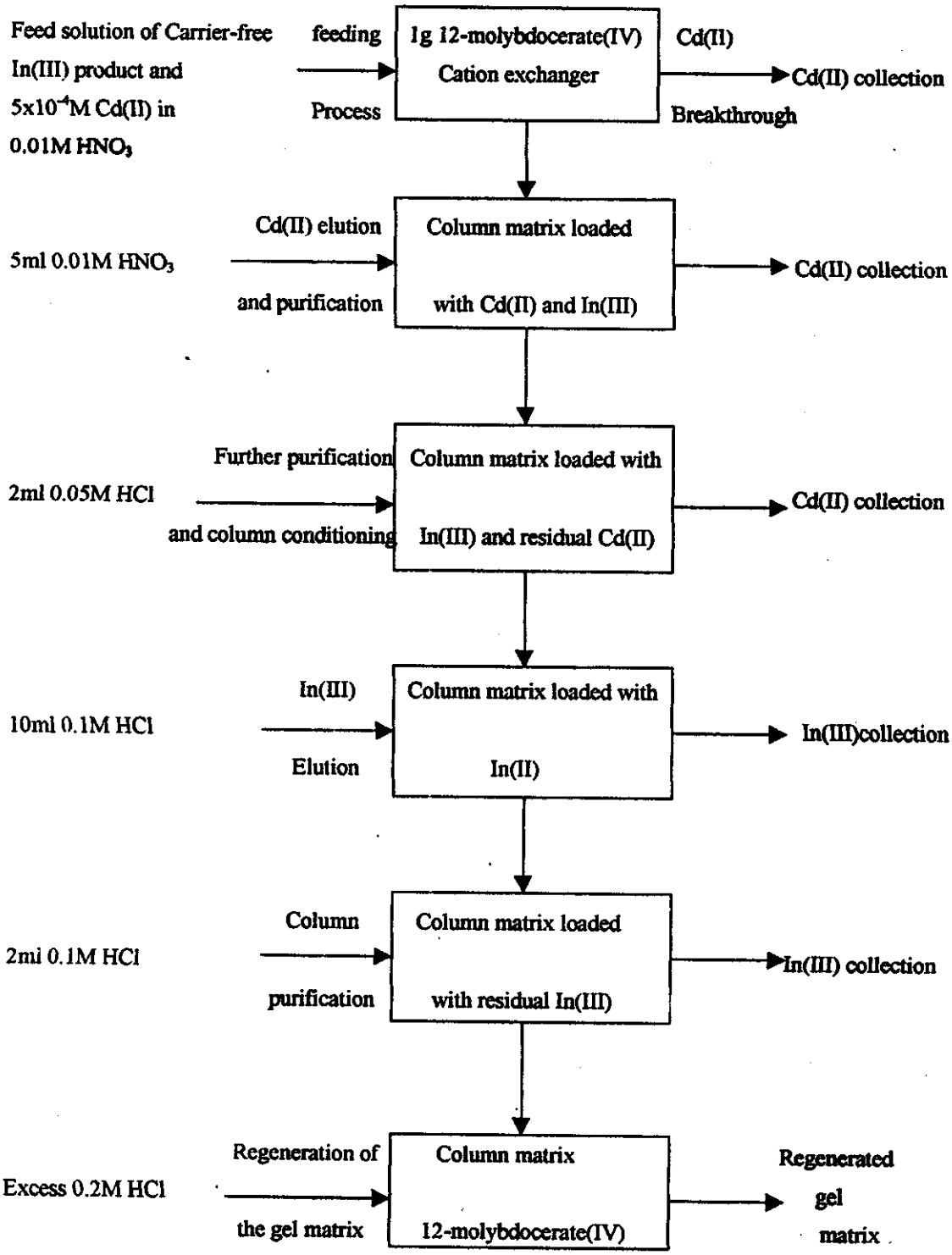

Fig.52. Proposed schematic diagram for separation of carrier-free In(III) from cyclotron irradiated Cd(III) targets by chromatographic column frontal method.

Figure 52 shows the proposed schematic diagram for separation of carrier-free In(III) from its irradiated Cd(II) target by the chromatographic column frontal method.

3.2.3 Regeneration of the Column Matrix

To replace the higher valency indium(III) ion which may be remaining on the exchanger by one of lower valency (i.e H^+); the conversion is carried out by using relatively concentrated acid solution. Therefore; The conversion of the bed matrix to the H^+-form was carried out with passing sufficient volume (about 30 times the matrix volume) of 0.2M nitric or hydrochloric acid solutions through the chromatographic column bed at a flow rate of 0.5 ml/min to ensure the complete conversion of the molybdocerate matrix to the H^+-form.

3.3 Silver (I) - Indium (III) Couple

3.3.1 Distribution Behaviour Investigations

3.3.1.1 Static studies

The distribution behaviour of the silver(I) and indium(III) radiotracers in 0.005-0.5M nitric acid solutions on 12-molybdocerate(IV) matrix were individually investigated by the batch equilibration method in a shaker thermostat adjusted at 25±1°C.

3.3.1.1.1 Effect of H^+- ion Concentration

Figure 53 shows the effect of nitric acid concentration on the distribution behaviour of $5x10^{-4}$M silver(I) on 12-molybdocerate (IV) at 25±1°C. It is obvious that Ag(I)have high affinity towards the sorbent material with almost constant K_d values of about 1034 ml/g in dilute acid solution of concentrations up to around 0.1M HNO_3. Thereafter; the corresponding K_d values linearly decrease to 149ml/g with increasing the acid concentration up to 0.5M HNO_3. At acid concentrations ≤ 0.1M HNO_3, silver(I) ions have distinct tendency to form species of Ag^+ which are tightly retained onto the matrix by ion exchange reaction with the exchangeable counter H^+- sites on the surface of the 12-molybdocerate (IV) matrix. At acid concentrations ≥0.1M HNO_3, the concentration of the competing H^+ ions in solutions increases and silver(I) ions tend to form $Ag(NO_3)$ molecular species; which may contribute to the observed decrease in the corresponding distribution coefficient values.

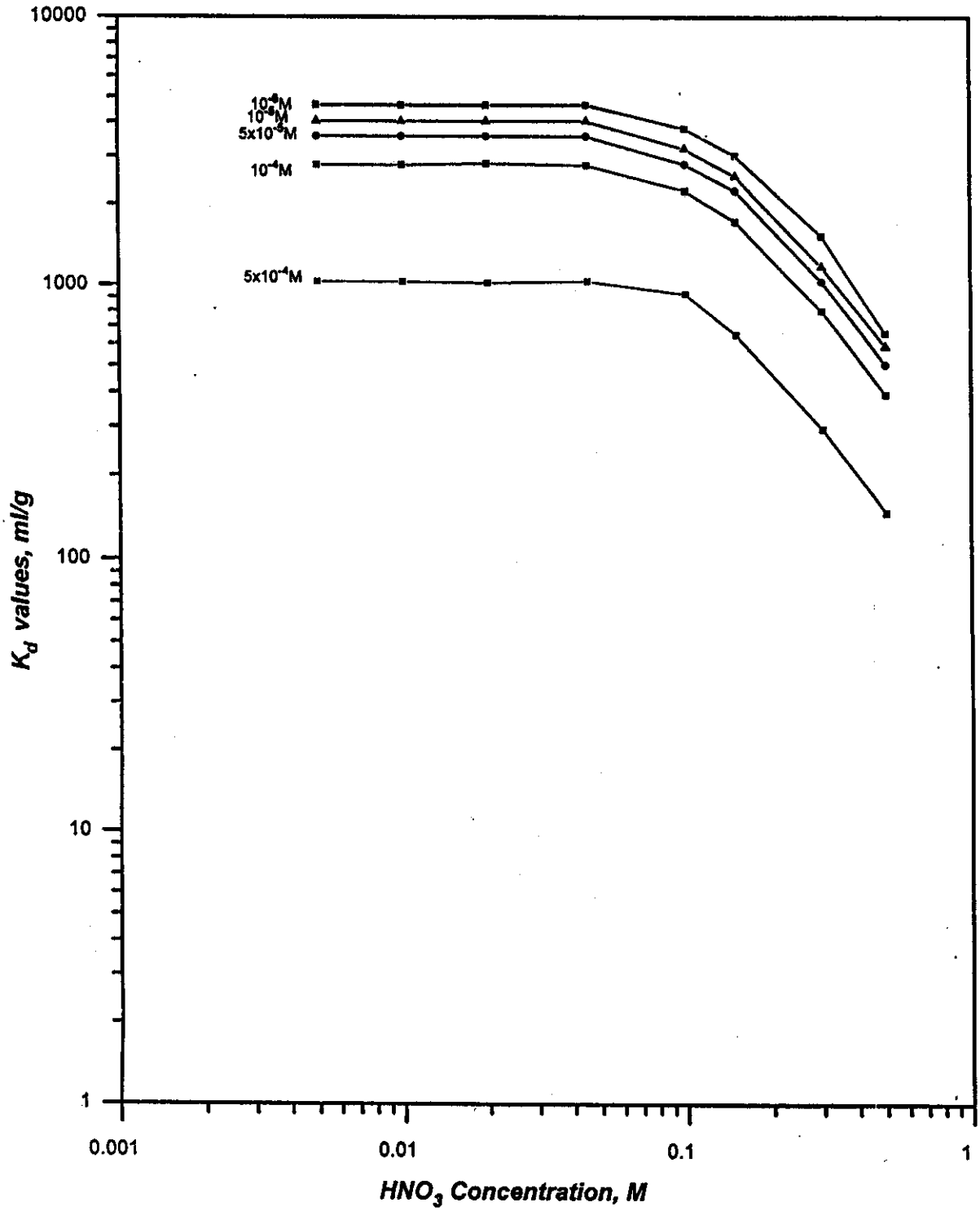

Fig.53.Distribution coefficient (K_d) values of Ag(I) in HNO_3 acid solutions on 12-molybdocerate (IV) at different Ag(I) concentrations(25±1 °C).

The interaction of Ag(I) in HNO_3acid solutions ≥0.1M with the MoCe(IV) gel follows more or less an ideal cation exchange mechanism described by the following equation:

$$\overline{R^-H^+} + Ag^+_{solution} \longleftrightarrow \overline{R^-Ag^+} + H^+_{solution}$$

where $\overline{R^-H^+}$ is the solid cation exchanger (MoCe) containing the exchangeable H^+ ions.

The retention of Ag^+ onto heteropoly acid ion exchangers such as ammonium phosphomolybdate (AMP) and ammonium phosphotungstate (AWP) as well as 12-molybdocerate(IV), is characterized by a plateau of almost constant K_d values in dilute acid solutions of concentrations up to around 0.1M acid[152, 153]. The high selectivity of the heteropolyacids and their salts for large monovalent cations (LMC) such as Ag^+; Cs^+ and Tl^+ may be attributed to their inorganic nature and chemical structure. The retention of LMC increases with the increase in their non-hydrated ionic diameter to form insoluble heteropoly acid salts via covalent bonding. It is observed that the K_d values of Ag(I)>In(III) (Fig.53 compared to Fig.36). The large non-hydrated ionic radii; small hydrated radii, of Ag^+ ion (1.15A°) compared to In (0.85A°)[155, 156]allows it to approach more closely to the negative sites of attachment on the cation exchanger by an electrostatic bounding force.

3.3.1.1.2 Effect of Concentration of the Radiotracers

Figures 53 and 36 show the effect of metal ions concentrations on the distribution behaviours of Ag(I) and In(III) radiotracers [ranging from 10^{-6} to $5x10^{-4}$ M] in HNO_3 acid solutions on 12-molybdocerate (IV) gel. It is obvious that the K_d values of Ag(I) and In(III) decrease with increasing the corresponding metal ions concentration. However, at comparable conditions, silver(I) ions are more strongly retained onto the 12-molybdocerate(IV) matrix than its indium(III) product. So, separation of

macro or micro amounts [≥ $5x10^{-4}$M Ag(I)] of Ag target in ≤0.1M HNO_3 from the indium(III) product present in trace amount [<<10^{-6}M In(III)] could be achieved onto 12-molybdocerate (IV) columns.

3.3.1.2 Dynamic studies

The breakthrough characteristics of Ag(I) and In(III) from 1g MoCe(IV) columns were individually investigated in 0.01; 0.05; 0.1 and 0.2M HNO_3 acid solutions containing different metal ions concentrations. In breakthrough technique the feed solution was continuously passed through the column bed at a flow rate of 1ml/min and room temperature (25°C). The column effluents were radiometrically analysed and the counting rates (C_v) of equal volume fractions were compared with standard samples (C_o). The obtained results were drawn in the form of breakthrough curves (C_v /C_o, % vs. effluent volume, ml).

3.3.1.2.1 Effect of Concentration of the Radiotracers

Figure 54 (curves a, b and c) shows that the breakthrough of Ag(I) in 0.2M HNO_3 acid solutions are delayed to higher effluent volumes with decreasing the metal ions concentration in the feed solution. However 10^{-5}M In(III) in 0.2M HNO_3 acid solution (Curve d) demonstrates immediate breakthrough of In(III) radiotracer, the positions of 100% In(III) and 1% Ag(I) breakthrough (i.e, In-Ag resolution) are delayed towards higher effluent volumes with decreasing the target concentration in the feed solution.

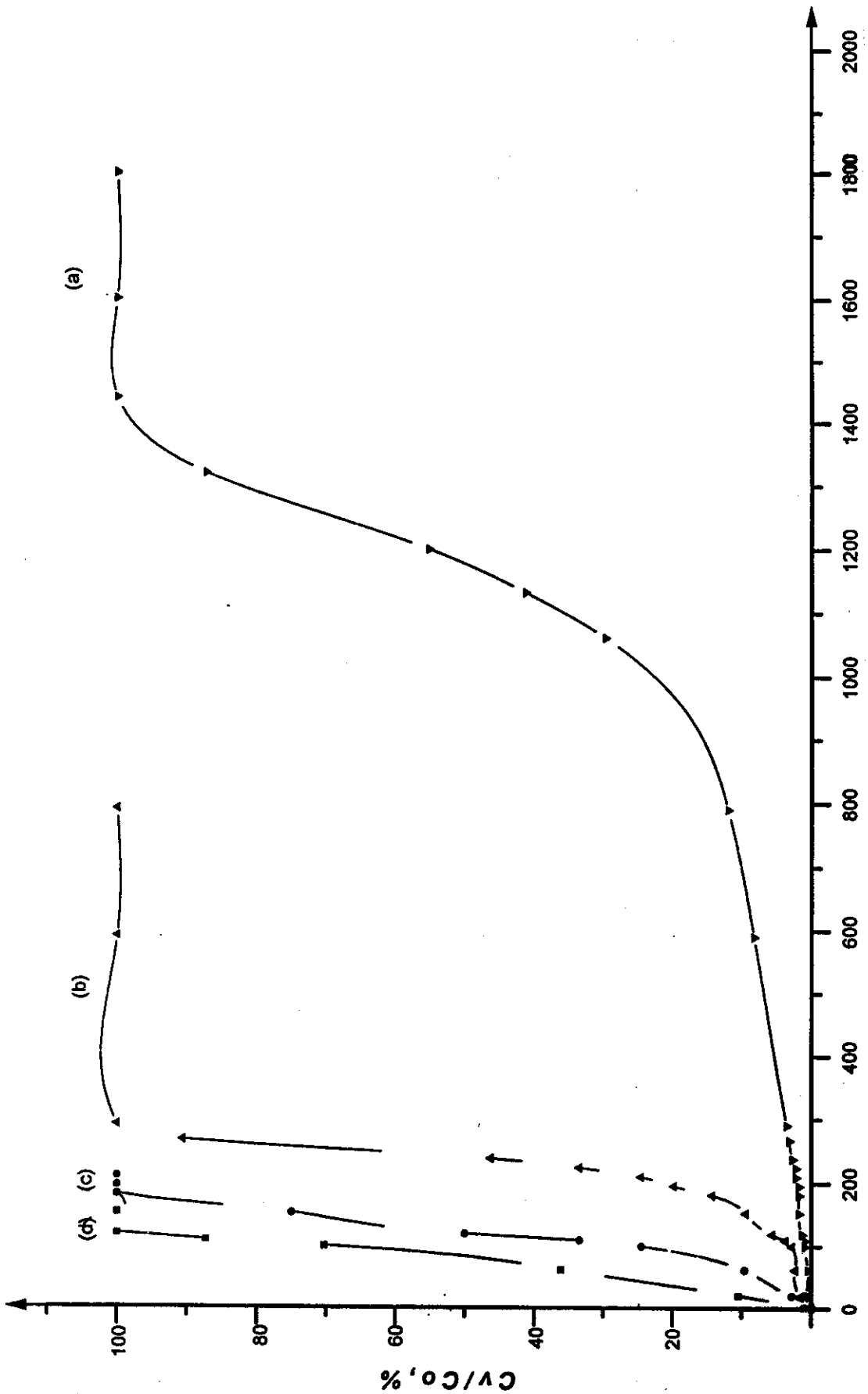

Fig.54. Breakthrough curves of In(III) and Ag(I) in 0.2M HNO_3 from 1g 12-molybdocerate(IV) columns (0.6cmi.dx3.5cm) at a flow rate of 1ml/min as a function of metal ions concentrations
(a)10^{-5}M Ag(I) (b)$5x10^{-5}$M Ag(I) (c)10^{-4}M Ag(I) (d)10^{-5}M In(III)

Taking into consideration that the sorption affinity of indium would be seriously affected by the silver concentration in solution, the distribution ratio of indium would decrease with increasing the silver concentration. So, chromatographic columns packed with adequate amounts of the molybdate matrix would achieve quantitative uptake of the silver(I) target dissolved in ?0.1M acid solutions, with distinct separation resolution from its indium(III) product.

3.3.1.2.2 Effect of Chemical Composition of the Feed Solution

Figures 54-57 show the effect of concentration of nitric acid in the feed solutions on the individual breakthrough behaviour of silver(I) and indium(III) from 1g 12-molybdocerate columns. It is obvious that the breakthrough of Ag(I) and In(III) are delayed; to higher effluent volumes, as the concentration of nitric acid was decreased from 0.2 to 0.01M acid. This observation is in accordance with the increase in K_d values at lower acidity of the equilibration solution. Therefore; dilute nitric acid solutions will meet with the column loading and washing process to achieve high uptake values and delayed breakthrough of the respective(mainly Ag^+) radiotracers.

3.3.2Chromatographic Column Separations

It is clear from the aforementioned distribution coefficient values that silver(I) ions in nitric acid solutions have marked sorption affinity towards the 12-molybdocerate (IV) matrix compared with its indium(III) product, under similar experimental conditions. Table 12 illustrates the separation factor [α] values of silver(I) from indium(III) in nitric acid solutions at different concentrations of acid and metal ions. The separation factor [α] values reflect the versatility of 12-

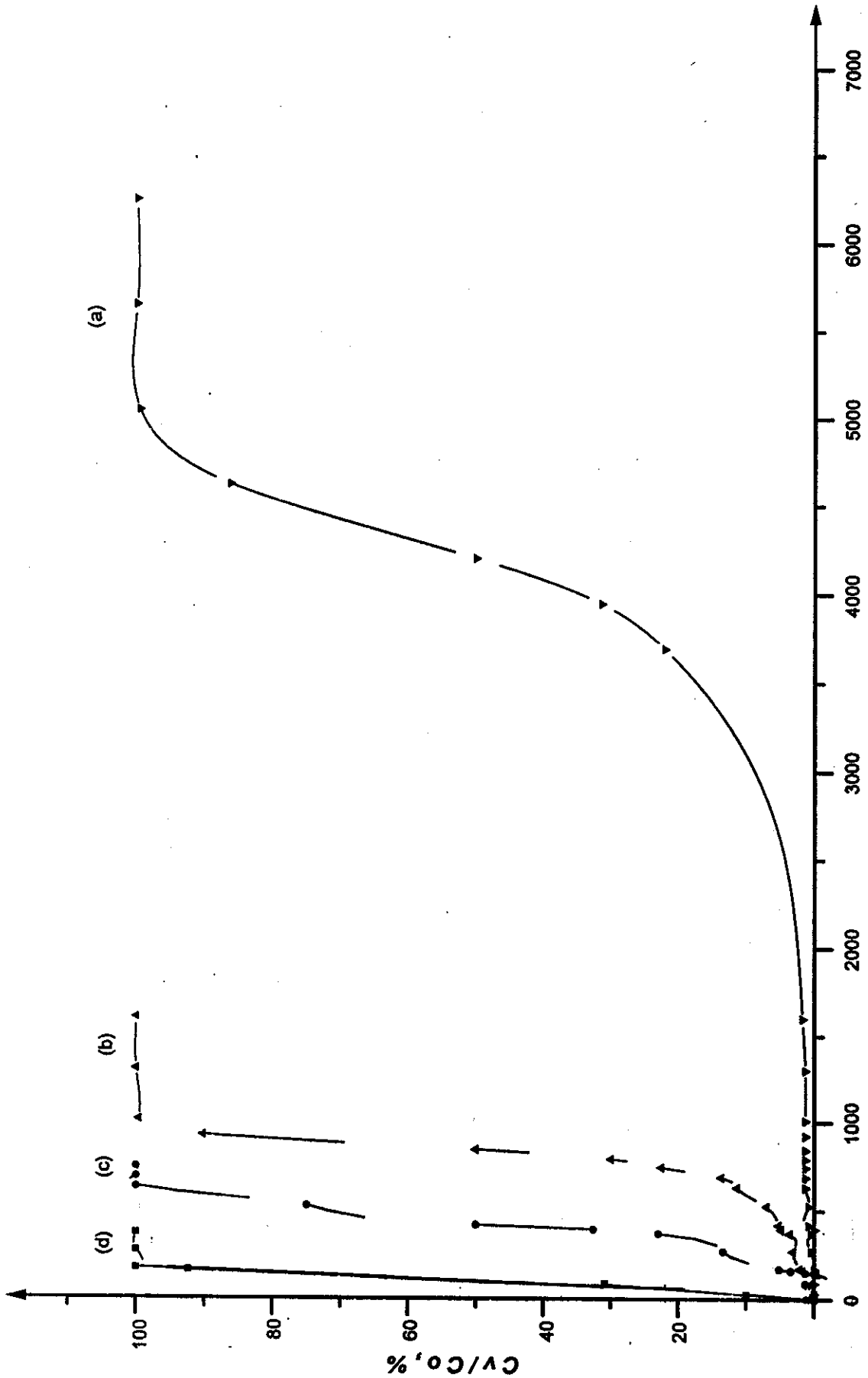

Fig.55. Breakthrough curves of In(III) and Ag(I) in 0.1M HNO_3 from 1g 12-molybdocerate(IV) columns (0.6cm i.d x 3.5cm) at a flow rate of 1ml/min as a function of metal ions concentratuions (a)10^{-5}M Ag(I) (b)$5x10^{-5}$M Ag(I) (c)10^{-4}M Ag(I) (d)10^{-5}M In(III)

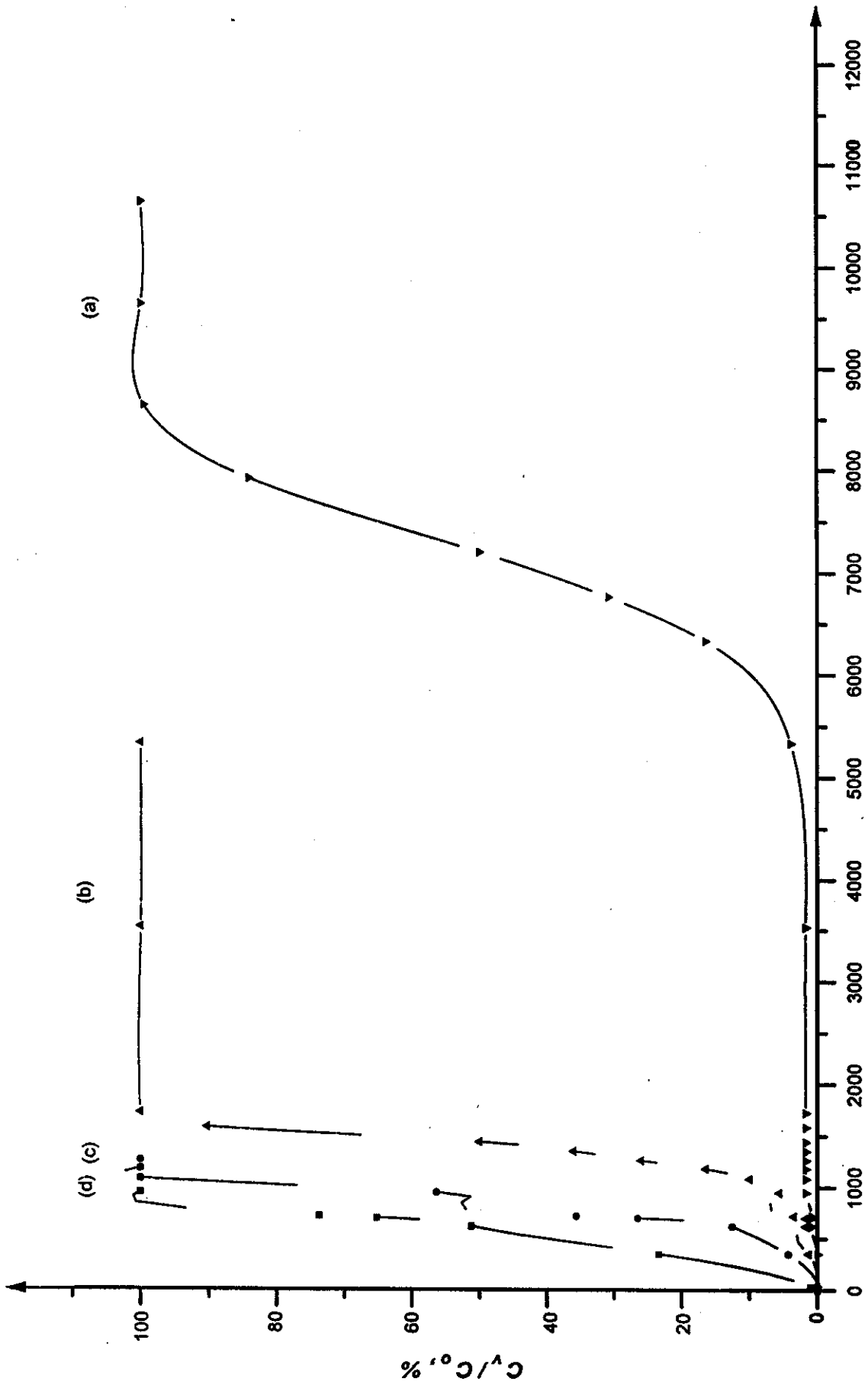

Fig.56. Breakthrough curves of In(III) and Ag(I) in 0.05M HNO_3 from 1g 12-molybdocerate(IV) columns (0.6cm i.d x 3.5cm) at a flow rate of 1ml/min as a function of metal ions concentrations (a)10^{-5}M Ag(I) (b)$5x10^{-5}$M Ag(I) (c)10^{-4}M Ag(I) (d)10^{-5}M In(III)

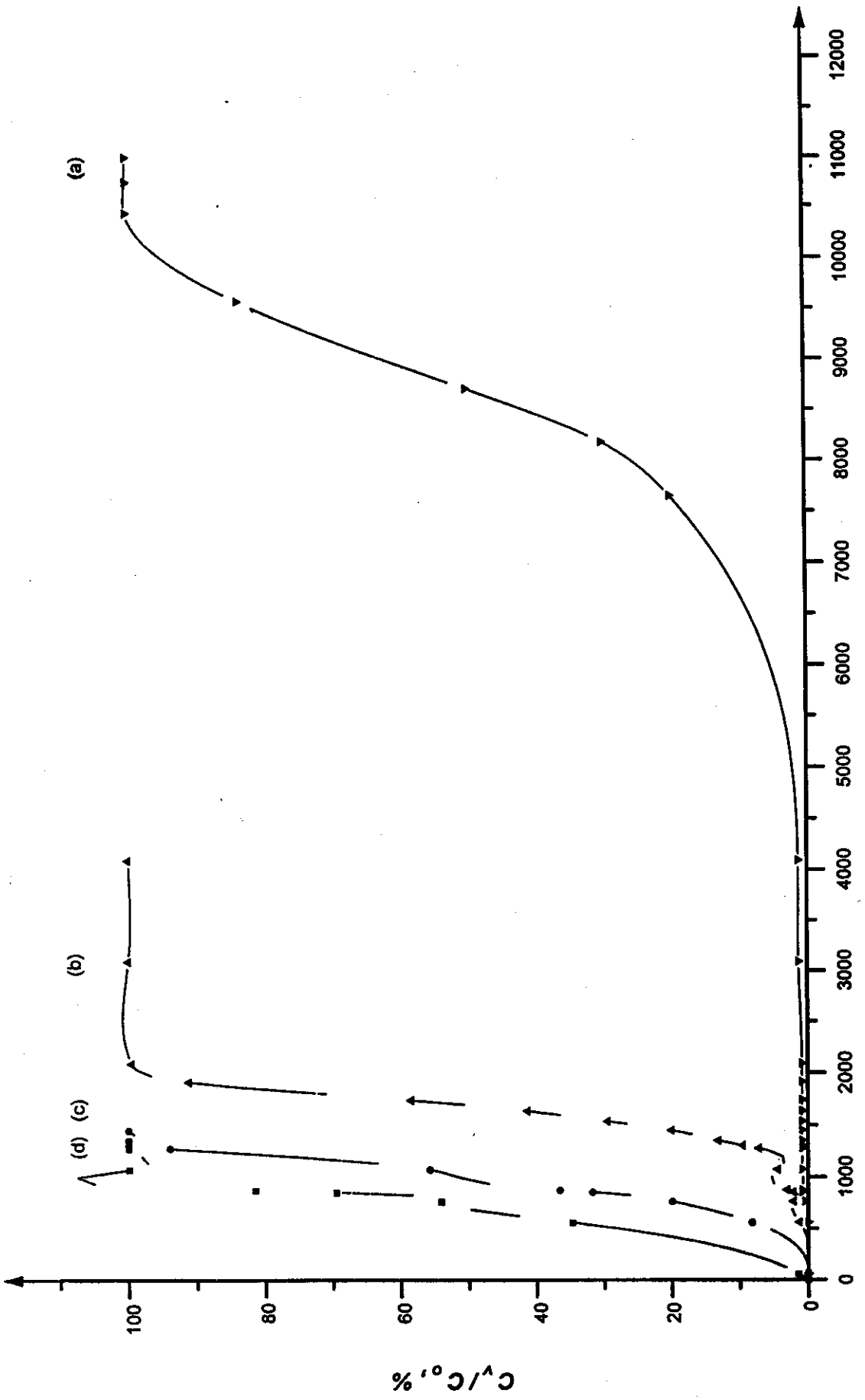

Fig.57. Breakthrough curves of In(III) and Ag(I) in 0.01M HNO_3 from 1g 12-molybdocerate(IV) columns(0.6cm i.d x 3.5cm) at a flow rate of 1ml/min as a function of metal ions concentrations
(a)10^{-5}M Ag(I) (b)$5x10^{-5}$M Ag(I) (c)10^{-4}M Ag(I) (d)10^{-5}M In(III)

Table 12. Individual distribution coefficients (K_d)values and separation factores (α) of In(III)-Ag(I) couple in HNO_3 acid solutions on 12-molybdocerate (IV)

Metal ion Concentration; M		Concentration of the equilibrating solutions											
		0.01M HNO_3			0.05 M HNO_3			0.1M HNO_3			0.2 M HNO_3		
		Distribution coefficient (K_d) values, ml/g											
		In^{3+}	Ag^+		In^{3+}	Ag^+		In^{3+}	Ag^+		In^{3+}	Ag^+	
Product In^{3+}	Target Ag^+	Separation factor α =Kd (Ag) / Kd (In)											
		K_d	K_d	α	K_d	K_d	α	K_d	K_d	α	K_d	K_d	α
$5x10^{-4}$	$5x10^{-4}$	150	1034	6.89	150	1034	6.89	120	829	6.91	66	500	7.58
10^{-4}		200	1034	5.17	200	1034	5.17	161	829	5.15	97	500	5.15
$5x10^{-5}$		249	1034	4.15	249	1034	4.15	200	829	4.15	123	500	4.07
10^{-5}		307	1034	3.37	307	1034	3.37	250	829	3.32	149	500	3.36
$5x10^{-4}$	10^{-4}	150	2800	18.7	150	2800	18.7	120	2200	18.3	66	1400	21.2
10^{-4}		200	2800	14	200	2800	14	161	2200	13.7	97	1400	14.4
$5x10^{-5}$		249	2800	11.2	249	2800	11.2	200	2200	11	123	1400	11.4
10^{-5}		307	2800	9.12	307	2800	9.12	250	2200	8.8	149	1400	9.4
$5x10^{-4}$	$5x10^{-5}$	150	3558	23.7	150	3558	23.7	120	2867	23.9	66	1850	28
10^{-4}		200	3558	17.8	200	3558	17.8	161	2867	17.8	97	1850	19.07
$5x10^{-5}$		249	3558	14.3	249	3558	14.3	200	2867	14.3	123	1850	15.04
10^{-5}		307	3558	11.6	307	3558	11.6	250	2867	11.5	149	1850	12.42
$5x10^{-4}$	10^{-5}	150	4046	26.9	150	4046	26.9	120	3244	27	66	2000	30.3
10^{-4}		200	4046	20.2	200	4046	20.2	161	3244	20.1	97	2000	20.6
$5x10^{-5}$		249	4046	16.2	249	4046	16.2	200	3244	16.2	123	2000	16.3
10^{-5}		307	4046	13.2	307	4046	13.2	250	3244	12.98	149	2000	13.4

Promising separation of indium(III) from silver(I) can be achieved more or less completely by virtue of the differences in their sorption affinity towards the molybdocerate matrix particularly at lower (≤0.1M) acid concentrations to obtain quantitatively retention of Ag^+. Table 13 compiles the breakthrough characteristics of Ag(I) and In(III) in HNO_3 acid solutions at different concentrations of acid and metal ions. Consequently, the separation process of a mixture solution of Ag(I) and In(III) has been investigated using small chromatographic columns of 1g 12-molybdocerate(IV) matrix by both elution and frontal separation methods.

3.3.2.1 Elution Chromatography

Elution performance of the silver(I)-indium(III) couple was examined using chromatographic columns of (0.6 cm i.d x 3.5 cm) packed each with 1g of 12-molybdocerate (IV) matrix loaded with 5ml mixture solution consists of $5x10^{-4}$ M silver (I) and 10^{-5} M indium(III) in 0.2, 0.1, 0.05 and 0.01M HNO_3 at a flow rate of 1ml/min. However a small leakage of Ag(I) (about 4.2%) is obtained when loading with 0.2M HNO_3 acid, quantitative retention on the sorbent matrix was achieved with 0.1, 0.05 and 0.01M HNO_3 acid solutions.

3.3.2.1.1 Effect of Chemical Composition of the Eluent

Figure 58 (curves a,b,c and d) displays the effect of acid concentrations; 0.2, 0.1, 0.05 and 0.01M nitric acid solutions as eluents, on the elution profiles and yields of silver(I)-indium(III) couple dissolved in 0.01M HNO_3 from 1g 12-molybdocerate (IV) columns at flow rate 1ml/min. It is clear that In(III) is readily eluted in the form of a sharp elution profile with 5ml of 0.2 and 0.1M HNO_3 acid solutions. It was found that about 98% of the indium(III) radioactivity loaded onto the

Table 13. Breakthrough characteristics of Ag (I) and In (III) in HNO_3 acid solutions from 1g 12- molybdocerate (IV) colums at a flow rate of 1ml/min

Metal ion conc., M	Character	Concentration of HNO_3, M							
		0.01		0.05		0.1		0.2	
		Ag	In	Ag	In	Ag	In	Ag	In
10^{-5}	V(1%)	765	56	633	35	369	3	106	2
	V(50%)	8700	850	7200	700	4200	150	1200	100
	V(100%)	10440	1275	8640	945	5040	173	1440	120
	C, meq/g	8.7×10^{-2}	2.6×10^{-2}	7.2×10^{-2}	2.1×10^{-2}	4.2×10^{-2}	1.5×10^{-3}	1.2×10^{-2}	3×10^{-3}
5×10^{-5}	V(1%)	153	11	126	7	74	2	21	1
	V(50%)	1740	170	1440	140	840	30	240	20
	V(100%)	2088	255	1728	189	1008	35	288	24
	C, meq/g	8.7×10^{-2}	2.6×10^{-2}	7.2×10^{-2}	2.1×10^{-2}	4.2×10^{-2}	1.5×10^{-3}	1.2×10^{-2}	3×10^{-3}
10^{-4}	V(1%)	76	6	63	4	37	1	10	1
	V(50%)	870	85	720	70	420	15	120	10
	V(100%)	1305	128	1080	94	630	17	180	12
	C, meq/g	8.7×10^{-2}	2.6×10^{-2}	7.2×10^{-2}	2.1×10^{-2}	4.2×10^{-2}	1.5×10^{-3}	1.2×10^{-2}	3×10^{-3}
5×10^{-4}	V(1%)	15	1	12	1	7	1	2	1
	V(50%)	175	17	144	14	84	3	24	2
	V(100%)	209	26	173	19	100	4	29	3
	C, meq/g	8.7×10^{-2}	2.6×10^{-2}	7.2×10^{-2}	2.1×10^{-2}	4.2×10^{-2}	1.5×10^{-3}	1.2×10^{-2}	3×10^{-3}

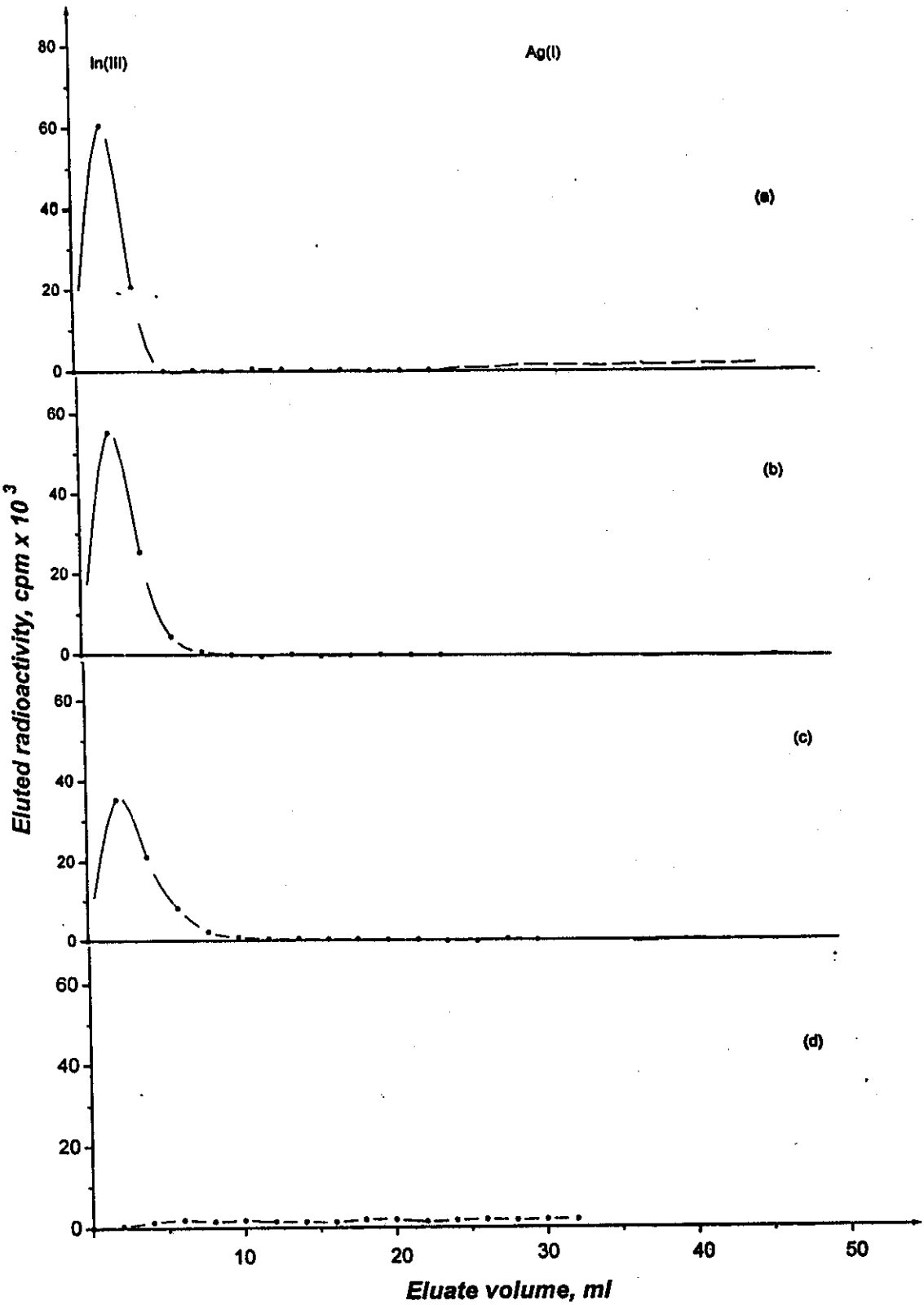

Fig.58. ELution curves of In(III) from Ag(I) onto 1g 12-molybdocerate columns (0.6cm i.d x 3.5cm) with (a)0.2 (b)0.1 (c)0.05M (d)0.01M HNO_3 acid solutions at a flow rate of 1ml/min.

column is eluted and concentrated in the first 5ml of 0.2M nitric acid. On the other hand; about 89%, 23% and 3.4% of the eluated indium(III) radioactivity were obtained in the first 5ml 0.1, 0.05 and 0.01 M acid; respectively. It is obvious that as the acid concentration increases; the corresponding elution efficiency of In(III) increases and distribution of the eluted radioactivity is concentrated in smaller eluate volumes. The chromatographic elution behaviour of Ag(I) and In(III) are more or less in agreement with the previously obtained batch distribution and dynamic studies data.

3.3.2.1.2 Effect of Flow Rate of the Eluent

Figures 59-62 (curves a, b and c) display the elution profiles of indium(III) and silver(I) radiotracers from 1g 12-molybdocerate(IV) columns with 0.2, 0.1, 0.05 and 0.01M nitric acid solutions at flow rates of 0.5, 1 and 2ml/min; respectively. It is distinct from the figures that the positions of the maximum elution peaks of In(III) were not markedly changed with changing the flow rate in 0.2 and 0.1M acid solutions, whereas they displaced to higher eluate volumes with increasing the flow rate of the dilute acid eluents (0.05M and 0.01M acid). This may be due to slow sorption/desorption kinetics of the indium(III) radiotracers on the surface of the molybdocerate matrix into the eluent [slow diffusion mechanism]. The distribution (i.e, volume concentration) of the eluted Ag(I) radioactivity in the different eluate fractions gives shallow-tailed elution profiles with increasing the eluent flow rate. It was found that about 98.2%, 93.4.3% and 89.7% of the indium(III) radioactivity are obtained in the first 4ml 0.2M HNO_3 acid eluate at flow rates 0.5; 1 and 2ml/min; respectively. On the other hand; about 6.3%, 4.2% and 2.8% of the eluated silver(I) radioactivity were obtained with 20ml 0.2M HNO_3 acid at flow rates 0.5, 1 and 2 ml/min; respectively.

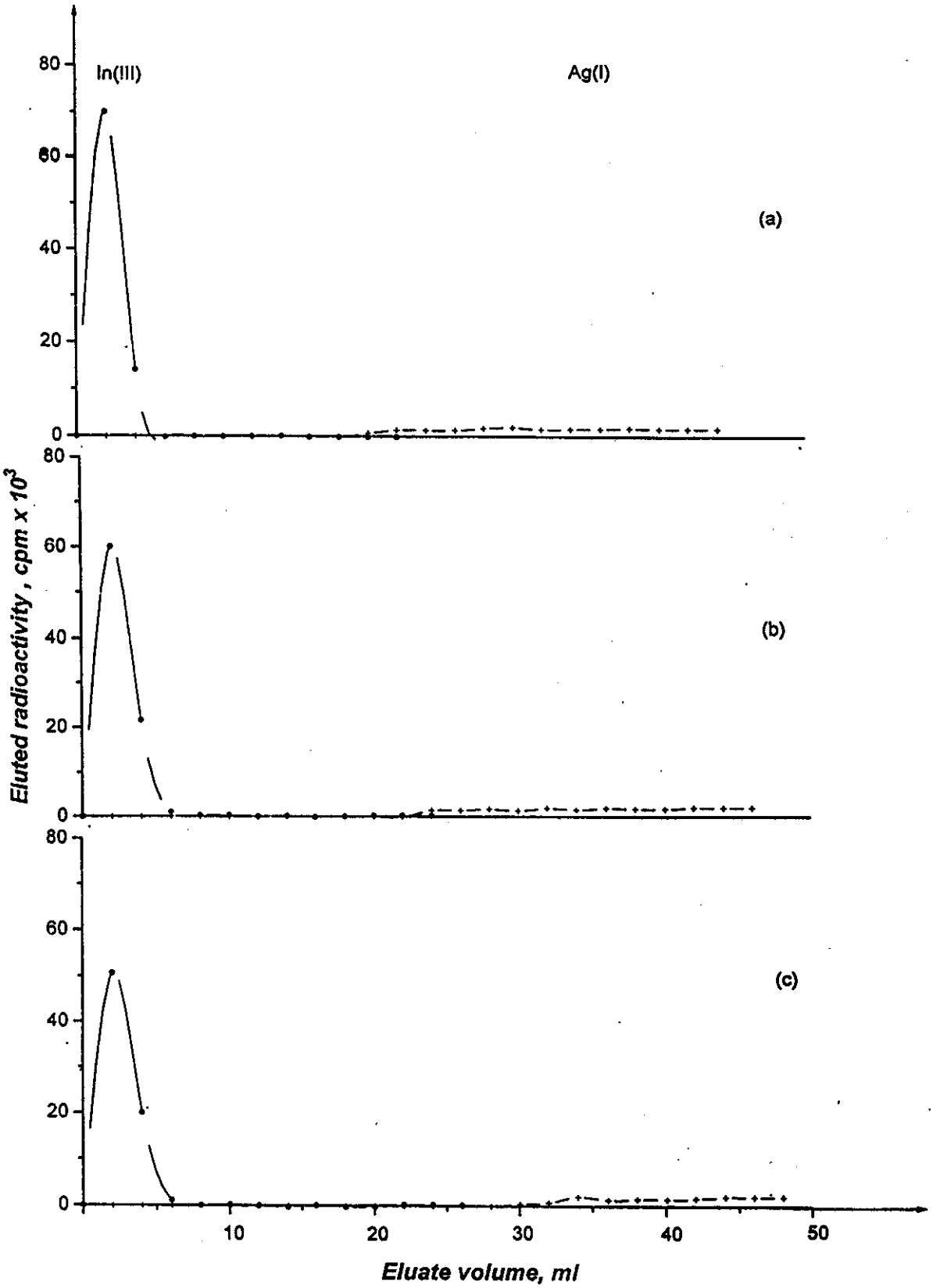

Fig.59.Elution curves of In(III) from Ag(I) onto 1g 12-molybdocerate columns (0.6cm i.d x 3.5cm) with 0.2M HNO_3 at a flow rate of (a)0.5ml/min (b)1.0ml/min (c)2.0ml/min.

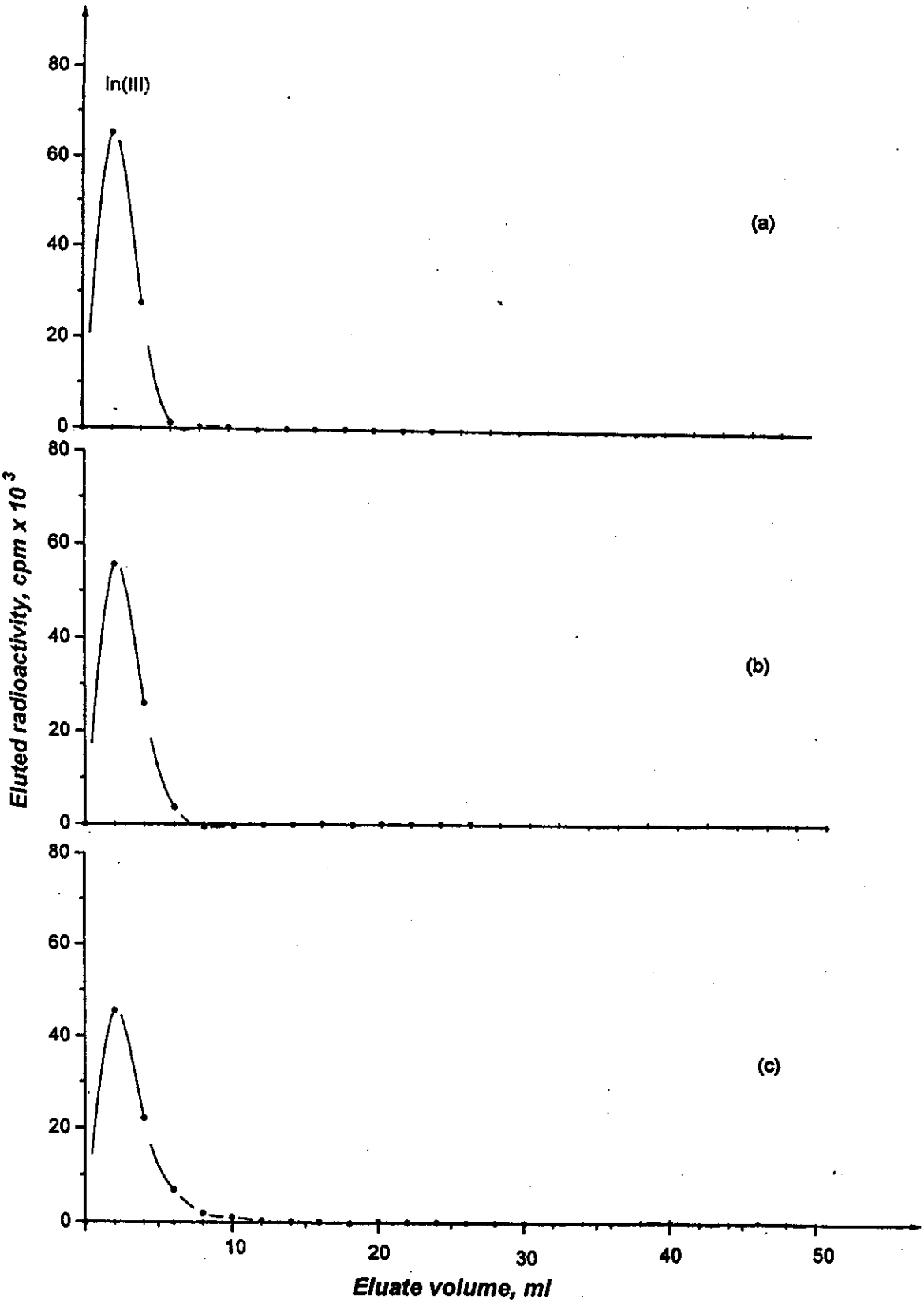

Fig.60. Elution curves of In(III) from Ag(I) onto 1g 12-molybdocerate columns (0.6cm i.d x 3.5cm) with 0.1M HNO_3 at a flow rate of
(a) 0.5 ml/min (b) 1.0 ml/min (c) 2.0ml/min

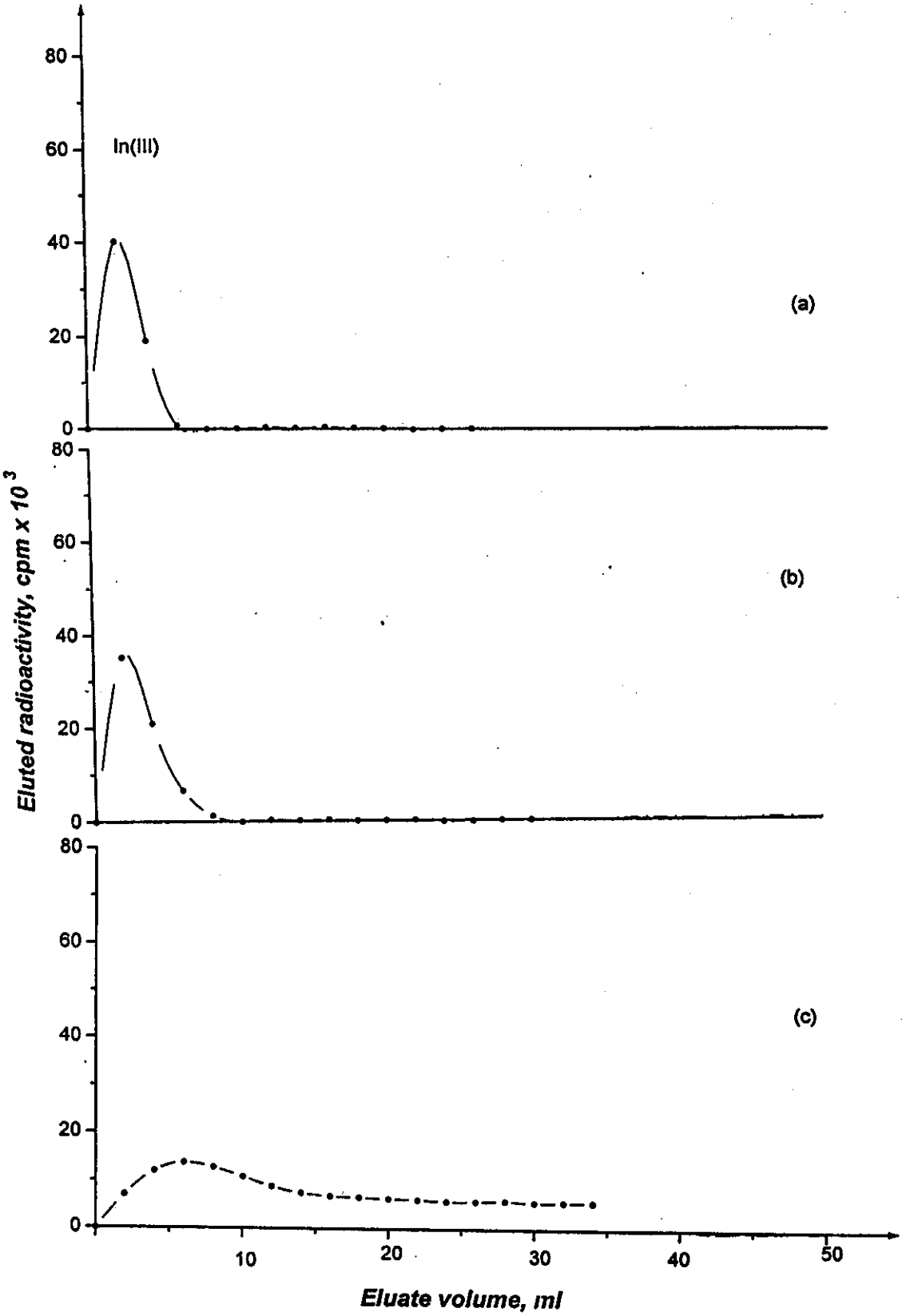

Fig.61.Elution curves of In(III) from Ag(I) onto 1g 12-molybdocerate columns (0.6cm i.d x 3.5cm) with0.05M HNO_3 at a flow rate of (a)0.5ml/min (b)1.0ml/min (c)2.0ml/min

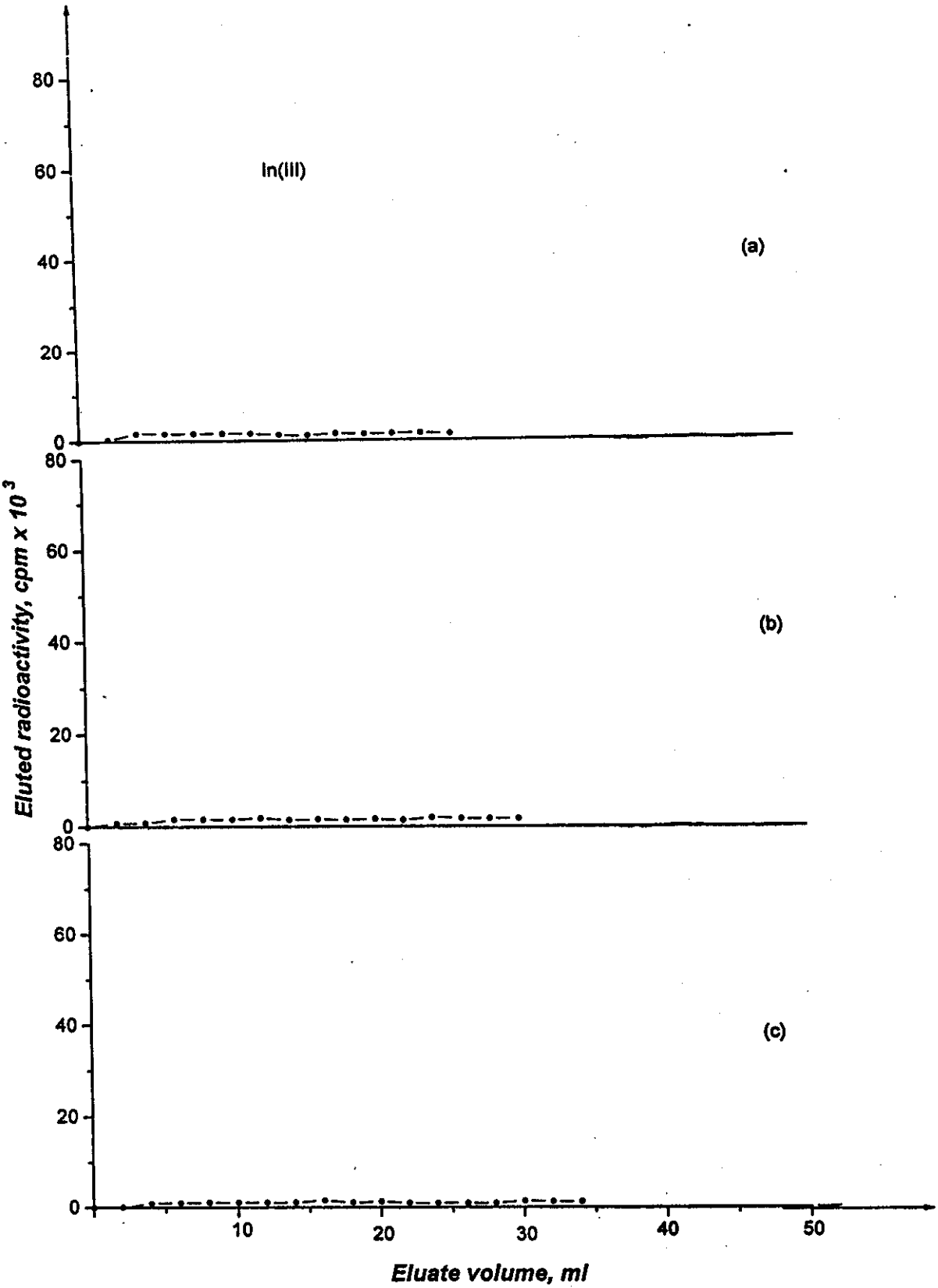

Fig.62. ELution curves of In(III) from Ag(I) onto 1g 12-molybdocerate(IV) columns (0.6cm i.d x 3.5cm) with 0.01M HNO_3 at a flow rate of

(a)0.5ml/min (b)1.0ml/min (c)2.0ml/min

3.3.2.1.3 Recommended Procedure for Elution Separation of the Silver(I) – Indium (III) Couple

In case of small amounts of the target material; not more than 15% of the total sorption capacity of the sorbent matrix in small solute volume, the chromatographic column elution method is recommended for radiochemical separation of the silver(I) - indium(III) couple. In this process, 5ml mixture solution consists of $5x10^{-4}$M silver (I) and 10^{-5}M indium (III) in 0.01M HNO_3 acid solution was loaded onto 1g 12-molybdocerate (IV) column (0.6 cm i.d x 3.5 cm). Silver(I) and indium(III) were quantitatively sorbed onto the column matrix as verified by radiometric measurements of the column effluents. Elution of the sorbed In(III) from the column matrix is carried out with 10ml 0.1M HNO_3 acid solution at flow rate 1 ml/ min. Figure 63 displays the obtained elution data of In(III) from Ag(I) onto 1g 12-molybdocerate(IV) column with 0.1M HNO_3 at a flow rate of 1ml/min. It was found that about 56.4% of the loaded indium(III) radioactivity was eluted and concentrated in the first 3ml 0.1M HNO_3 acid eluate. The elution yield of indium(III) is in the order of 98.6% of the total In(III) radioactivity loaded onto the column. The obtained elution yield is higher than that obtained from cation and anion exchange columns; AG 50W-X4 and Dowex 2x8 (i.e, 95% and 85%), respectively [80-122]. Purification of the bed matrix from any residual In(III) retained onto the gel matrix is carried out with passing 4ml 0.2M HNO_3 at the same flow rate. Regeneration of the strongly retained Ag(I) is eluted with 20ml 1M HNO_3 acid solution at flow rate of 1ml/min ,whereas, about 98.8% of Ag(I) radioactivity was eluted (Fig.63).

Figure 64 illustrates a proposed schematic diagram for separation of carrier-free In(III) radioisotope from its Ag(I) target solute by chromatographic column elution method.

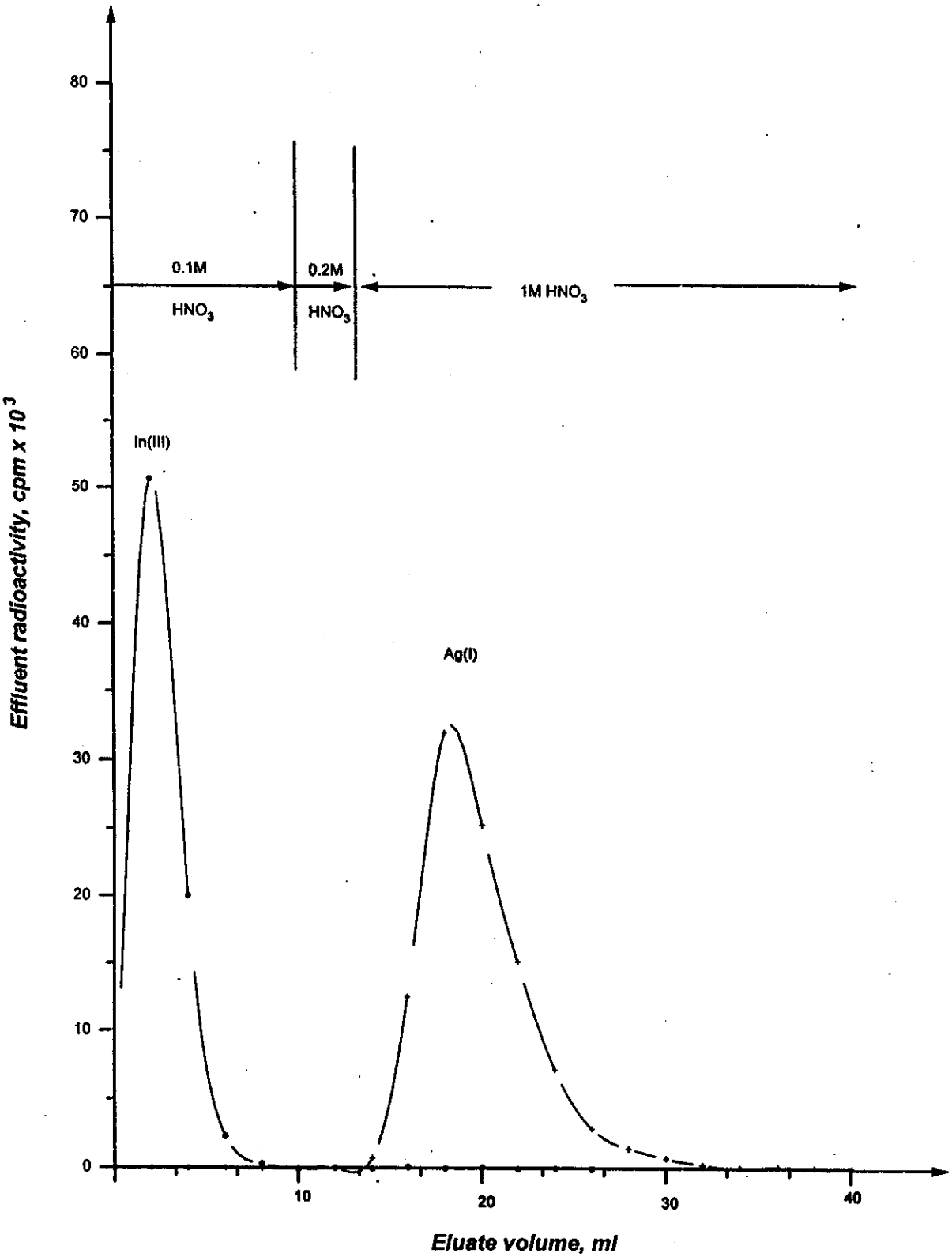

Fig.63. Typical elution profiles of In(III) from Ag(I) onto 1g 12-molybdocerate(IV) columns (0.6cm i.d x 3.5cm) with 0.1, 0.2 and 1M HNO_3 at flow rate 1ml/min.

3.3.2.2 Frontal Chromatography

For radiochemical processing of the cyclotron produced radioisotopes; the irradiated Ag(I) target material and the product In(III) radiotracer are usually present in relatively high solute volumes; about 80ml of the etching solution[80, 81]. Therefore; the continuous separation technique is of great importance in practice compared to the elution method. In this technique, a mixture solution containing 10^{-4} M silver (I) and 10^{-5} M indium (III) in 0.1M nitric acid solution was continuously added to 1g 12-molybdocerate(IV) column.

3.3.2.2.1 Recommended Procedure for Frontal Separation of the Silver (I)- Indium (III) Couple

The previously obtained breakthrough characteristics as well as the elution profiles data explore the optimum operating conditions for separation of indium(III) radiotracer from bulk amounts of the silver(I) target. Figure 65 display that Ag(I)-In(III) separation can be achieved onto small chromatographic columns, packed each with 1g 12-molybdocerate(IV) gel (0.6cm i.d x 3.5cm), fed with 200ml mixture solution of 10^{-4}M Ag(I) and 10^{-5}M In(III) radiotracers in 0.01M HNO_3 acid at a flow rate of 1ml/min. It is observed that the mixture constituent; indium(III); with the least affinity for the molybdate gel immediately passed along the column matrix leaving the strongly sorbed silver(I) build up onto the complex bed matrix. The retained In(III) was eluted from the column bed with passing 10ml of 0.1M HNO_3 acid solution at flow rate of 0.5ml/min. Purification of the bed matrix from any residual In(III) is carried out with passing further 4ml of 0.2M HNO_3 acid at the same flow rate. Thereafter, Ag(I) is eluted with 20ml of 1M HNO_3 acid solution at flow rate of 1ml/min.

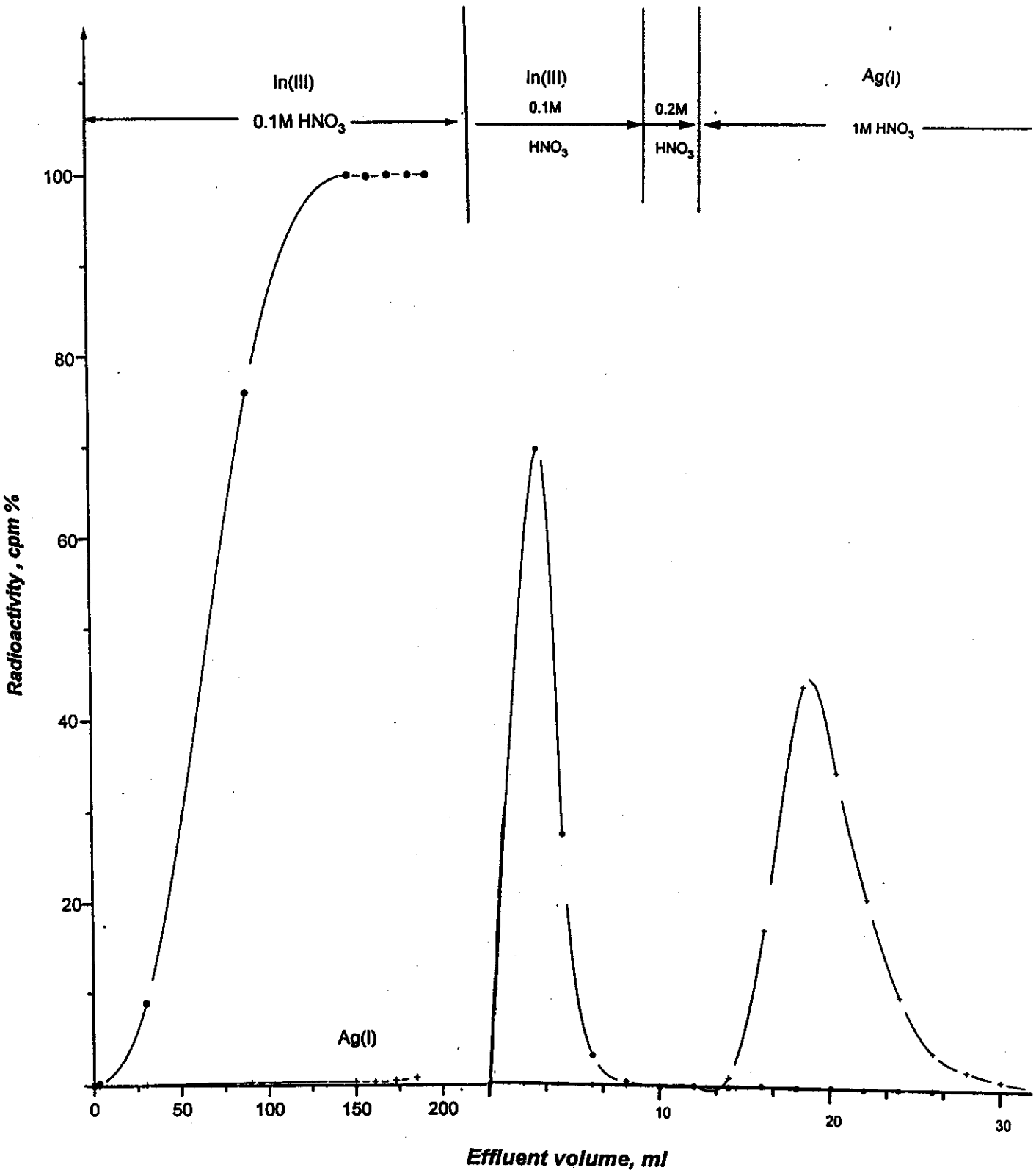

Fig.65. Frontal separation of a mixture solution containing 10^{-4}M Ag(I) and 10^{-5}M In(III) from 1g 12-molybdocerate(IV) columns (0.6cm i.d x 3.5cm) with HNO_3 acid solution.

Figure 66 shows the proposed schematic diagram for separation of carrier-free In(III) from its Ag(I) target by the chromatographic column frontal method.

3.3.3 Regeneration of the Column Matrix

To replace the strongly retained Ag(I) ions remaining onto the sorbent surface by hydrogen ion (i.e, conversion of the column bed into the H^+-form) was carried out by using relatively concentrated HNO_3 acid solution. To insure the complete conversion of the molybdate matrix to the H^+-form, sufficient volume (about 30 times the matrix volume) of 1M nitric acid solution was passed through the column bed at a flow rate of 0.5 ml/min.

3.3.4 Quality Control Testes

3.3.4.1 Chemical Purity of Indium (III) Eluates

Presence of any chemical impurities in the indium(III) eluate; originating from either the back of the target holder; the molybdocerate matrix and / or from the eluents; will markedly affect the use of the indium(III) eluates for nuclear medicine applications and chemical quality of the prepared radiopharmaceutical. The indium (III) eluates were analyzed spectrophotometrically[75,159] for the presence of molybdenum and cerium as chemical contaminants originating from the sorbent matrix. It was found that the concentration of cerium in the eluates was under the detection limit of the method, 1.0μg Ce/ml. On the other hand; the concentration of molybdenum was found to be in the range of 1-3μg Mo/ml in 0.1M HCl. Molybdenum and cerium concentrations in the eluates are below the restricted limit for nuclear medicine applications[85,93,96,100].

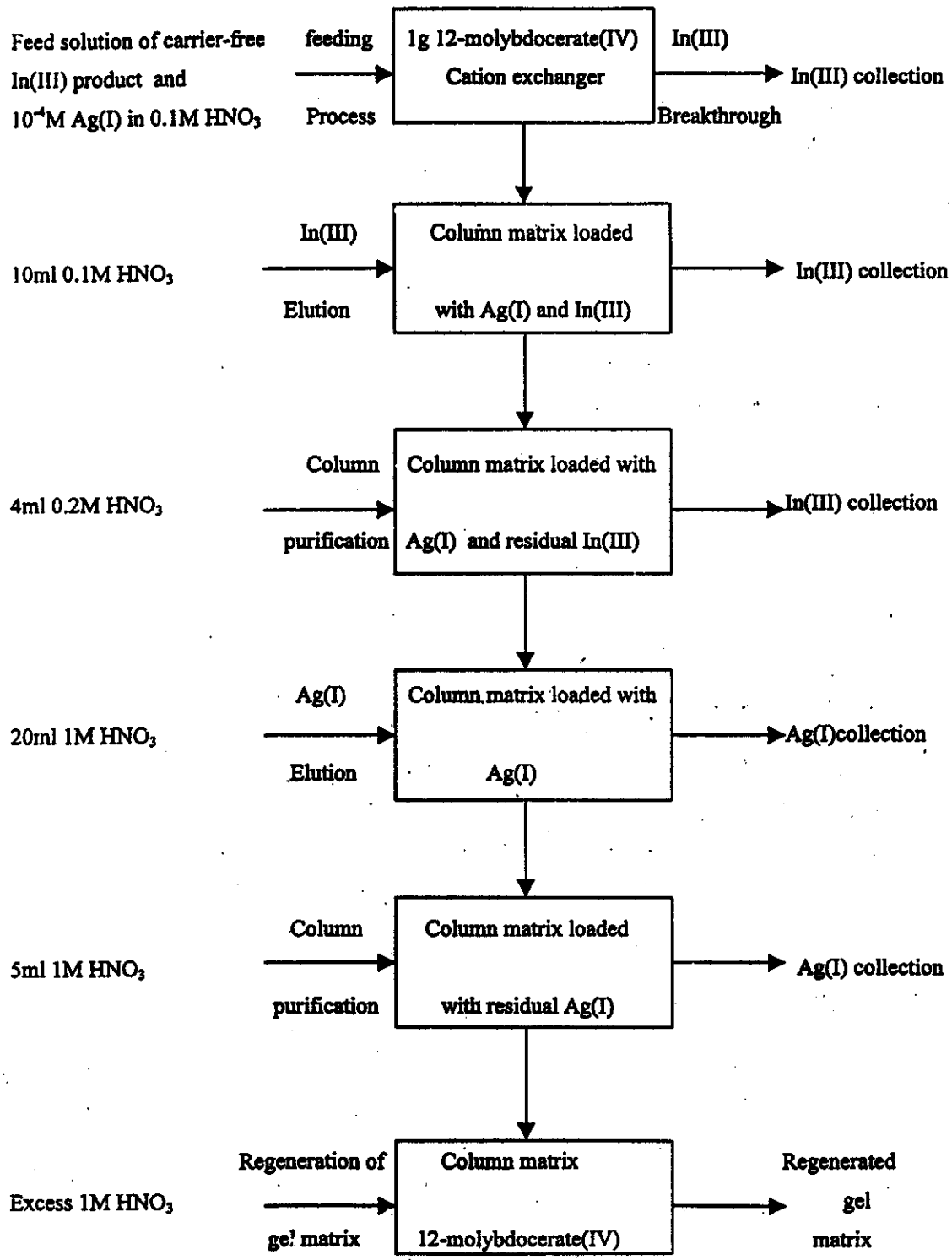

Fig.66. Proposed schematic diagram for separation of carrier-free In(III) from cyclotron irradiated Ag(I) targets by chromatographic column frontal method.

3.3.4.2 Radionuclidic Purity of Indium(III) Eluates

The radionuclidic purity of indium(III) eluates is defined as the proportion of the desired indium(III) radioactivity to the total eluate radioactivity. The presence of any other radionuclidic contaminants e.g ^{72}Cd, ^{110m}Ag and ^{64}Cu; of higher radiation energies or undesirable mode of decay; may affect the quality of diagnostic pictures and cause high radiation doses to the patient. Therefore; the radionuclidic purity, of indium(III) eluates, was confirmed by high-resolution gamma ray spectroscopy using high purity germanium (HPGe) detector coupled to multichannel analyzer. Figure 67 shows the gamma spectra of indium (III) eluates of siver(I)-indium(III) mixture measured immediately after separation. It is observed that only the photo peaks (88.23, 138.33, 190.95, 334.4, 416.99, 490.7, 557.14, 723.6, 819.34, 1281.77, 1497.29, 1761.2, 1770 and 2112.3 keV) corresponding to $^{114m,116m}In(III)$ are the main detected γ-energies. It was found that radionuclidic contaminants in each eluate was less than 0.1% of the $^{114m}In(III)$ radioactivity at the time of separation. Therefore, the corresponding radionuclidic purity is higher than 99.9%.

3.3.4.3 Radiochemical Purity of Indium(III) Eluates

Radiochemical purity is defined as the percent of indium(III) radioactivity present in the desired chemical form to the total radioactivity. The presence of any other chemical forms beside the desired form give poor quality products and consequence poor quality images attributed to dislocation in the target organ and consequently high background contribution from the surrounding tissues. The radiochemical purity of indium(III) eluates was assessed by ascending paper chromatography; using stripes of Whatman No.1 filter paper in 85% methanol as a developing solvent[86].Figure 68 depicts a typical radio-

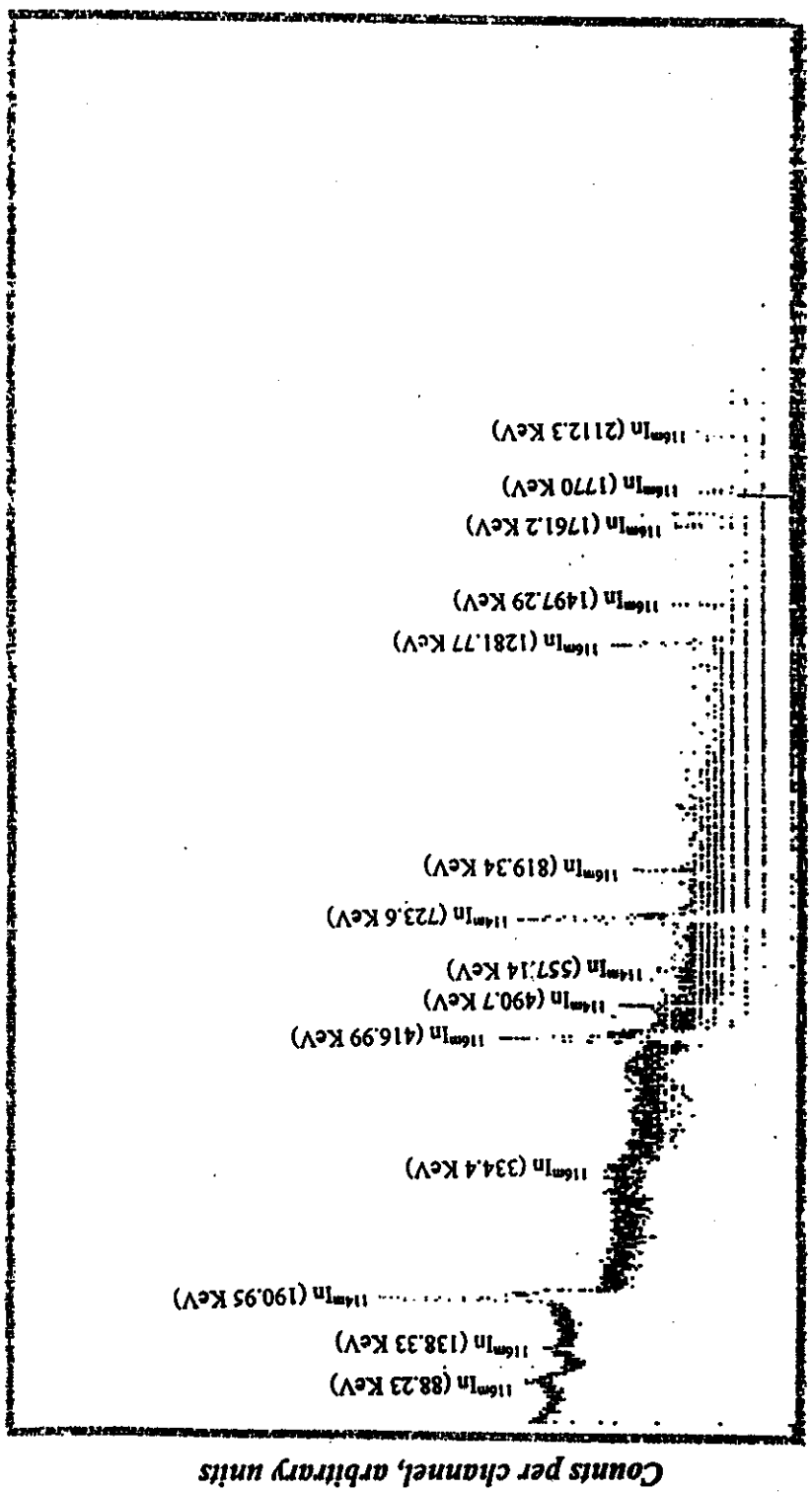

Fig.67.Gamma spectra of indium eluates from12-molybdocerate(IV) matrix.

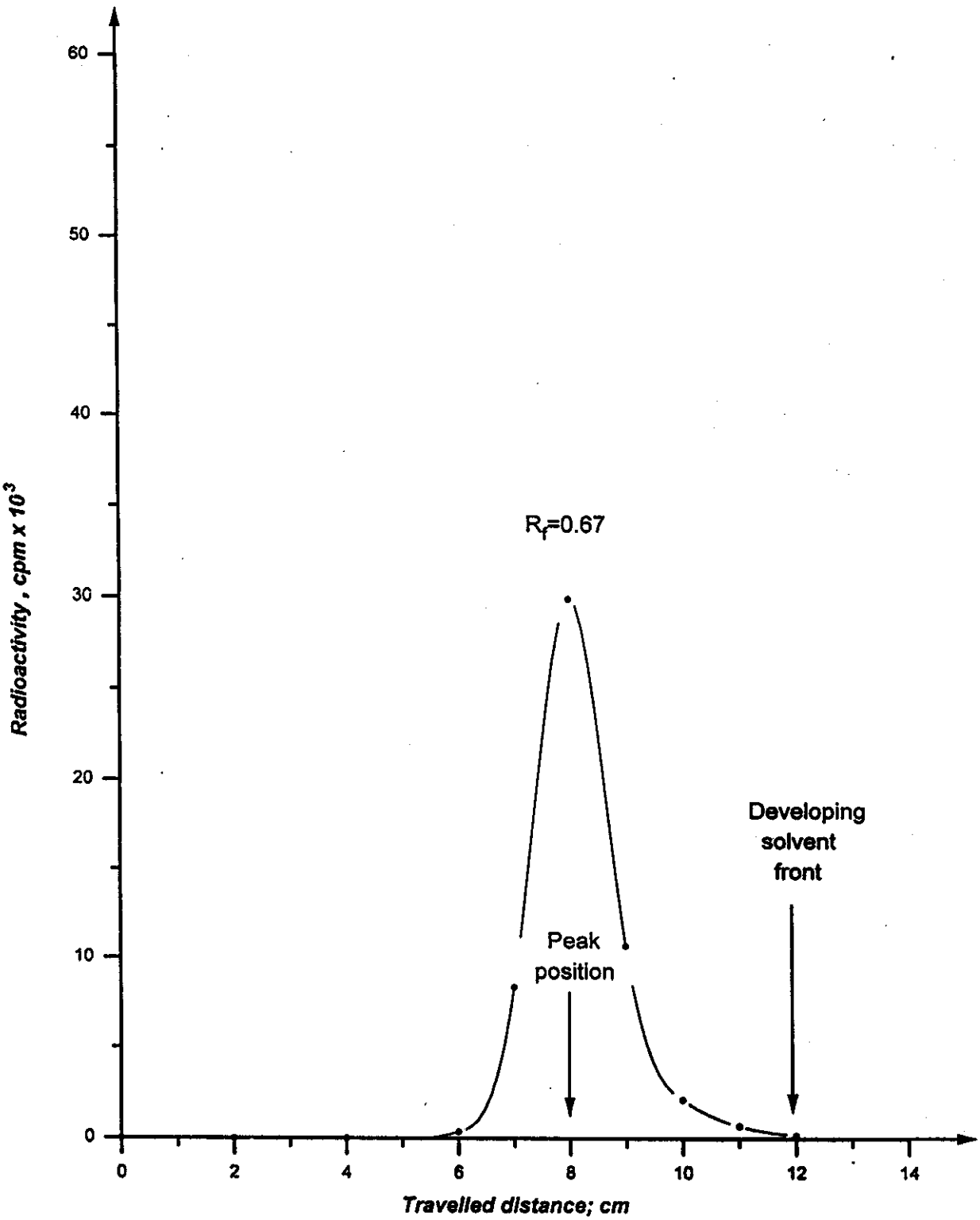

Fig.68. Radiochromatogram of indium(III) eluates from 12-molybdocerate column matrix.

chromatogram of indium(III) eluates from 12-molybdocerate(IV) column matrix . It is obvious that only one peak localized at R_f =0.67; which may be due to indium chloride $InCl_3$ radiotracer; has been observed[80,157]. The corresponding radiochemical purity was found to be about 92%. This value is in accordance with the recommended clinical specifications[95.96, 97,99].

3.4 Lead(II) - Thallium(I) Couple

3.4.1 Distribution Behaviour Investigations

3.4.1.1. Static Method

The distribution behaviour of the individual inactive lead(II) and thallium(I) radiotracer in 0.005-0.5M nitric and hydrochloric acid media on 12-molybdocerate(IV) gel were individually investigated by the batch equilibration method in a shaker thermostat adjusted at 25±1^{0}C. The corresponding concentration of lead(III) was determined by spectrophotometric method[159].

3.4.1.1.1 Effect of H^+-ion Concentration

Figure 69 display the corresponding K_d values of 10^{-6}M lead(II) in nitric acid media on 12-molybdocerate(IV) gel as a function of concentration of the equilibrating solution at 25±1^{0}C. In dilute nitric acid solutions up to around 0.05M, a sorption plateau with maximum K_d values of about 1250ml/g is obtained. The observed high K_d values of Pb(II) obtained at low acid concentrations presumably due to the formation of cationic species of Pb(II) such as $[Pb(OH)]^+$, Pb^{2+} and $[Pb(NO_3)]^+$ which are highly retained onto the moybdate matrix by cation exchange and/or hydolytic sorption mechanisms[25, 155]. On the other hand, the corresponding K_d values of Pb(II) in HNO_3 acid solutions linearly decrease with increasing the acid concentration up to 0.5M acid (80ml/g). The formation of molecular $[Pb(NO_3)_2]$ species as well as anionic non sorbable species of $[Pb(NO_3)_4]^{2-}$, $[Pb(NO_3)_5]^{3-}$ and $[Pb(NO_3)_6]^{4-}$ on the expense of the sorbable cations, at high acid concentrations would decrease the respective K_d values [26,156]. Furthermore, the competition between the exchanging Pb(II) cations and H^+ in solution to exchange with the counter H^+ ions on the 12-molybdocerate(IV) matrix may contribute to the decrease in the K_d

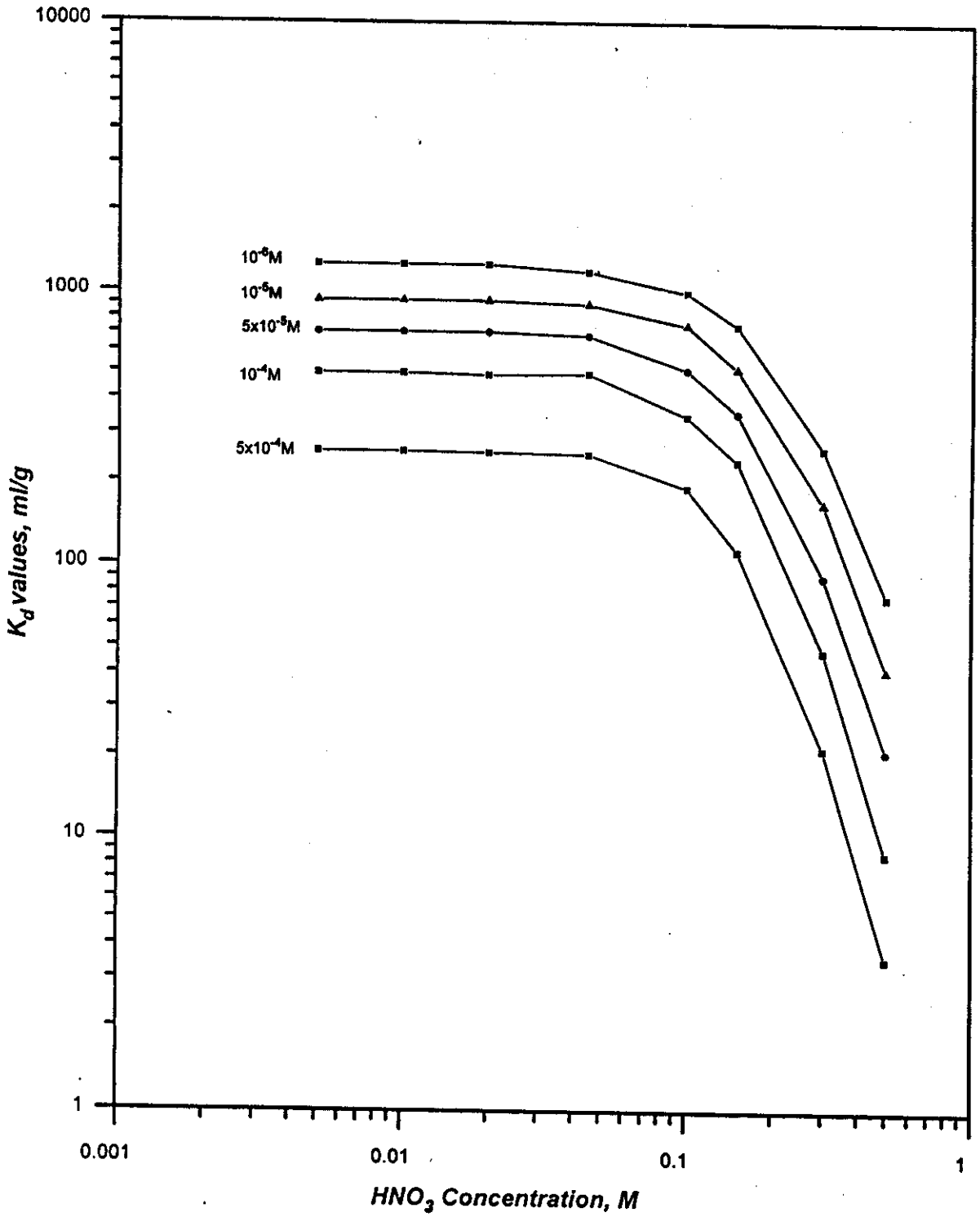

Fig.69. Distribution coefficient (K_d) values of Pb(II) in HNO_3 acid solutions on 12-molybdocerate (IV) at different Pb(II) concentrations(25±1 °C).

values with increasing the acid concentration. Figure 70 demonstrates the effect of HNO_3 acid concentration on the distribution behaviour of 10^{-6}M thallium(I) on the 12-molybdocerate(IV) matrix at 25±1°C. It is obvious that the distribution behaviour of Pb^{2+} and Tl^{+} are more or less similar. At low acid concentration up to around 0.1M HNO_3 thallium ions show high sorption affinity towards the MoCe(IV) gel with a sorption maximum plateau of almost constant K_d values at about 3500 ml/g. This observation is presumably attributed to the predominance of Tl^{+} species which are strongly held onto the sorbent matrix by ion exchange reaction with the counter H^{+}-ions of the exchangeable sites on the surface of the 12-molybdocerate(IV) matrix. At acid concentrations ≥0.1MHNO_3, the corresponding K_d values decrease to ~920ml/g at about 0.5M HNO_3 acid solution. The observed decrease in the corresponding distribution coefficient values may be due to the great tendency of the Tl(I) ions to form neutral low adsorbable molecular species; [$Tl(NO_3)$]. It is observed that the adsorbability and the corresponding K_d values of Tl(I)>Pb(II) as shown in Figure 69 compared to Figure 70. This observation can be explained on the basis of high selectivity of the heteropolyacid 12-molybdocerate(IV) cation exchanger for large monovalent Tl(I) cation. The large non-hydrated ionic radii and the small hydrated radii of Tl^{+} ion (1.48A°) allows it to approach more closely to the negative sites of attachment on the surface of the cation exchanger and fixation by strong electrostatic bounding force than Pb^{2+}(1.23A°)[155,156].

3.4.1.1.2 Effect of acid Anion

Figure 71 depicts the sorption behaviour of 10^{-6}M Pb(II) ions on 12-molybdocerate(IV) gel in hydrochloric acid solutions at 25±1°C.

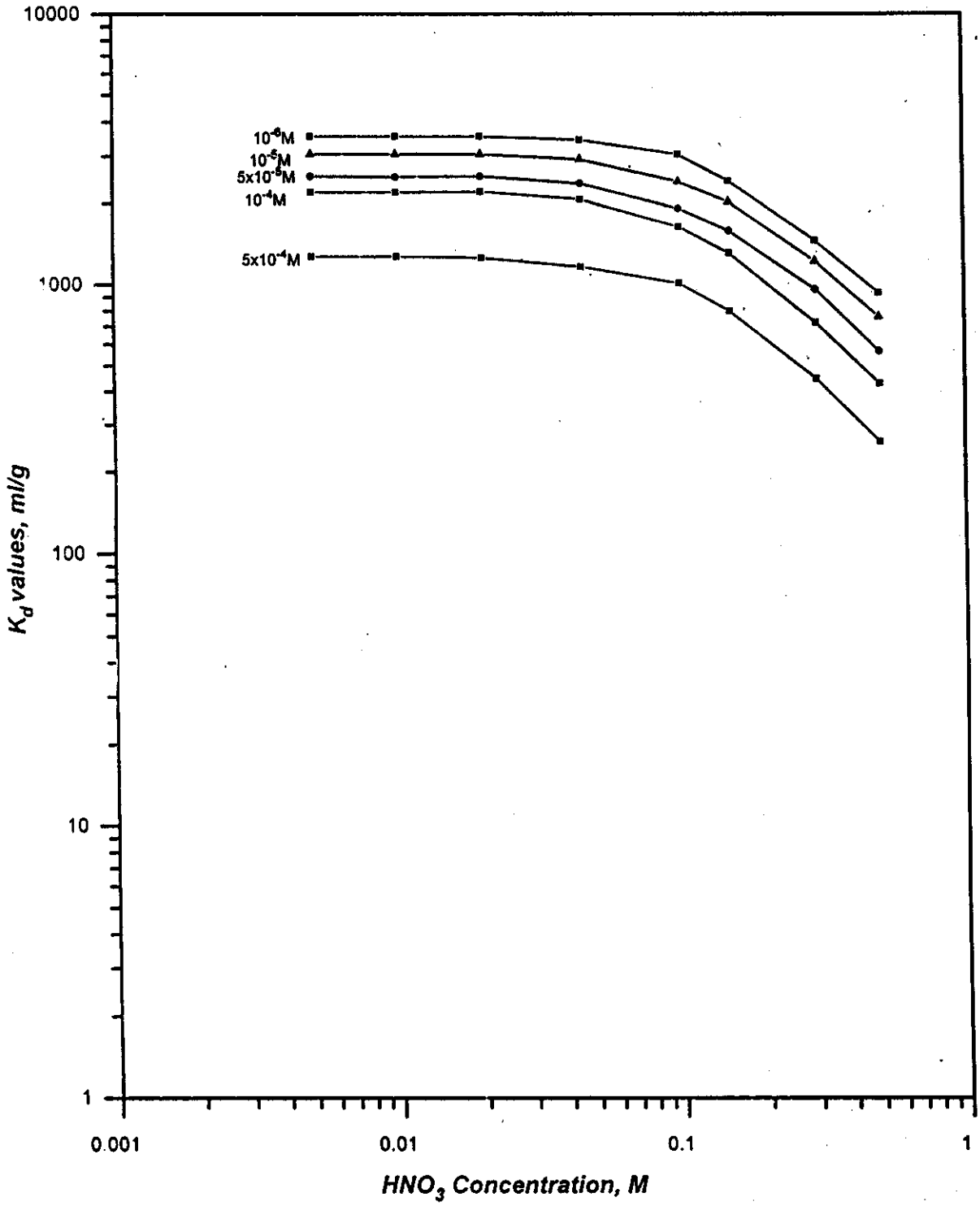

Fig.70. Distribution coefficient (K_d) values of Tl(I) in HNO_3 acid solutions on 12-molybdocerate (IV) at different Tl(I) concentrations(25±1 °C).

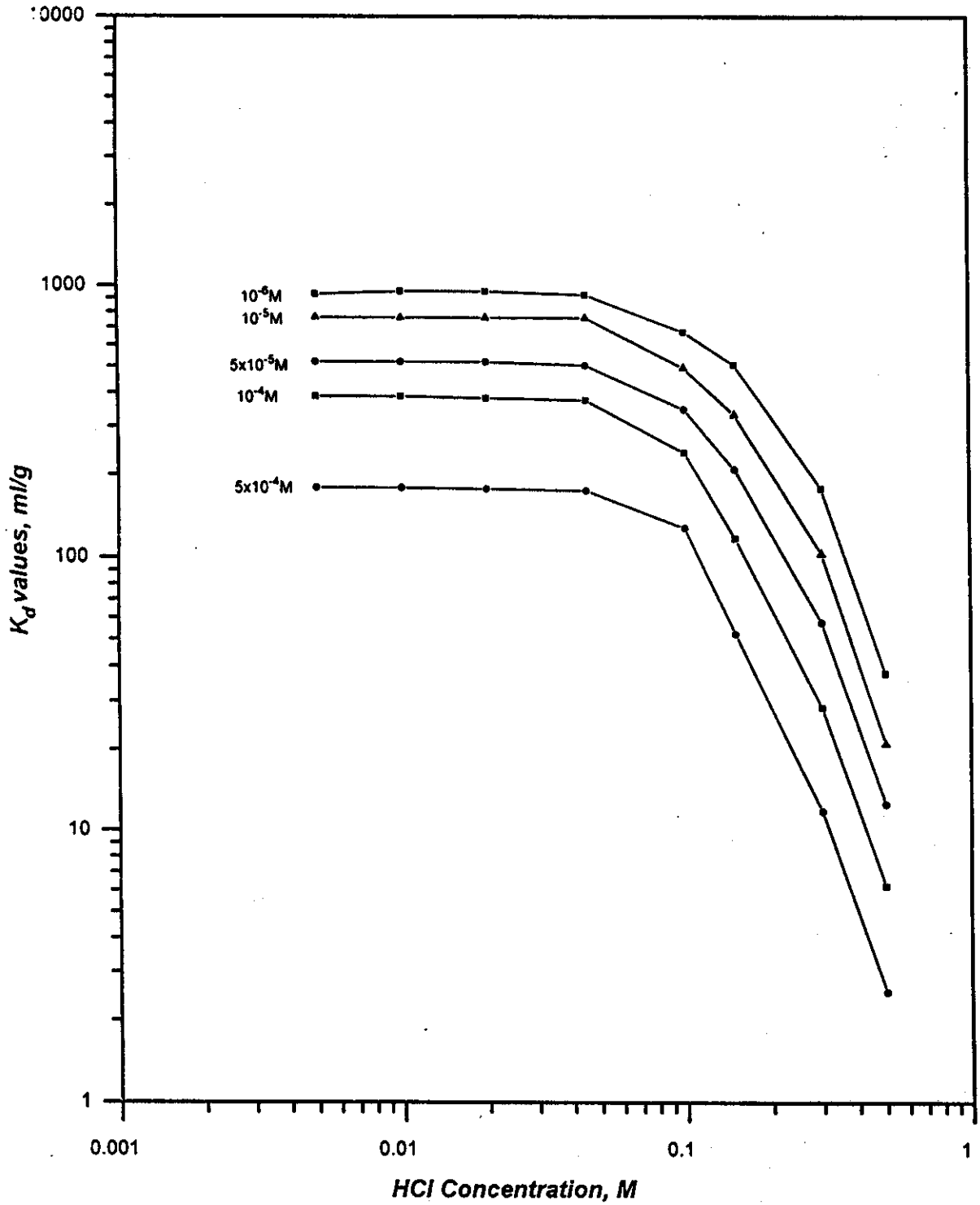

Fig.71. Distribution coefficient (K_d) values of Pb(II) in HCl acid solutions on 12-molybdocerate (IV) at different Pb(II) concentrations(25±1 °C).

It is clear that the high K_d values of Pb(II) in dilute acid solutions; 997ml/g at 0.05M HCl, and decrease markedly with increasing the acid concentration ?0.03M to reach to 40ml/g in 0.5M HCl acid solution. Lead(II) ions have a high tendency to form cationic species of $[Pb(OH)]^+$, Pb^{2+} and $[Pb(Cl)]^+$, in dilute acid solutions, which are tightly held onto the surface of 12-molybdocerate(IV) matrix by hydrolytic sorption and /or cation exchange mechanisms [24, 154]. At high acid concentrations Pb(II) ions shows a great tendency for complex formation with the Cl^- anions of the hydrochloric acid forming low and non sorbable anionic species of Pb(II): $[Pb(Cl)_2]$, $[Pb(Cl)_4]^{2-}$ and $[Pb(Cl)_6]^{4-}$ which contribute to the observed decrease of the K_d values[25,155]. Figures 69 and 71 indicate that however the sorption of Pb(II) in HNO3 and HCl acid solutions are similar; its sorption behaviour depends to a great extent on the concentration of the competing H^+ ions in solution as well as on the conjugated acid anion, where the K_d values in HNO_3 acid media are more higher than those in HCl acid solutions, at comparable conditions. This behaviour may be attributed to different association affinity of NO_3^- and Cl^- anions with Pb(II) in HNO_3 and HCl acid solutions to form less adsorbable stable complexes. On the other hand, Figures 70 and 72 show that the sorption behaviour and the corresponding K_d values of thallium(I) are seriously affected with the acid anion of the equilibrating media. It is obvious that the K_d values of Tl(I) in HNO_3 acid are higher than that in HCl acid solutions at comparable experimental conditions. This observation may be attributed to the high association affinity of thallium(I) towards Cl^- anions in hydrochloric acid solution forming more stable chloride complexes than NO_3^- anions in nitric acid solution, i.e, less stable strongly absorbed nitrate complexes[25,155, 156].

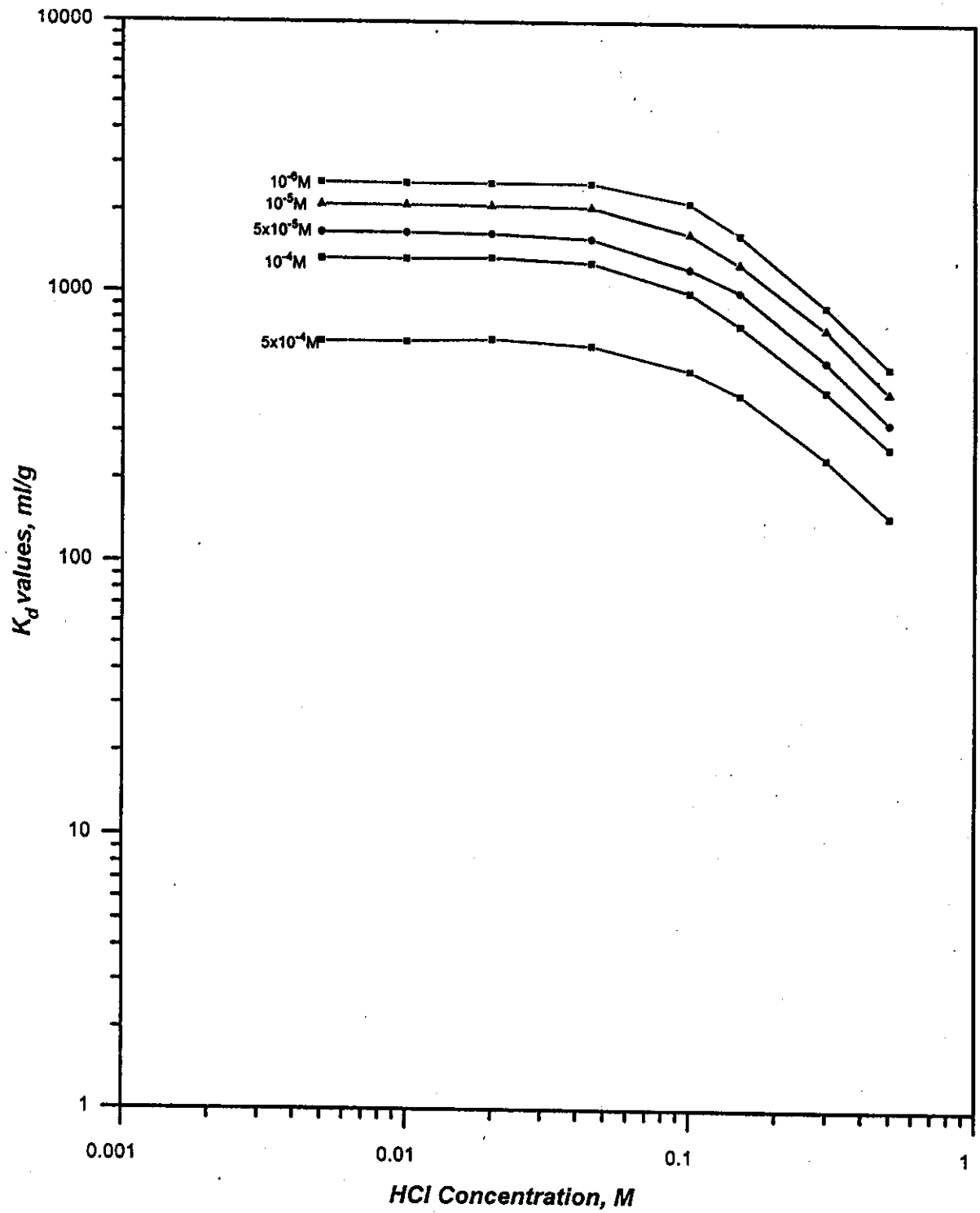

Fig.72. Distribution coefficient (K_d) values of Tl(I) in HCl acid solutions on 12-molybdocerate (IV) at different Tl(I) concentrations(25±1 °C).

3.4.1.1.3 Effect of Concentration of the Metal Ions

Figures (69 and 70) and (71 and 72) depicts the effect of lead(II) and thallium(I) concentrations, ranging from 10^{-6} to $5x10^{-4}$M, in nitric and hydrochloric acid solutions on their distribution behaviour on 12-molybdocerate(IV) gel. In all cases, the distribution coefficient (K_d) values of the respective Pb(II) and Tl(I) ions decrease with increasing the concentration of the ions in the equilibrating medium. At comparable conditions, the corresponding distribution coefficient (K_d) values of lead(II) are lower than that of thallium(I). It indicates that lead(II) ions are less strongly held on the 12-molybdocerate(IV) gel than its thallium(I) product at similar conditions. Therefore, the obtained observations are promising to meet the actual separation conditions of the cyclotron produced thallium(I) product from lead(II) precursor on 12-molybdocerate(IV) gel columns.

3.4.1.2 Dynamic Studies

Retention uptake of the 12-molybdocerate(IV) gel for different concentrations of the respective lead(II) and thallium(I) ions in 0.05 and 0.2M nitric and hydrochloric acid solution were individually investigated using the chromatographic column breakthrough technique. In this technique, feed solutions of the respective Pb(II) and Tl(I) ions in the proper acid solution were continuously passed through the column bed at a flow rate of 1ml/min and room temperature (25°C). The column effluents were collected in equal volume fractions and analyzed spectrophotometrically for Pb(II) and radiometrically for Tl(I). The concentration (C_v) of equal volume fractions were compared with standard samples (C_o) and the Corresponding breakthrough curves (C_v/C_o, % vs. effluent volume) for Pb(II) and Tl(I) were withdrawn.

3.4.1.2.1. Effect of Concentration of the Metal Ions

Figure 73 (curves a, b, c, d and e) depicts the breakthrough profile of 10^{-5}M Tl(I) and 10^{-5}, $5x10^{-5}$, 10^{-4} and $5x10^{-4}$M Pb(II) in 0.05M HNO_3 acid solution from 1g 12-molybdocerate(IV) column matrix. Plots of Figure 73 (curves b,c and d) indicate that the higher the concentration of Pb(II) in the feed solution, the faster dynamic equilibrium and breakthrough of lead(II) in 0.05M HNO_3 acid are obtained. So, the position of saturation uptake of 12-molybdocerate(IV) gel for lead(II) [C_v/C_o=100%] and 1% Tl(I) breakthrough can be improved towards lower effluent volumes (i.e., Pb-Tl resolution) the higher the concentration of the Pb(II) precursor in the feed solution. Taking into consideration that thallium(I) as the product radiotracer is in trace amounts while its lead(II) precursor would be present in micro amounts. Consequently, chromatographic columns packed with adequate amounts of the MoCe(IV) matrix would be ultimately sufficient for quantitative uptake of Tl(I) with sufficiently distinct separation from its Pb(II) precursor.

3.4.1.2.2 Effect of Chemical Composition and Nature of the Feed Solution

Figures 73 and 74 demonstrate the individual breakthrough behaviour of lead(II) and thallium(I) from 1g 12-molybdocerate(IV) columns as a function of nitric acid concentration. It is distinct that the breakthrough of both Pb(II) and Tl(I) are improved; to smaller effluent volumes, with increasing the acid concentration from 0.01 to 0.2M HNO_3 acid solutions. This observation is in accordance with the decrease in the k_d values at higher acidity of equilibrium solution. On the other hand, Figures 75 and 76 illustrate more or less similar breakthrough behaviour trend for both Pb(II)andTl(I) with increasing the concentration

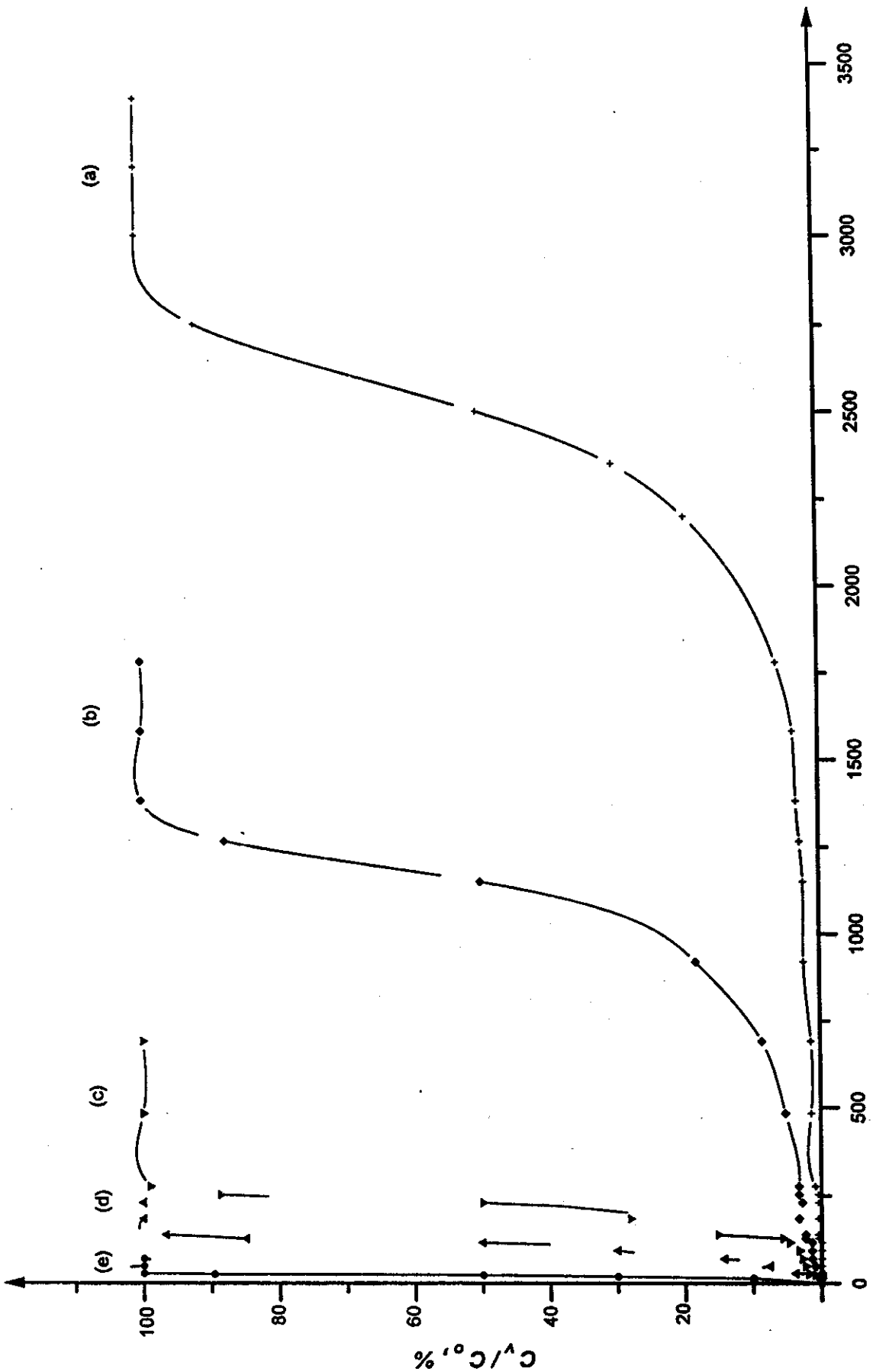

Fig.73. Breakthrough curves of Pb(II) and Tl(I) in 0.05M HNO_3 from 1g 12-molybdocerate(IV) columns (0.6cm i.d x 3.5cm) at flow rate 1ml/min as a function of metal ions concentrations.
(a) 10^{-5}M Tl(I) (b)10^{-5}M Pb(II) (c)$5x10^{-5}$M Pb(II) (d)10^{-4}M Pb(II) (e)$5x10^{-4}$M Pb(II)

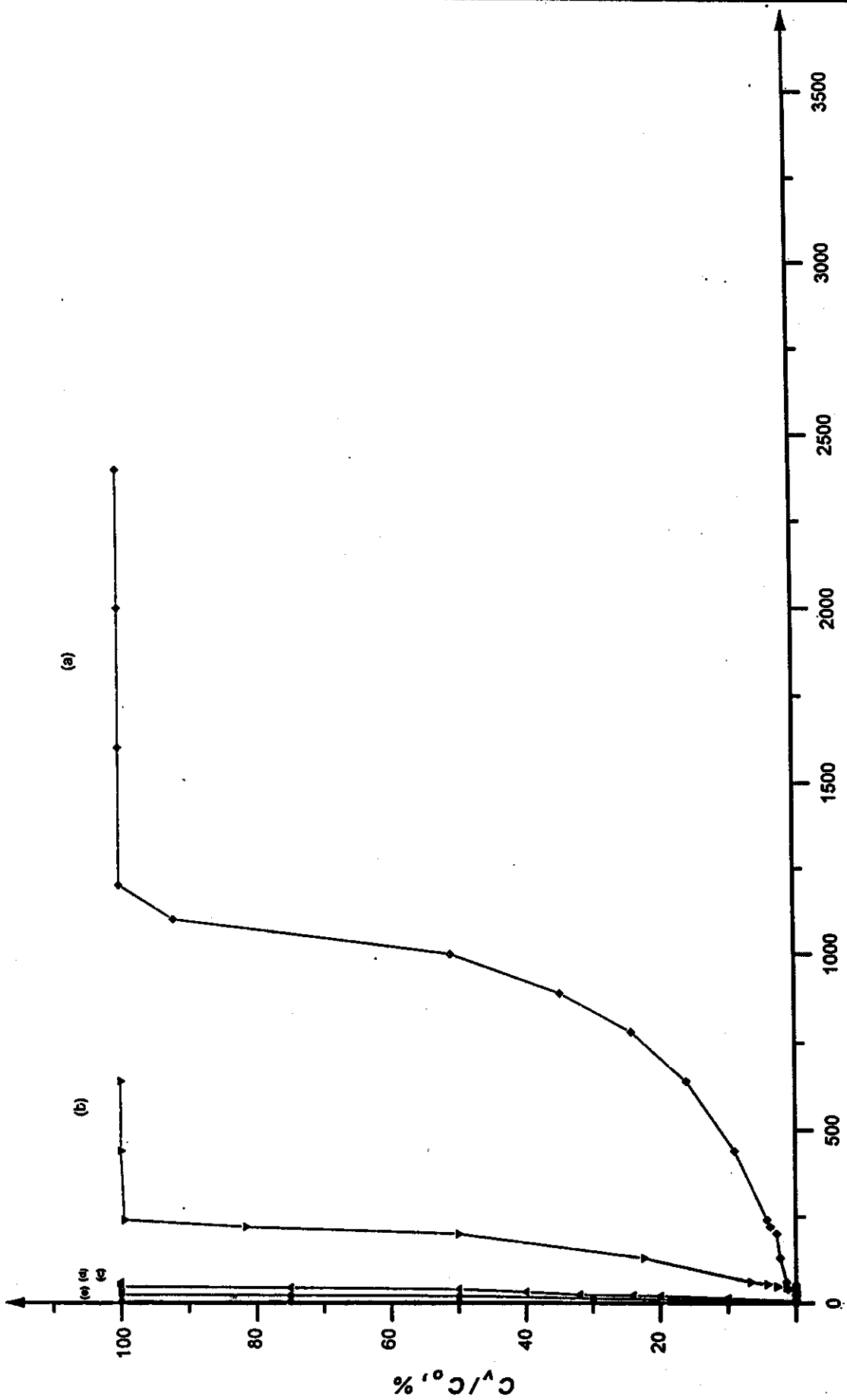

Fig.74. Breakthrough curves of Pb(II) and Tl(I) in 0.2M HNO_3 from 1g 12-molybdocerate(IV) columns (0.6cm i.d x 3.5cm) at flow rate of 1ml/min as a function of metals ions concentrations. (a)10^{-5}M Pb(II) (b)$5x10^{-5}$M Pb(II) (c)10^{-4}M Pb(II) (d)$5x10^{-4}$M Pb(II)

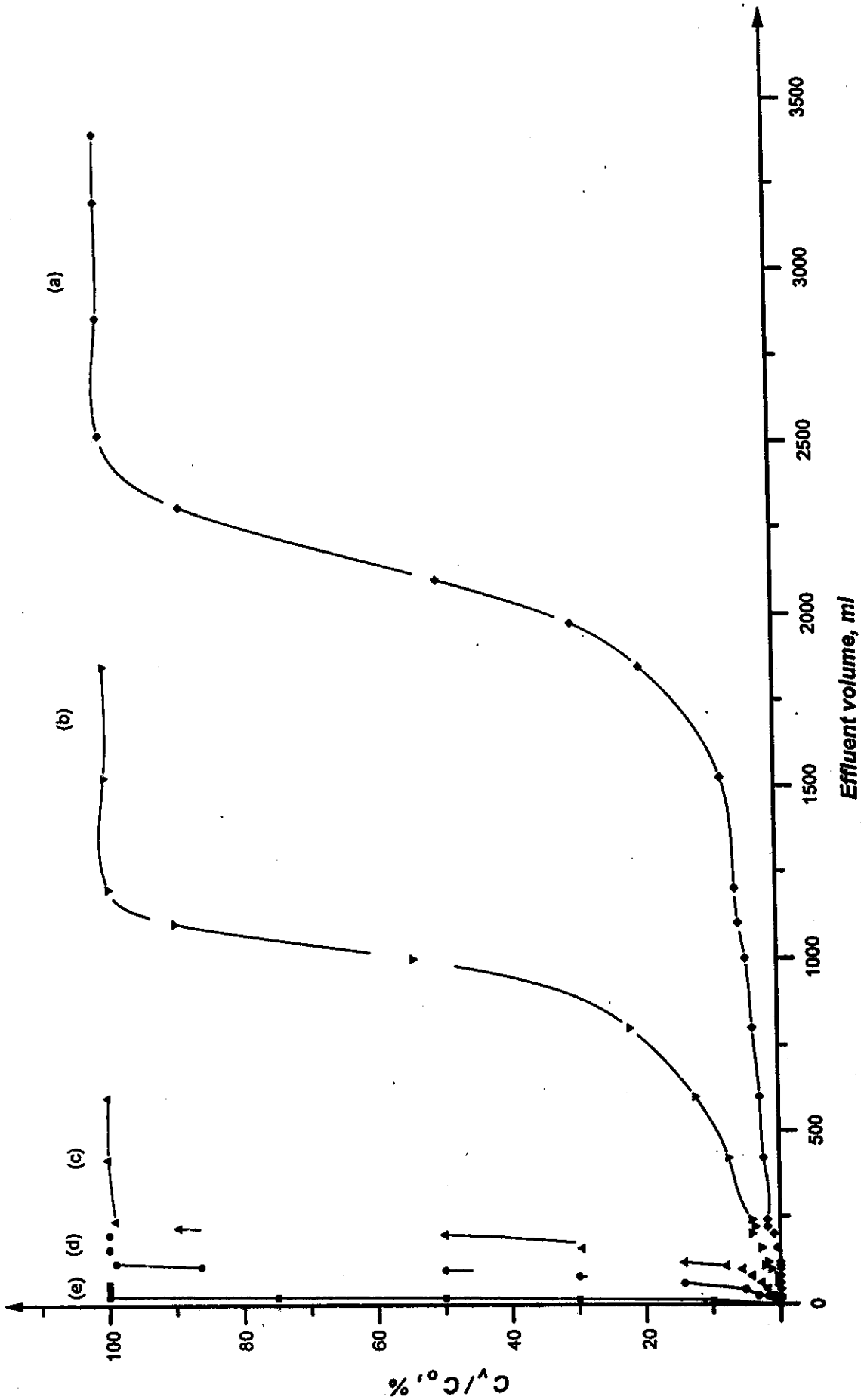

Fig.75. Breakthrough curves of Pb(II) and Tl(I) in 0.05M HCl from 1g 12-molybdocerate(IV) columns (0.6cm i.d x 3.5cm) at flow rate of 1ml/min as a function of metal ions concentrations. (a)10^{-5}M Tl(I) (b)10^{-5}M Pb(II) (c)$5x10^{-5}$M Pb(II) (d)10^{-4}M Pb(II) (e)$5x10^{-4}$M Pb(II)

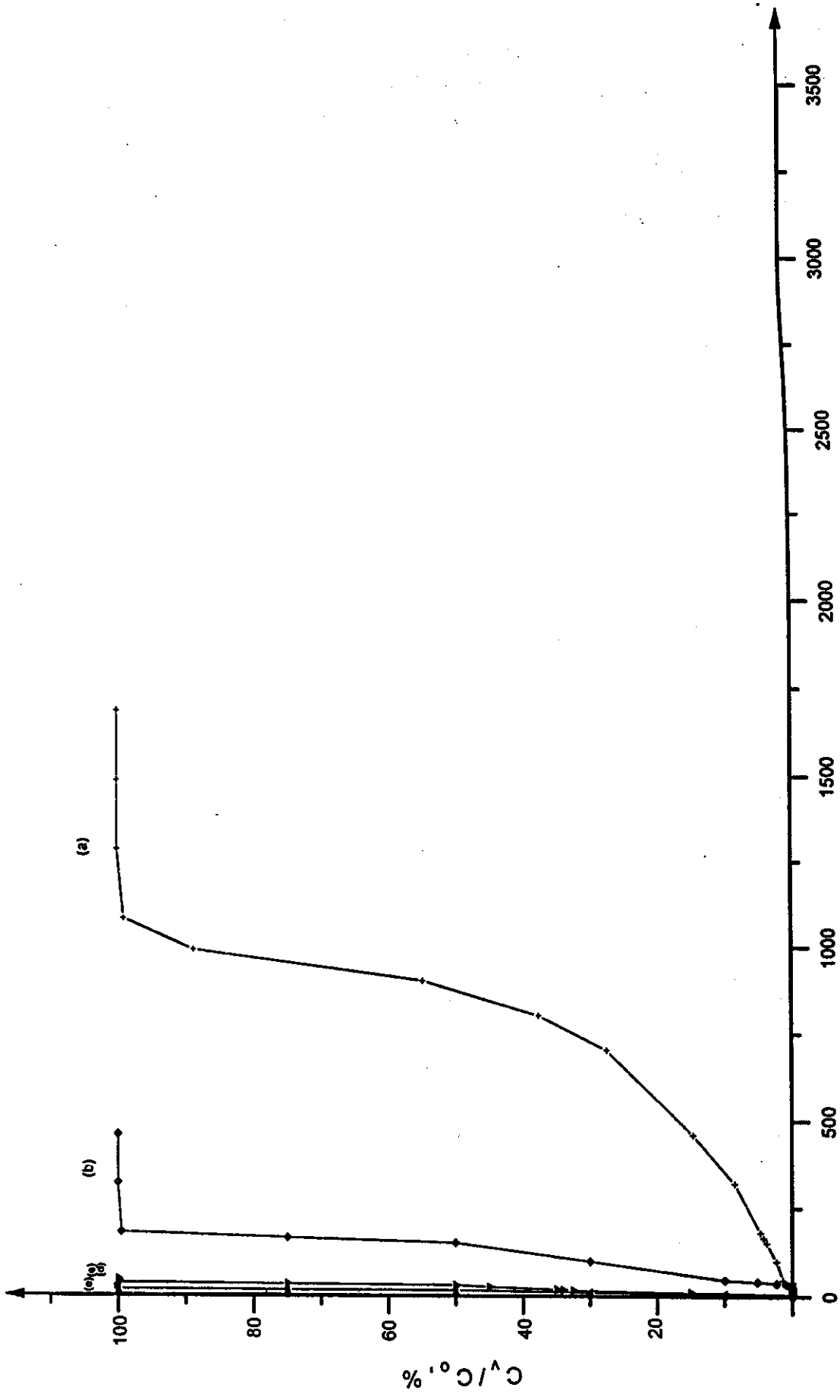

Fig.76. Breakthrough curves of Pb(II) and Tl(I) in 0.2M HCl from 1g 12-molybdocerate(IV) columns (0.6cm i.d x 3.5cm) at flow rate 1ml/min as a function of metal ions concentrations. (a)10^{-5}M Tl(I) (b)10^{-5}M Pb(II) (c)$5x10^{-5}$M Pb(II) (d)10^{-4}M Pb(II) (e)$5x10^{-4}$M Pb(II)

of HCl acid in the feed solution, as well as in HNO_3 acid solutions. It is distinct from Figures 73-76 that the breakthrough of Pb(II) and Tl(I) is more faster from hydrochloric acid than from nitric acid solutions, at comparable feeding conditions. This is in accordance with the previously obtained K_d values. This strongly suggests that, dilute nitric acid solutions would be more suitable media for the column loading and washing processes, where higher uptake values and delayed breakthrough for thallium(I) would be achieved under the investigated experimental conditions. At the other extreme, relatively concentrated hydrochloric acid is more preferable in elution process.

3.4.2 Chromatographic Column Separations

It is clear from the aforementioned distribution coefficient (K_d) values that thallium(I) ions in dilute and concentrated nitric and hydrochloric acid solutions have distinct sorption affinity towards the 12-molybdocerate(IV) matrix, with coparable lower sorption affinity for Pb(II) ions. Table 14 compiles the thallium(I)-lead(II) separation factor [α] values in nitric and hydrochloric acid solutions at different concentrations of acid and metal ions. The separation factor [α] values for thallium(I)-lead(II) in different acid solutions reflect the versatility of 12-molybdocerate(IV) to achieve their separation from each other by using the chromatogrphic column elution method. It is clear that matrix solutions of $\leq 10^{-5}$M Tl(I) and $\geq 5\times10^{-4}$M Pb(II) in 0.05 and 0.2M nitric and hydrochloric acid solution had the highest separation factor [α] values. Furthermore, it is observed that the thallium(I)-lead(II) separation factors [α] in hydrochloric acid solutions are much higher than in nitric acid solutions and 0.2M acid>0.05M acid.

Table 14. Individual distribution coefficients (K_d)values and separation factores (α) of Pb(II) / Tl(I) couple in HCl and HNO_3 acid solutions on 12-molybdocerate(IV)

Metal ion Concentration; M		Concentration of the equilibrating solutions											
		0.05M HCl			0.2M HCl			0.05M HNO_3			0.2M HNO_3		
		Distribution coefficient (K_d) values, ml/g											
		Tl^+	Pb^{2+}		Tl^+	Pb^{2+}		Tl^+	Pb^2		Tl^+	Pb^{2+}	
Product Tl^+	Precursor Pb^{2+}	Separation factor $\alpha=K_d(Tl) / K_d(Pb)$											
		K_d	K_d	α	K_d	K_d	α	K_d	K_d	α	K_d	K_d	α
$5x10^{-4}$	$5x10^{-4}$	600	175	3.43	320	28	11.43	1200	240	5	630	56	1.125
10^{-4}		1300	175	7.43	590	28	21.07	1975	240	8.23	1150	56	20.54
$5x10^{-5}$		1600	175	9.14	750	28	26.79	2400	240	10	1400	56	25
10^{-5}		2000	175	11.43	960	28	34.29	2950	240	12.29	1800	56	32.14
$5x10^{-4}$	10^{-4}	600	340	1.76	320	62	5.16	1200	450	2.67	630	120	5.25
10^{-4}		1300	340	3.82	590	62	9.52	1975	450	4.39	1150	120	9.58
$5x10^{-5}$		1600	340	4.71	750	62	12.09	2400	450	5.33	1400	120	11.67
10^{-5}		2000	340	5.88	960	62	15.48	2950	450	6.56	1800	120	15
$5x10^{-4}$	$5x10^{-5}$	600	450	1.33	320	125	2.56	1200	630	1.9	630	185	3.41
10^{-4}		1300	450	2.89	590	125	4.72	1975	630	3.13	1150	185	6.22
$5x10^{-5}$		1600	450	3.56	750	125	6	2400	630	3.81	1400	185	7.57
10^{-5}		2000	450	4.44	960	125	7.68	2950	630	4.68	1800	185	9.73
$5x10^{-4}$	10^{-5}	600	690	0.87	320	190	1.68	1200	890	1.35	630	290	2.17
10^{-4}		1300	690	1.88	590	190	3.11	1975	890	2.22	1150	290	3.97
$5x10^{-5}$		1600	690	2.32	750	190	3.95	2400	890	2.69	1400	290	4.83
10^{-5}		2000	690	2.89	960	190	5.05	2950	890	3.31	1800	290	6.21

Therefore, promising separation of thallium(I) from lead(II) can be achieved, more or less, completely by virtue of the differences in their sorption affinity towards the molybdocerate(IV) matrix, particularly, at high acid concentrations (≤0.2M). On the other hand, Table 15 compiles the breakthrough characteristics of Pb(II) and Tl(I) in nitric and hydrochloric acid solutions at different concentrations of acid and metal ions. Hence, separation of lead(II)-thallium(I) couple has been investigated by both elution and frontal separation methods using small chromatographic columns of 12-molybdocerate(IV) bed matrix.

3.4.2.1 Elution Chromatography

Elution performance of lead(II)-thallium(I) couple was conducted using chromatographic columns of (0.6cm i.d x 3.5cm) packed each with 1g 12-molybdocerate(IV) matrix loaded with 5ml mixture solution consists of $5x10^{-4}$M Pb(II) and 10^{-5}M Tl(I) in 0.05 and 0.2M nitric and hydrochloric acid solutions at flow rate of 0.5 ml/min.

3.4.2.1.1 Effect of Nature and Concentration of the Eluent

Lead(II) and thallium(I) elution performances were investigated as a function of type and concentration of the acid eluents. Figure 77 demonstrates the affect of 0.2 and 0.05M nitric acid solutions, as eluents, on the elution profiles and yields of the Pb(II)-Tl(I) couple from 1g 12-molybdocerate(IV) columns at a flow rate of 0.5ml/min. It is distinct that Pb(II) is readily eluted in the form of sharp elution profile with 5ml 0.2and relatively broad delayed peak with 0.05M HNO_3 acid solutions at a flow rate of 0.5ml/min. It was found that about 96.2% and 87% of the lead(II) ions loaded onto the column matrix are eluted and concentrated in the first 5ml and 10ml 0.2 and 0.05M HNO_3 acid eluates; respectively.

Table 15. Breakthrough characteristics of Pb(II) and Tl(I) in HCl and HNO_3 acid solutions from 1g 12-molybdocerate(IV) columns at a flow rate of 1ml/min

Metal ion conc., M	Character	Concentration of HCl, M				Concentration of HNO_3, M			
		0.05		0.2		0.05		0.2	
		Pb	Tl	Pb	Tl	Pb	Tl	Pb	Tl
10^{-5}	V(1%)	60	184	5	70	69	220	6	78
	V(50%)	1000	2100	150	900	1150	2500	200	1000
	V(100%)	1200	2520	180	1080	1380	3000	240	1200
	C, meq/g	$2x10^{-2}$	$2.1x10^{-2}$	$3x10^{-3}$	$9x10^{-3}$	$2.3x10^{-2}$	$2.5x10^{-2}$	$4x10^{-3}$	$1x10^{-2}$
$5x10^{-5}$	V(1%)	12	37	1	14	14	44	1	16
	V(50%)	200	420	30	180	230	500	40	200
	V(100%)	240	504	36	216	276	600	48	240
	C, meq/g	$2x10^{-2}$	$2.1x10^{-2}$	$3x10^{-3}$	$9x10^{-3}$	$2.3x10^{-2}$	$2.5x10^{-2}$	$4x10^{-3}$	$1x10^{-2}$
10^{-4}	V(1%)	6	18	1	7	7	22	1	8
	V(50%)	100	210	15	90	115	250	20	100
	V(100%)	120	252	18	108	138	300	24	120
	C, meq/g	$2x10^{-2}$	$2.1x10^{-2}$	$3x10^{-3}$	$9x10^{-3}$	$2.3x10^{-2}$	$2.5x10^{-2}$	$4x10^{-3}$	$1x10^{-2}$
$5x10^{-4}$	V(1%)	1	4	1	2	2	5	1	2
	V(50%)	20	42	3	18	23	50	4	20
	V(100%)	24	51	4	22	28	60	5	24
	C, meq/g	$2x1^{-2}$	$2.1x10^{-2}$	$3x10^{-3}$	$9x10^{-3}$	$2.3x10^{-2}$	$2.5x10^{-2}$	$4x10^{-3}$	$1x10^{-2}$

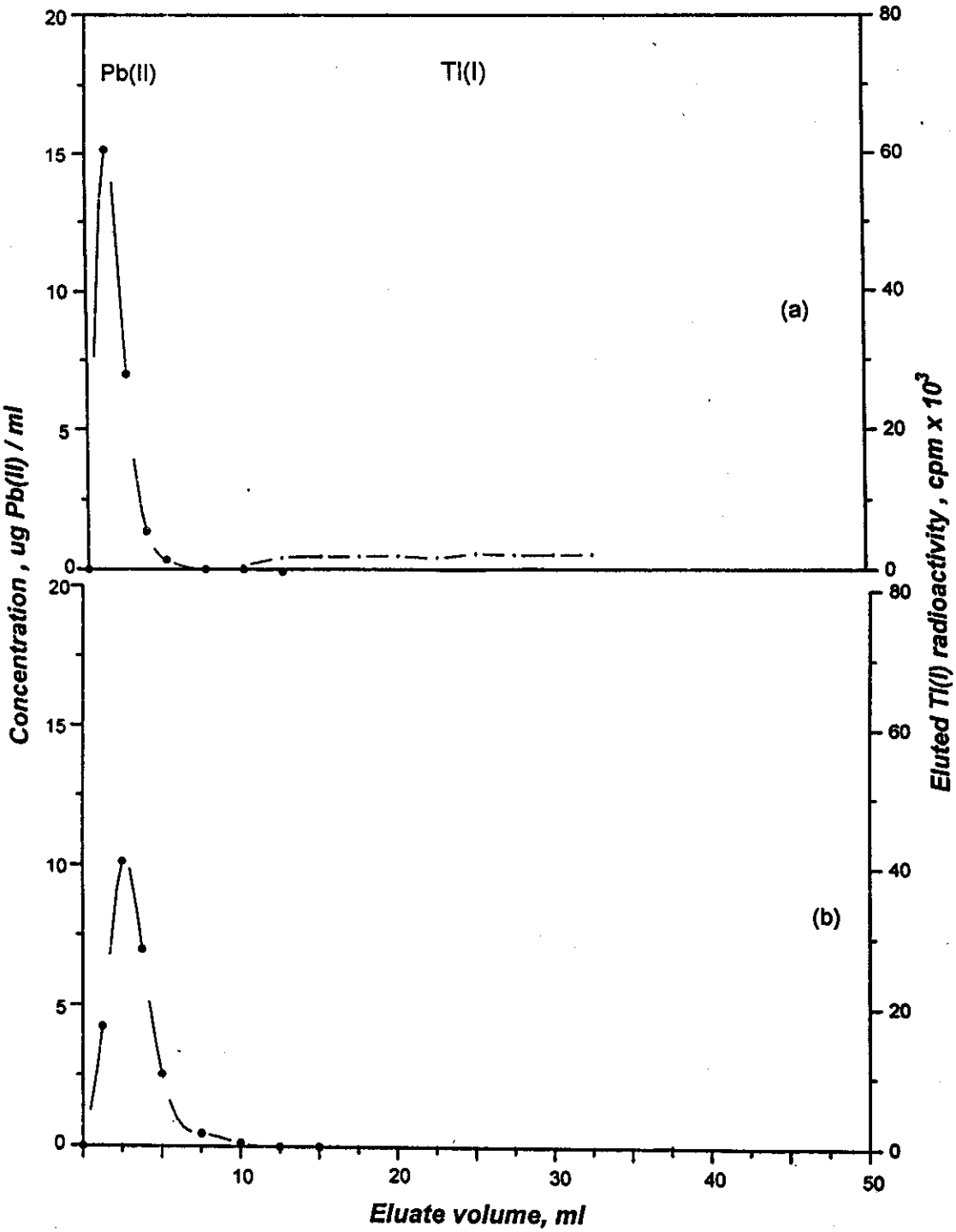

Fig.77.Elution curves of Pb(II) from Tl(I) onto 1g 12-molybdocerate(IV) columns(0.6cmx3.5cm) with (a)0.2 (b)0.05M HNO_3 acid solutions at flow rate of 0.5ml/min.

While, thallium(I) was quantitatively retained onto the sorbent matrix in 0.05M HNO_3 acid, a small leakage of thallium(I) (about 7.6%) was achieved in 0.2M HNO_3 acid solution at a flow rate of 0.5ml/min. As a consequence, the corresponding elution efficiency increases and the distribution of the eluted radioactivity is concentrated in smaller eluate volume with acid concentration. At other extreme, Figure 78 shows the elution profiles of the respective cations with 0.2 and 0.05M HCl acid solution. It was found that about 98.4 and 89% of the Pb(II) ions is eluted in the first 8ml of 0.2 and 0.05M HCl acid eluate; respectively. Moreover; it is observed from figures 77 and 78 that the chromatographic behaviour of Pb(II) and Tl(I) are more or less in accordance with the previously obtained batch distribution and dynamic studies data.

3.4.2.1.2 Effect of Flow Rate of the Eluent

Figures 79 and 80 show the effect of flow rate (i.e., 0.5, 1 and 2 ml/min) on the elution profiles of lead(II) and thallium(I) in 0.2 and 0.05M HCl acid solutions from 1g 12-molybdocerate(IV) columns; respectively. It is obvious that the positions of the maximum elution peaks of lead(II) are displaced to higher eluate volumes with increasing the flow rate of the eluent and / or decreasing the acid concentrations. Moreover, the obtained broad and; somewhat, diffused aft-boundaries of the Pb(II) elution profiles with increasing the flow rate may be due to slow sorption/desorption kinetics of lead(II) ions on the surface of the molybdocerate(IV) matrix into the eluent [i.e, slow diffusion mechanisms]. The distribution (i.e, volume concentration) of the eluated Tl(I) radioactivity in the different eluate fractions of 0.2M HCl gives shallow-tailed profiles at all the investigated flow rates.

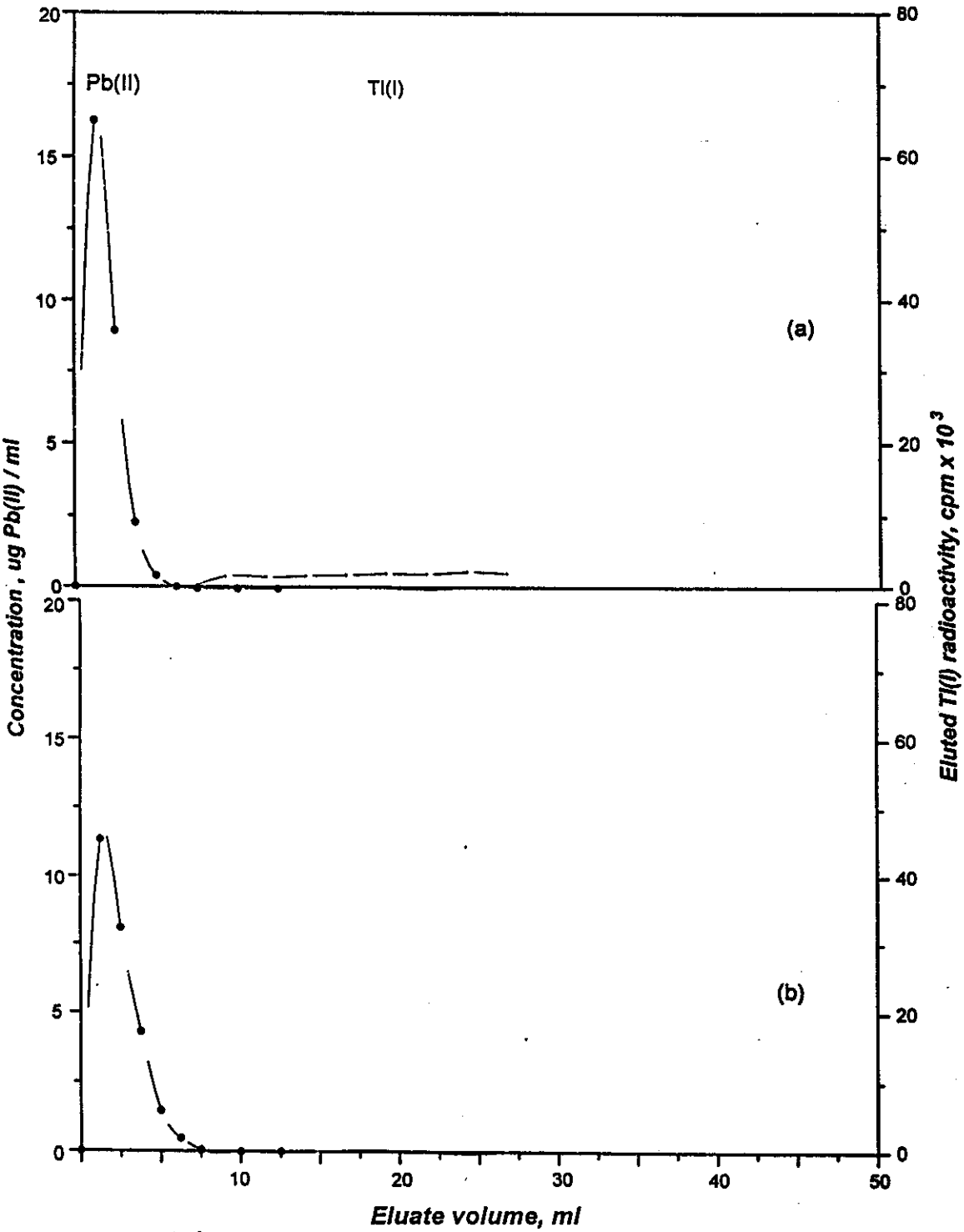

Fig.78. Elution curves of Pb(II) from Tl(I) onto 1g 12-molybdocerate(IV) columns (0.6cm i.d x3.5cm) with (a)0.2 (b) 0.05M HCl acid solutions at flow rate of 0.5ml/min.

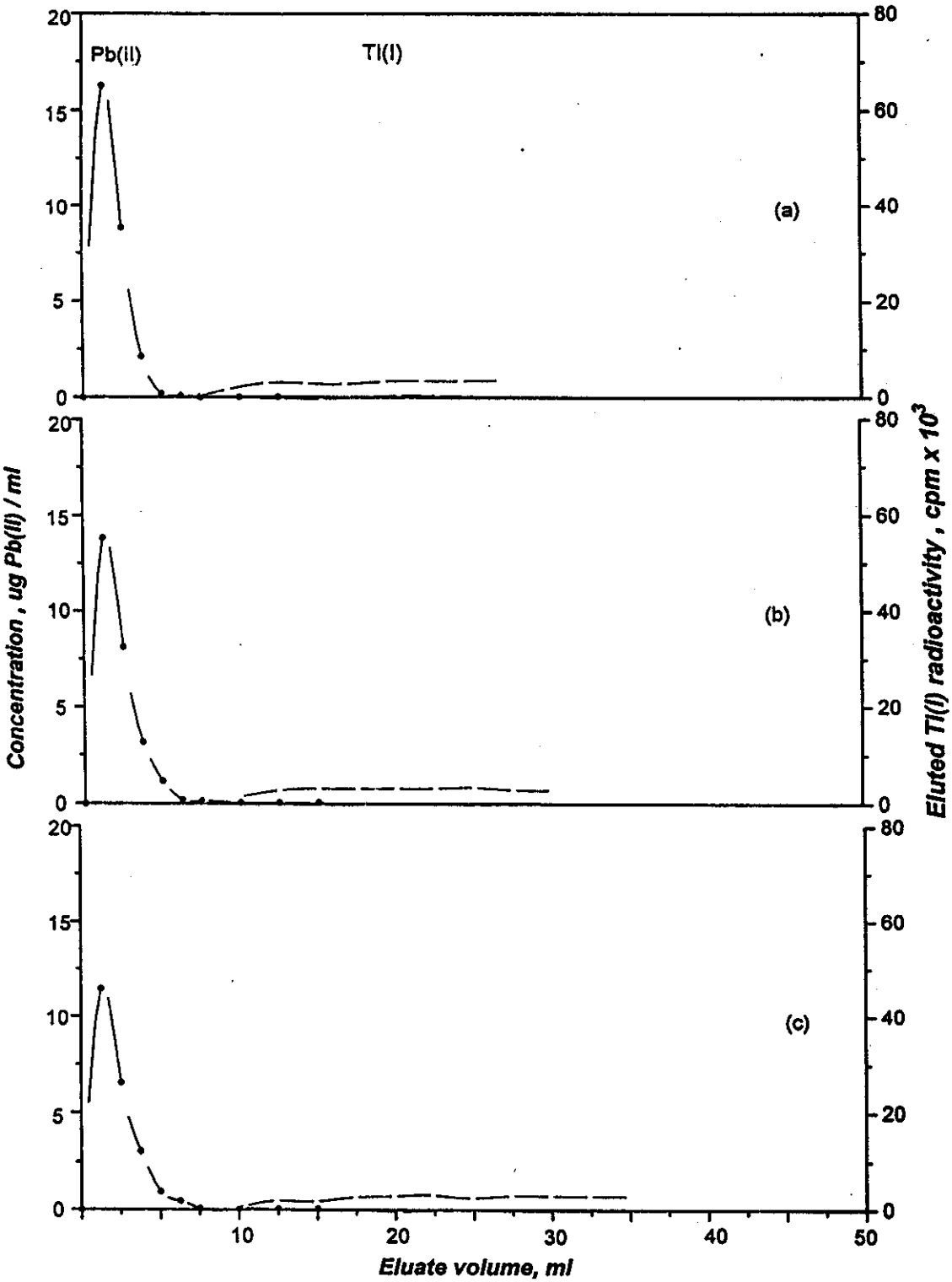

Fig.79. Elution curves of Pb(II) from Tl(I) onto 1g 12-molybdocerate(IV) columns (0.6cm i.d x 3.5cm) with 0.2M HCl at a flow rate of (a)0.5ml/min (b)1.0ml/min (c)2.0ml/min

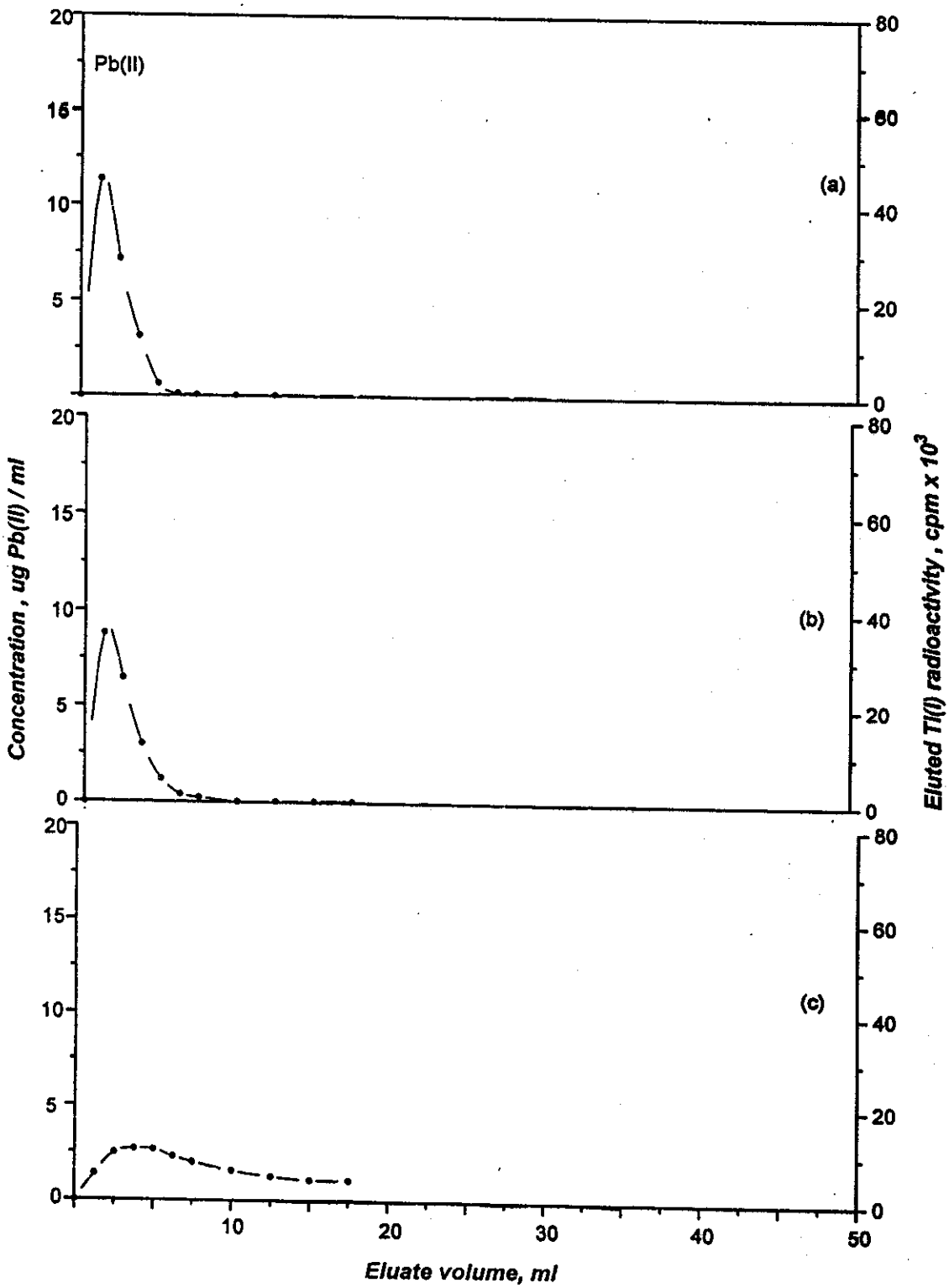

Fig.80. Elution curves of Pb(II) from Tl(I) onto 1g 12-molybdocerate(IV) columns (0.6cm i.d x 3.5cm) with 0.05M HCl at a flow rate of
(a)0.5ml/min (b)1.0ml/min (c)2.0ml/min

Figures 81 and 82 show that the elutionof Tl(I) and Pb(II) with nitric acid solutions (0.2 and 0.05M) has more or less similar elution behaviour trends as in HCl solutions at comparable flow rate. It was found that about 96.2%, 88.4% and 76.8% of Pb(II) are obtained in the first 5ml of 0.2M HNO_3 acid as eluate at flow rate of 0.5, 1 and 2ml/min, respectively ,whereas, about 8.5%, 5.8% and 3.7% of the eluted Tl(I) radioactivity were obtained with 15ml 0.2M HNO_3 acid solution. On the other hand, about 98.4%, 92.3% and 83.6% of the Pb(II) are obtained in the first 5ml of 0.2M HCl acid eluates at flow rates of 0.5, 1, and 2ml/min; respectively, whereas, about 11.4%, 9.7% and 5.6% of Tl(I) radioactivity were obtained with 15ml 0.2M HCl acid solution.

3.4.2.1.3 Recommended Procedure for Elution Separation of the Lead(II)- Thallium(I) Couple

In case of small solute volumes, the chromatographic column elution mode is recommended for separation of the lead(II) - thallium(I) couple since the amounts of lead(II) precursor, by any way, must not exceed fifteen percent of the total sorption capacity of the sorbent matrix. In this process, 5ml of the mixture solution consists of 10^{-5}M Tl(I) radiotracer and $5x10^{-4}$M Pb(II) in 0.01M HNO_3 acid solution was loaded onto 1g 12-molybdocerate(IV) column. Quantitative sorption of both Pb(II) and Tl(I) onto the sorbent matrix was verified by spectrophotometric and/or radiometric measurments of the column effluents. Elution and purification of the bed matrix from the retained Pb(II) achieved with passing 7ml 0.05M HNO_3 acid solution at a flow rate of 0.5ml/min. Further purification of the column matrix from any residual Pb(II) ions held onto MoCe(IV) matrix and conditioning the bed matrix for Tl(I) elution is carried out using 2ml 0.05M HCl at the same

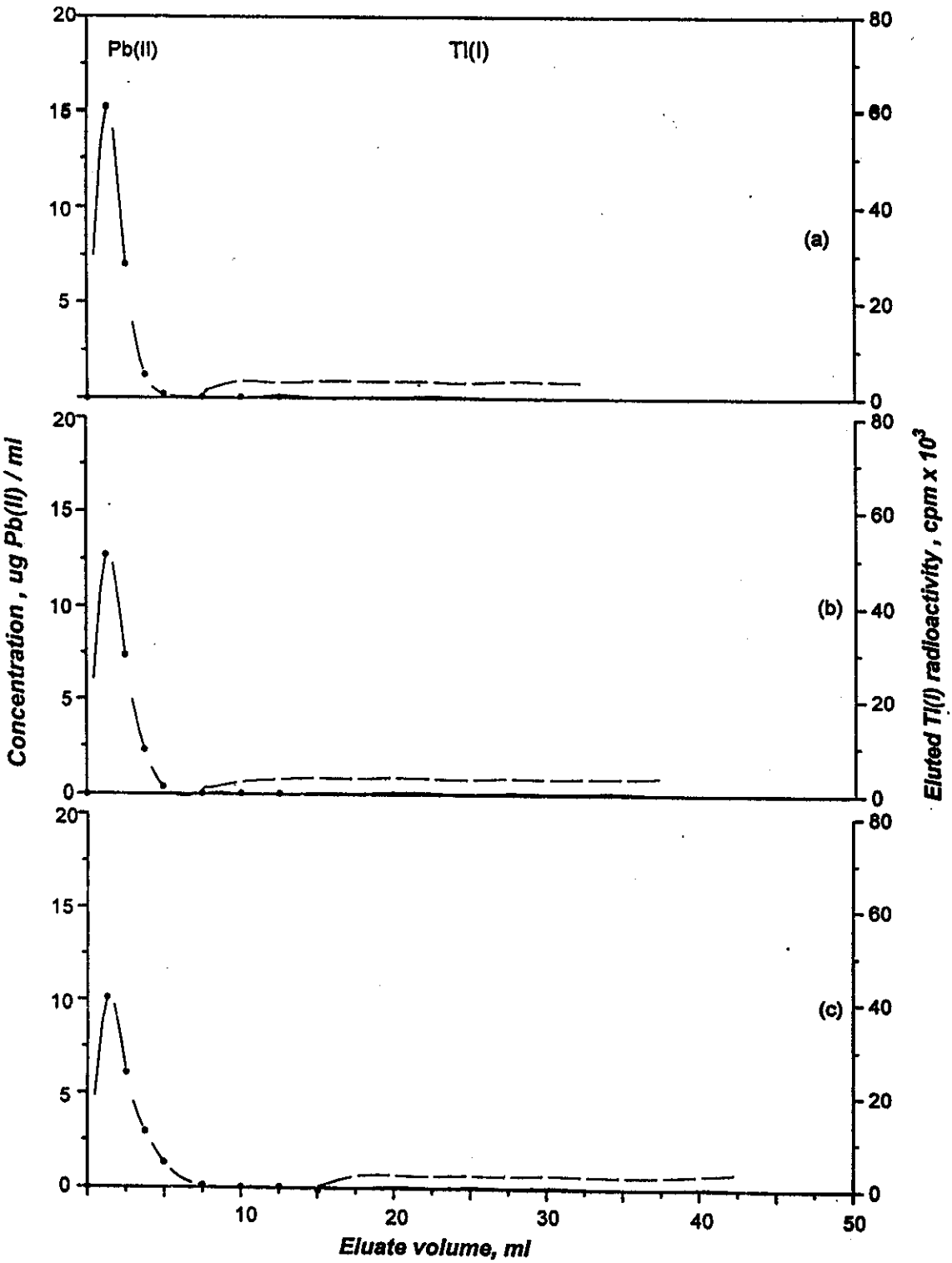

Fig.81. Elution curves of Pb(II) from Tl(I) onto 1g 12-molybdocerate(IV) columns (0.6cm i.d x 3.5cm) with 0.2M HNO_3 at a flow rate of
(a)0.5ml/min (b)1.0ml/min (c)2.0ml/min

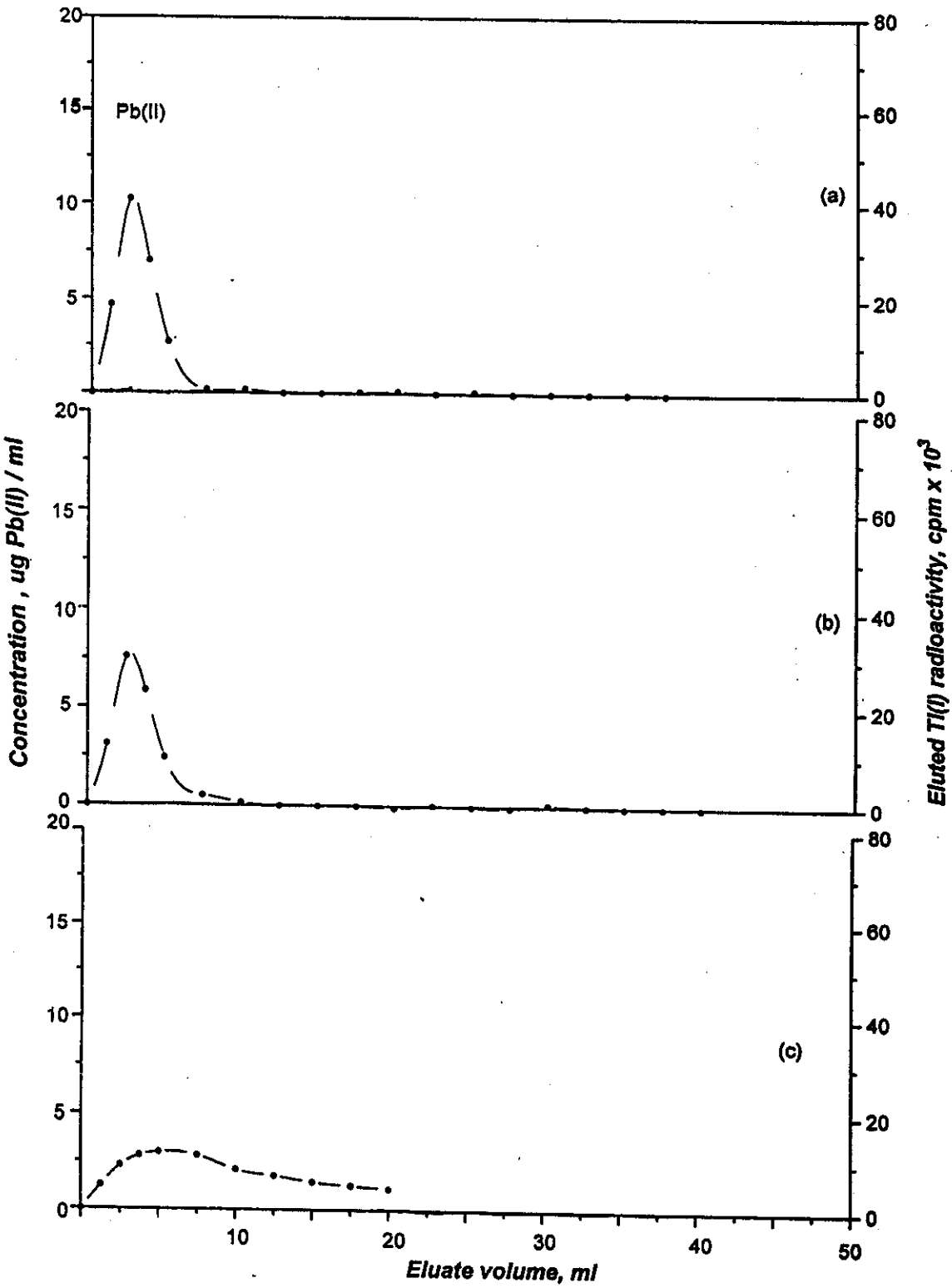

Fig.82. ELution curves of Pb(II) from Tl(I) onto 1g 12-molybdocerate(IV) columns (0.6cm I.d x 3.5cm) with 0.05M HNO_3 at a flow rate of
(a)0.5ml/min (b)1.0ml/min (c)2.0ml/min

flow rate. Thereafter, the tightly retained Tl(I) is eluted with 18ml 1M HCl acid solution at flow rate of 0.5ml/min. Figure 83 demonstrate the elution profiles of Pb(II) and Tl(I) from 1g 12-molybdocerate(IV) column with 0.05M HNO_3 , 0.05 and 1M HCl acid solutions at a flow rate of 0.5ml/min; respectively. It was found that about 87% of the loaded Pb(II) radioactivity was eluted and concentrated in the first 5ml 0.05M HNO_3, whereas about 97% of the Tl(I) radioactivity were eluted with 25ml 1M HCl acid solution. The elution yield of thallium(I) was found to be about 92.4% of the total Tl(I) radioactivity loaded onto the column matrix. The observed elution yield is high compared with those obtained from anion exchange columns; Dowex 1x8 (200-400 mesh) and AG1-X4 (i.e., 50-55% and 68%); respectively[10,126]. Figure 84 demonstrates the proposed schematic diagram for separation of carrier-free Tl(I) from its Pb(II) precursor by chromatographic column elution method.

3.4.2.2 Frontal Chromatography

In radiochemical processing of the cyclotron produced radioisotopes, the Pb(II) precursor and the product Tl(II) radiotracer are in relatively high solute volumes of around 50ml of the etching solution [10,124]. Consequently, the continuous feeding technique for Pb(II)-Tl(I) separation is of great importance, in practice, compared to the elution method. In this technique, mixture solutions of $5x10^{-4}$M Pb(II) and 10^{-5}M Tl(I) in 0.05M HCl acid solution is continuously added to 1g MoCe(IV) columns.

3.4.2.2.1 Recommended Procedure for Frontal separation of Lead(II)-Thallium(I) Couple

The previously obtained breakthrough characteristics as well as the elution profiles data indicate the optimum operating conditions for

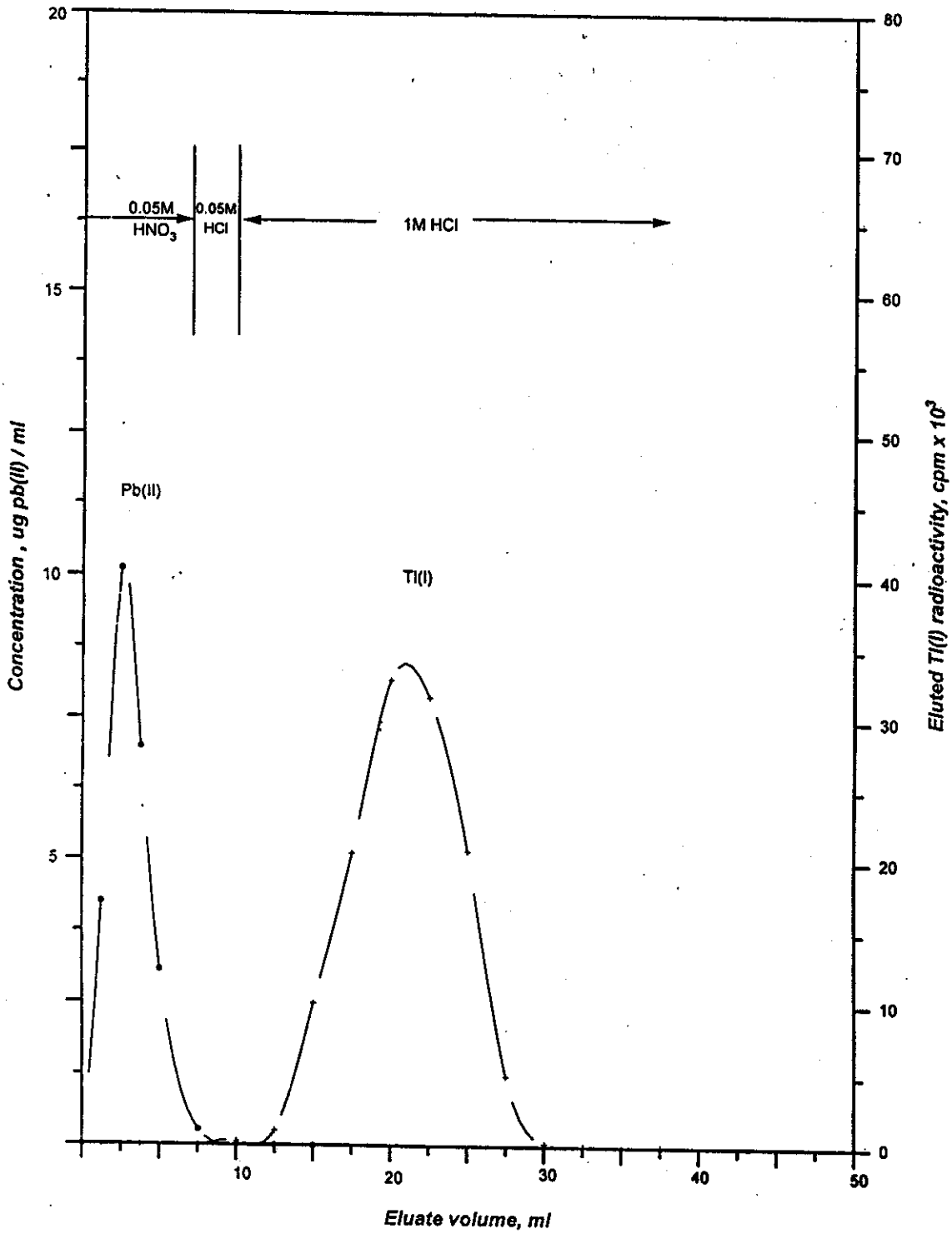

Fig.83.Typical elution profiles of Tl(I) from Pb(II) onto 1g 12-molybdocerate(IV) columns (0.6cmx3.5cm) with HNO_3 and HCl acid solutions at flow rate of 0.5ml/min.

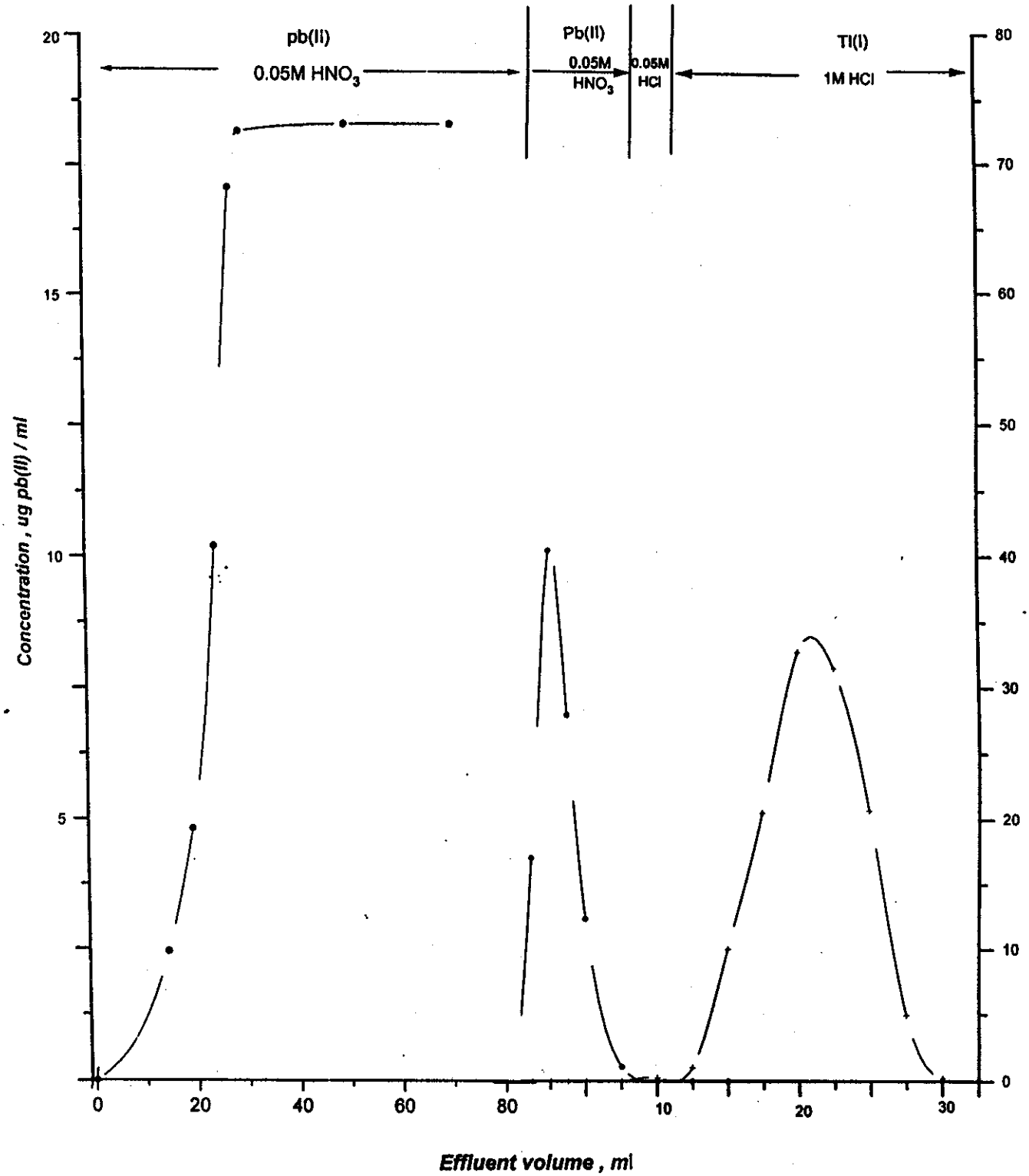

Fig.85. Frontal separation of mixture solution containing $5x10^{-4}$M Pb(II) and 10^{-5}M Tl(I) from 1g 12-molybdocerate(IV) column (0.6cm x 3.5cm) with HNO_3 and HCl acid solutions.

separation of Tl(I) radiotracer from its Pb(II) precursor. Figure 85 demonstrate that Pb(II)-Tl(I) separation can be achieved by feeding mixture solution of $5x10^{-4}$M Pb(II) and 10^{-5}M Tl(I) radiotracers in 0.05M HNO_3 acid solution through small chromatographic column packed with 1g 12-molybdocerte(IV) gel (0.6cm i.d x 3.5cm) at a flow rate of 1ml/min. It is clear that the mixture constituent lead(II), with the weakest tendency for the sorbent matrix, was immediately migrated through the column, whereas, thallium(I) with the strongest affinity for the MoCe(IV) gel accumulates onto the sorbent matrix of the column in agreement with the previously obtained breakthrough characteristics. The remaining Pb(II) ions is eluted and purified from the column with 7ml 0.05M HNO_3 acid at a flow rate of 1ml/min. Further purification and column conditioning is carried out with passing 2ml 0.05M HCl acid at the same flow rate. Thereafter, Tl(I) is eluted with 18ml 1M HCl acid solution at a flow rate of 1ml/min. Figure 86 illustrates the proposed schematic diagram for separation of the Pb(II)-Tl(I) couple by chromatographic column frontal method.

3.4.3 Regeneration of the Column Matrix:

To replace the tightly held thallium(I) ions remaining onto the sorbent surface by hydrogen ion(i.e., conversion of the column bed into the H^+-form) was carried out by using relatively concentrated acid solution. Therefore, to ensure complete conversion of the bed matrix to the H^+-form sufficient volume (about 30 times of the matrix volume) of 1M nitric or hydrochloric acid solutions was passed through the column matrix at a flow rate of 0.5ml/min.

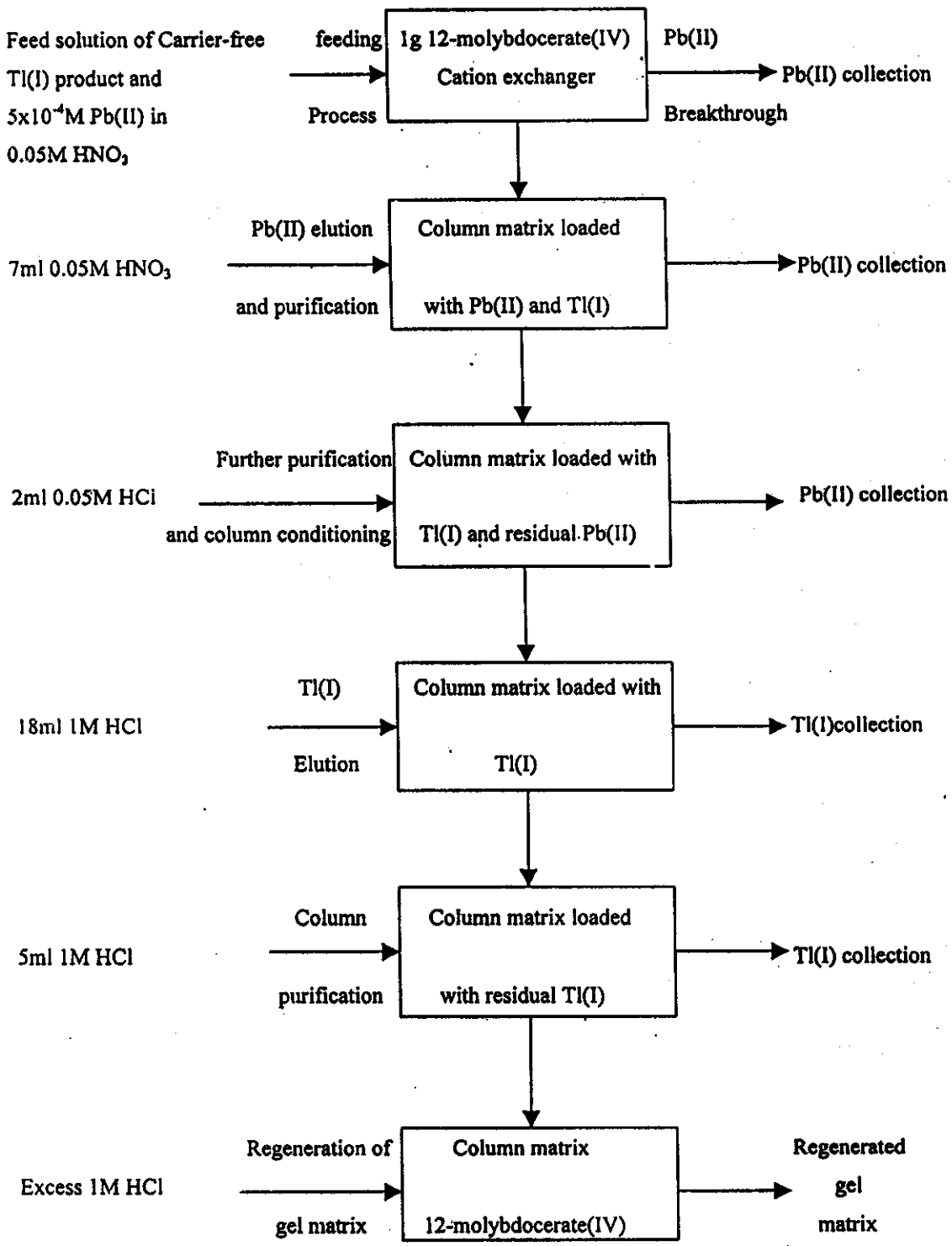

Fig.86. Proposed schematic diagram for separation of carrier-free Tl(I) from cyclotron produced Pb(II) precursor by chromatographic column frontal method.

3.4.4 Quality Control Testes

3.4.4.1 Chemical Purity of Thallium(I) Eluates

Presence of any chemical impurities in the thallium(I) eluates will markedly affect its use for nuclear medicine applications[128,133]. The chemical impurities may be originated form the sorbent matrix and/or the eluents. The used chemicals are of analytical reagent grade; therefore, its concentration as chemical impurities was eliminated. The thallium(I) eluates were analyzed spectrophotometrically[75,159] for the presence of molybdenum and cerium as a chemical contaminants originated from the 12-molybdocerate(IV) matrix. Cerium and molybdenum concentrations in the eluates are dependent on the concentration of the acid eluents (0.01-1M acid) and on the working temperature (about 25°C). It was found that the cerium and molybdenium concentrations are about 1μg Ce/ml and in the range of 2-4μg Mo/ml in 1M acid. These concentrations are below the restricted limits for nuclear medicine applications[130,132].

3.4.4.2 Radionuclidic Purity of Thallium(I) Eluates

The Presence of other radionuclides; of longer half-lives, higher photon energies and/or mode of decay above to an accepted level, will increase the radiation exposure dose to the patient and give bad diagnostic quality pictures[129,131,134]. The radionuclidic purity of thallium(I) eluates is defined as the proportion of the desired thallium(I) radionuclide to the total eluate radioactivity. The radionuclidic purity of the thallium(I) eluates, was confirmed by high-resolution gamma spectrometry using high purity germanium (HPGe) detector coupled to multichannel analyzer. Figure 87 shows the gamma spectra of thallium(I) eluates measured immediately after separation. It is observed that photo peaks (70.82, 80.2, 134, 208.2, 265.7, 316.8, 367.9, 457.2, 564.2, 579.3, 704.6, 828.3, 1021.5, 1139.9, 1205.7, 1385.3, 1411.3) corresponding to

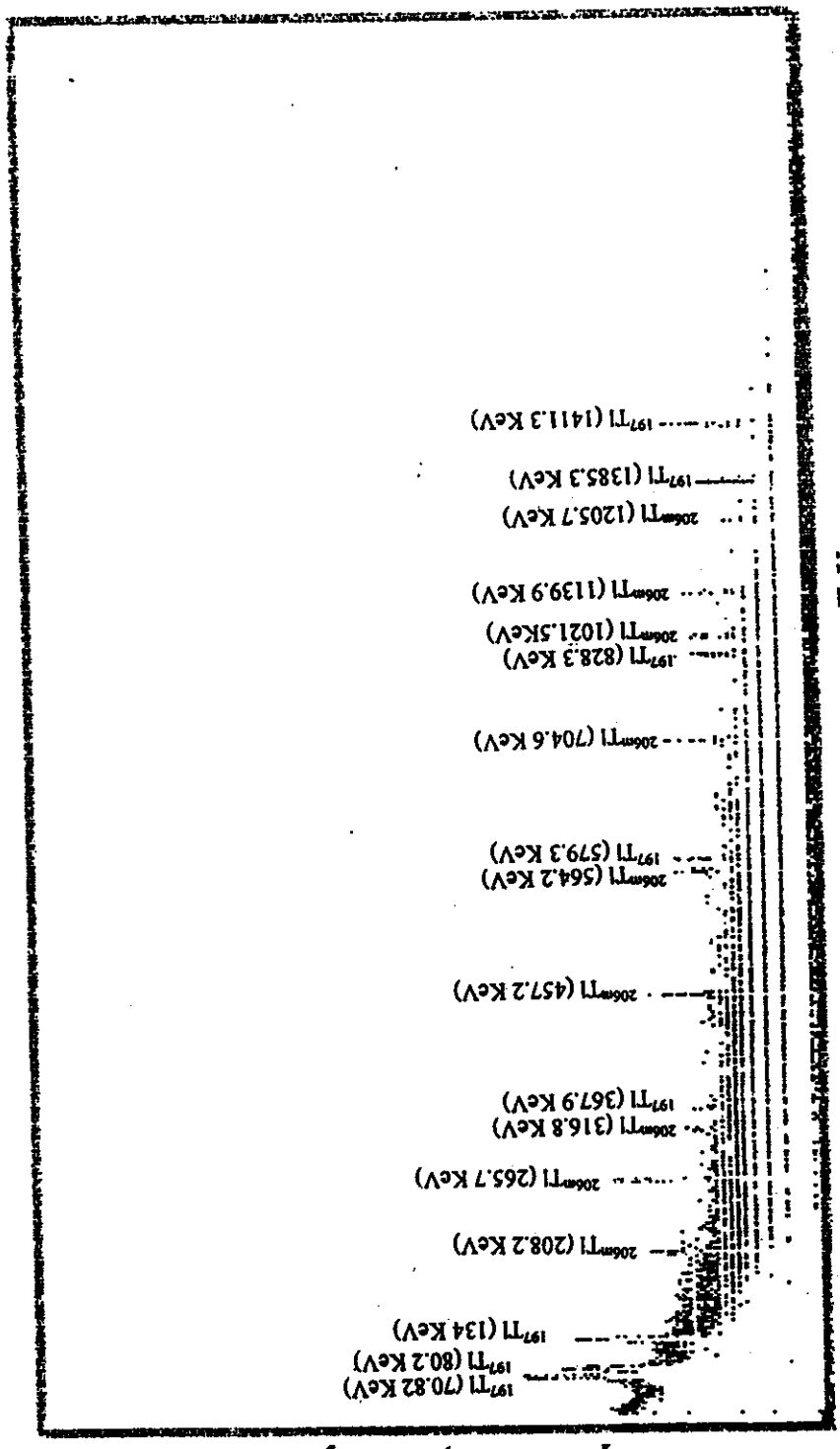

Fig.87.Gamma spectra of thallium eluates from12-molybdocerate(IV) matrix.

^{197,206m}Tl(I) are the main detected gamma energies. The corresponding radionuclidic purity was found to be higher than 99.9%.

3.4.4.3. Radiochemical Purity of Thallium(I) Eluates

The radiochemical purity is defined as the percent of the thallium(I) radioactivity in the desired chemical form to the total radioactivity. The presence of different radiochemical forms give poor quality images due to poor localization in the origin of interest and the high background from the surrounding tissues[128,130,131]. The radiochemical purity of thallium(I) eluates was assessed by ascending paper chromatography; using stripes of Whatman No.1 filter paper in methanol as a developing solvent[8, 43]. Figure 88 display a typical radiochromatogram of thallium(I) eluates from 12-molybdocerate column matrix. The radiochromatogram shows one only peak localized at R_f=0.58. Whereas; the retardation factor (R_f) represents the traveled distance from the base line to the peak position divided by the distance from the base line to the solvent front. The obtained R_f value may be due to thallium chloride; TlCl, radiotacer[8]. The corresponding radiochemical purity was found to be about 94%. This value is in agreement with the recommended specifications for use of thallium(I) for therapeutic and diagnostic purposes in nuclear medicine[41].

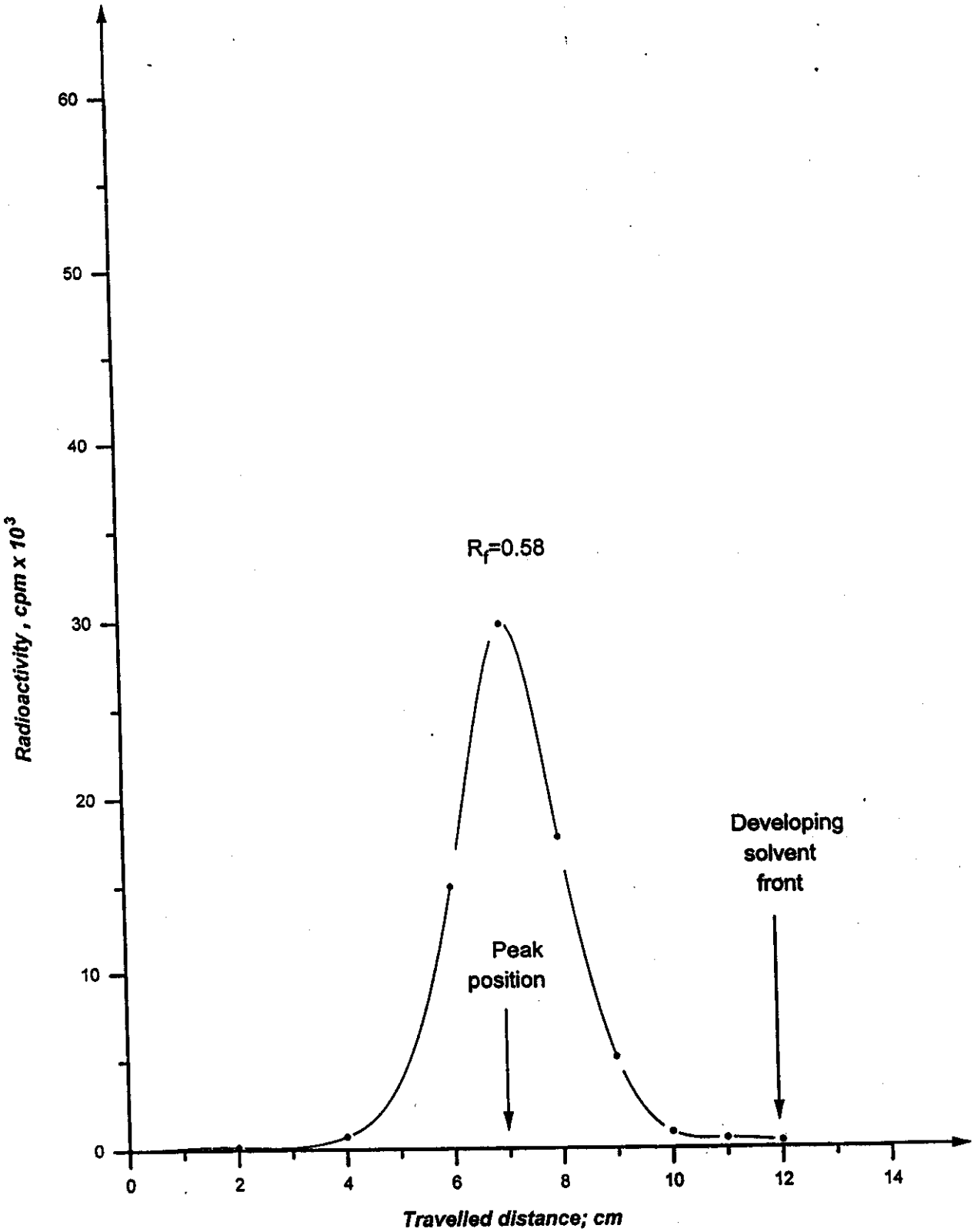

Fig.88.Radiochromatogram of thallium(I) eluates from 12-molybdocerate column matrix.